University of Nebraska - Lincoln

DigitalCommons@University of Nebraska - Lincoln

METHANOGEN METABOLIC FLEXIBILITY

Sean Carr
University of Nebraska-Lincoln, sean.carr@huskers.unl.edu

METHANOGEN METABOLIC FLEXIBILITY

by

Sean R. Carr

A DISSERTATION

Presented to the Faculty of

The Graduate College at the University of Nebraska

In Partial Fulfillment of Requirements

For the Degree of Doctor of Philosophy

Major: Biological Sciences

(Genetics, Cellular, and Molecular Biology)

Under the Supervision of Professor Nicole R. Buan

Lincoln, Nebraska

July, 2022

METHANOGEN METABOLIC FLEXIBILITY

Sean R. Carr, Ph.D.

University of Nebraska, 2022

Advisor: Nicole R. Buan

Methanogens are obligately anaerobic archaea which produce methane as a byproduct of their respiration. They are found across a wide diversity of environments and play an important role in cycling carbon in anaerobic spaces and the removal of harmful fermentation byproducts which would otherwise inhibit other organisms. Methanogens subsist on low-energy substrates which requires them to utilize a highly efficient central metabolism which greatly favors respiratory byproducts over biomass. This metabolic strategy creates high substrate:product conversion ratios which is industrially relevant for the production of biomethane, but may also allow for the production of value-added commodities. Particularly of interest are terpene compounds, as methanogen membranes are composed of isoprenoid lipids resulting in a higher flux through isoprenoid biosynthetic pathways compared to Eukarya and Bacteria. To assess the metabolic plasticity of methanogens, our laboratory has engineered the methanogen *Methanosarcina acetivorans* to produce the hemiterpene isoprene. We hypothesized that isoprene producing strains would result in a decreased growth phenotype corresponding to a depletion of metabolic precursors needed for isoprenoid membrane production. We found that the engineered methanogens responded well to the modification, directing up to 4% of total towards isoprene production and increasing overall biomass despite the

additional metabolic burden. Using flux balance analysis and RNA sequencing we investigated how the engineered strains respond to isoprene production and how production can be enhanced.

ACKNOWLEDGEMENTS

First, I would like to thank my advisor, Nicole R. Buan. Dr. Buan introduced to the fascinating world of archaea and instilled in me a passion for the odd and unusual which continues to drive me to better understand the natural world. Her passion for methanogens and uncovering the unknown shaped me into the scientist I am, and her infectious love of research continues to inspire me. Without her patient guidance and thoughtful insight this work would not have been possible. I would also like to thank my committee members (Dr. Ken Nickerson, Dr. Wayne Riekhof, Dr. Paul Blum, and Dr. Rebecca Roston) for their guidance through my thesis project and helping me work around difficult roadblocks along the way. A special thank you to Dr. Blum whose guidance and mentoring on applied microbiology and entrepreneurship have made me a better researcher and scientific communicator.

I would also like to thank my lab members, past and present, who made working in this laboratory a joyful experience. When I first joined the lab Jared Aldridge was instrumental in showing me the ropes and getting me acclimated to the graduate school mindset. Working alongside him on some of the most exciting projects I have been involved in was a highlight of my higher education. I would like to thank Jennie Catlett and Ethan Bender for their assistance in learning new techniques and helping me feel comfortable performing my own research in lab. Connor Hines, Morgan Price, and Darla Brennan also deserve a big thank you. As I transitioned from a junior to a senior graduate student, I found that in mentoring others you truly begin to understand what you have learned. I will continue to cherish the times we have spent in lab together whether it be conducting research or just spending time with one another.

TABLE OF CONTENTS

Chapter 4: Isoprene Production from Municipal Wastewater Biosolids by

Engineered Archaeon *Methanosarcina acetivorans*

**Chapter 5: Expression of isoprene synthase in *Methanosarcina acetivorans* reveals
energetic adaptations and links to amino acid biosynthesis**

Chapter 6: Metabolic Feedback Inhibition Influences Metabolite Secretion by the

Human Gut Symbiont *Bacteroides thetaiotaomicron*...140

Chapter 7: Metabolic synergy between human symbionts *Bacteroides* and

Methanobrevibacter 184

LIST OF MULTI-MEDIA OBJECTS

Chapter 1: The Anaerobic World of Methanogens

Life, in all of its diversity of scale and form, exists within a cycle of composition and decomposition. Though complex, this cycle can be clearly delineated between life with and without the presence of oxygen. In the aerobic space, small organic compounds are assembled into larger compounds of increasing complexity. As life grows larger and larger it requires exponentially greater amounts of energy and carbon to sustain itself. Through aerobic respiration, great amounts of energy are generated by the breaking down of complex molecules [1]. This creates a cycle of complex organisms consuming and breaking down less complex organisms, ever increasing in size until eventually the large organism dies. Once these large, complex biomasses expire, they are broken down by other aerobic organisms as much as possible, though they can only be degraded so far in an aerobic space. To further decompose complex organic structures to their base components, anaerobic degradation is necessary. Anaerobically, microbes respire and ferment organic matter to terminal degradation products, 1- and 2- carbon compounds which are unusable to the majority of life on Earth [2]. These terminal degradation products would accumulate ad infinitum, trapped without use, were there not a way to return them to a state usable for the carbon cycle. Methanogens gain energy not by the separation of complex compounds into smaller ones, but rather by the bioconversion of 1- and 2- carbon compounds into methane [2-6]. This gaseous methane then bubbles back into the aerobic world where it is consumed by methanotrophic organisms and is returned to the carbon cycle **(Figure 1)**. Without methanogens the world would be drowned in simple carbon compounds with no way to rebuild complex life.

The discovery of methanogens:

The discovery of methanogens was not a simple linear path. As with many microbes, their effects were recorded before the organisms themselves were observed. In the late 16th century, physicist and chemist Alessandro Volta recorded observations of flammable gases which emerged from reservoirs in marshland sediments [2]. When ignited these gases rapidly combusted into a brilliant blue flame, though the gas itself could be collected and transported, maintaining its combustive nature. It would not be until the 17th century that this flammable gas would be properly named by chemist August von Hofmann as methane. The properties and benefits of methane were characterized far before it was understood how it was most commonly created. Today we know methane for primarily two things: its use as a renewable fuel source as natural gas, and its potent effect as a greenhouse gas. Methane in the atmosphere has a 28 times greater warming effect than carbon dioxide and is believed to be a major contributing factor to global climate change [7-9]. Unbeknownst to the early scientists, however, this flammable gas was created not chemically, but by microorganisms, and those microbes themselves push the limits of what life is capable.

Before identification of the organism itself was achieved, the conditions by which microbial methane production could occur were characterized. In the late 1800s it was known that decaying plant biomass would produce methane though the mechanism was still unknown. Using similar techniques which Louis Pasteur utilized to prove the microbial nature of ethyl alcohol, researchers compared the methane produced by intestinal rumen supplemented with plant biomass with and without sterilization. When the rumen were sterilized via chemical and thermal means no methane were produced,

showing that it was not the simple 'decay' of the plant biomass which caused the formation of methane but rather a living biological process [3]. It would not be until 1933 that the organisms responsible for biomethane would be cultured and identified from river mud [10]. Originally thought to be bacteria, it was identified that these methanogens were capable of growing in inorganic medium with only simple carbon sources as their sole source of carbon and energy. These microbes would continue to be a curiosity in the microbial community and would become the focus of Dr. Carl Woese, who would use the ribosomal RNA sequence of methanogens as the foundation of archaea as an independent domain of life [4, 11].

Often called "The Third Domain," archaea represent life at its most primitive and diverse. To call archaea the Third domain however is somewhat of a misnomer as these organisms are some of the most evolutionarily ancient beings still in existence [12]. Methanogenic archaea have been identified in environments spanning the boundaries of life sustaining conditions, from acidic to alkaline (pH 3.0-10.2), thermophilic to psychrophilic (-2°C to 110°C), and including both fresh and saline aquatic environments [13]. Currently methanogens are of most interest due to their production of methane, both because of their ecological impact as a byproduct of agricultural production in livestock [14] and rice cultivation [15] and their use as a renewable source of natural gas [16, 17] as well as a high energy fuel source for rocket engines [18, 19].

Methanogen metabolism:

Despite their diversity of environments, methanogens are united by their unique central metabolism. All known methanogens are strict obligate anaerobes and produce methane as the primary byproduct of their central respiration [3]. As mentioned above,

methanogens grow in these anaerobic environments by the reduction of one carbon (C1)

compounds including carbon dioxide and carbon monoxide, methanol, methylamines,

and methyl sulfides as well as acetate [20-22]. It has also been demonstrated recently that

coal and long-chain alkanes can be utilized as a methanogenic substrates [23-27]. To

grow on these energy poor substrates methanogens have adopted a highly efficient central

respiratory pathway known as the Wolfe Cycle [6]. In the five best characterized versions

of this pathway substrates are reduced to methane while formate, primary and secondary

alcohols, or H_2 are oxidized to CO_2 with the assistance of the electron carrying molecules

Coenzyme M and Coenzyme B [20, 28]. Cofactors associated with the Wolfe cycle are

regenerated via a transmembrane ion gradient which also serves to produce ATP for the

methanogen via ATP synthase [29, 30]. These reactions yield a very small amount of

energy for the methanogen and as a result the methanogens only obtain between 0.5 and 2

moles of ATP per mole of substrate [20]. A result of this low energy yield is a higher

focus on respiration in methanogens than any other organism with over 99% of the

chemistry within the cell being directly tied to the Wolfe Cycle. This focus on central

respiration makes methanogens an ideal organism for the production of renewable

biofuels as the vast majority of feed substrate is converted efficiently to methane. It

should be noted, however, that while the Wolfe Cycle is highly conserved and

exceedingly efficient, it can also be modified to better serve biotechnological goals

without undermining the proficiency of methanogenic growth. In this dissertation we will

explore the metabolic flexibility of methanogens as well as the potential for their

application in biotechnology. For example, by overexpressing the cytoplasmic enzyme

complex heterodisulfide reductase (HdrABC), methane production in methanogens

grown on methanol has been shown to produce 30% extra methane without a detectable change in growth rate compared with a non-modified strain [31]. Additionally, it is possible that the regeneration of methanogenic cofactors may be more flexible in their regeneration than initially thought [32]. If a methanogen were to be engineered to produce a non-native metabolite where the formation of which allows for the regeneration of ferredoxin, F_{420}, coenzyme M or coenzyme B then production of that metabolite has the potential to increase the rate of methanogenesis while also producing the desired product [32].

Figures and legends:
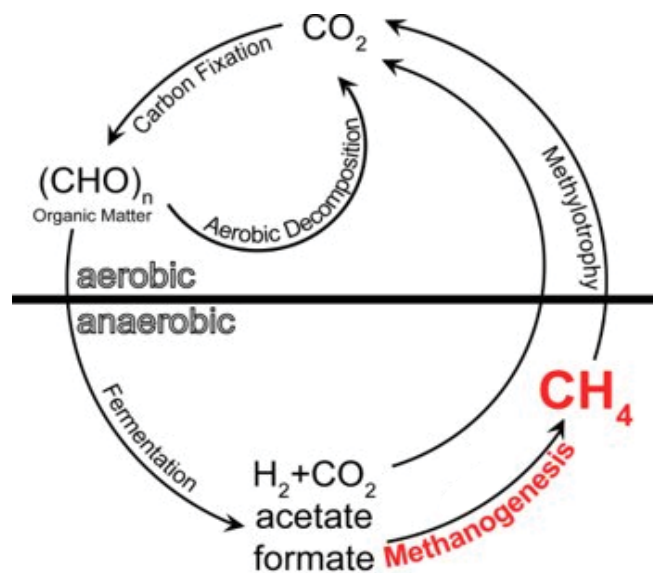
Figure 1: The global carbon cycle divided into aerobic and anaerobic segments. Large macromolecules are developed in the anaerobic portion of the carbon cycle through a series of methylotrophic and carbon fixing reactions leading to complex organic biomass. Decomposing organic biomass is fermented into its most basic 1- and 2-carbon forms anaerobically. 1- and 2- carbon compounds are utilized by methanogens and bioconverted into gaseous methane which returns to the aerobic segment of the carbon cycle (N. Buan).

References

1.   Schmidt-Rohr, K., *Oxygen is the high-energy molecule powering complex multicellular life: Fundamental corrections to traditional bioenergetics.* ACS omega, 2020. **5**(5): p. 2221-2233.

2.   Wolfe, R.S., *An historical overview of methanogenesis*, in *Methanogenesis*. 1993, Springer. p. 1-32.

3.   Ferry, J.G., *Methanogenesis: ecology, physiology, biochemistry & genetics*. 2012: Springer Science & Business Media.

4.   Balch, W., et al., *Methanogens: reevaluation of a unique biological group.* Microbiological reviews, 1979. **43**(2): p. 260.

5.   Rouviere, P.E. and R. Wolfe, *Novel biochemistry of methanogenesis.* Journal of Biological Chemistry, 1988. **263**(17): p. 7913-7916.

6.   Thauer, R.K., *The Wolfe cycle comes full circle.* Proceedings of the National Academy of Sciences, 2012. **109**(38): p. 15084-15085.

7.   Tilche, A. and M. Galatola, *The potential of bio-methane as bio-fuel/bio-energy for reducing greenhouse gas emissions: a qualitative assessment for Europe in a life cycle perspective.* Water Science and Technology, 2008. **57**(11): p. 1683-1692.

8.   Huttunen, J.T., et al., *Fluxes of methane, carbon dioxide and nitrous oxide in boreal lakes and potential anthropogenic effects on the aquatic greenhouse gas emissions.* Chemosphere, 2003. **52**(3): p. 609-621.

9.   Cicerone, R.J. and R.S. Oremland, *Biogeochemical aspects of atmospheric methane.* Global biogeochemical cycles, 1988. **2**(4): p. 299-327.

10.   Stephenson, M. and L.H. Stickland, *Hydrogenase: the bacterial formation of methane by the reduction of one-carbon compounds by molecular hydrogen.* Biochemical Journal, 1933. **27**(5): p. 1517.

11.   Woese, C.R. and G.E. Fox, *Phylogenetic structure of the prokaryotic domain: the primary kingdoms.* Proceedings of the National Academy of Sciences, 1977. **74**(11): p. 5088-5090.

12.   Barns, S.M., et al., *Perspectives on archaeal diversity, thermophily and monophyly from environmental rRNA sequences.* Proceedings of the National Academy of Sciences, 1996. **93**(17): p. 9188-9193.

13.   Martin, W.F. and F.L. Sousa, *Early microbial evolution: the age of anaerobes.* Cold Spring Harbor perspectives in biology, 2016. **8**(2): p. a018127.

14.   Johnson, K.A. and D.E. Johnson, *Methane emissions from cattle.* Journal of animal science, 1995. **73**(8): p. 2483-2492.

15.   Schütz, H., W. Seiler, and R. Conrad, *Processes involved in formation and emission of methane in rice paddies.* Biogeochemistry, 1989. **7**(1): p. 33-53.

16.   Huang, Z., et al., *Low carbon renewable natural gas production from coalbeds and implications for carbon capture and storage.* Nature communications, 2017. **8**(1): p. 1-11.

17.   Luo, G. and I. Angelidaki, *Integrated biogas upgrading and hydrogen utilization in an anaerobic reactor containing enriched hydrogenotrophic methanogenic culture.* Biotechnology and bioengineering, 2012. **109**(11): p. 2729-2736.

18.   Sheehan, S.W., *Electrochemical methane production from CO2 for orbital and interplanetary refueling.* Iscience, 2021: p. 102230.

19. Neill, T., et al., *Practical uses of liquid methane in rocket engine applications.* Acta Astronautica, 2009. **65**(5-6): p. 696-705.

20. Buan, N.R., *Methanogens: pushing the boundaries of biology.* Emerging Topics in Life Sciences, 2018. **2**(4): p. 629-646.

21. Daniels, L., et al., *Carbon monoxide oxidation by methanogenic bacteria.* Journal of Bacteriology, 1977. **132**(1): p. 118-126.

22. Rother, M. and W.W. Metcalf, *Anaerobic growth of Methanosarcina acetivorans C2A on carbon monoxide: an unusual way of life for a methanogenic archaeon.* Proceedings of the National Academy of Sciences, 2004. **101**(48): p. 16929-16934.

23. Mayumi, D., et al., *Methane production from coal by a single methanogen.* Science, 2016. **354**(6309): p. 222-225.

24. Zengler, K., et al., *Methane formation from long-chain alkanes by anaerobic microorganisms.* Nature, 1999. **401**(6750): p. 266-269.

25. Borrel, G., et al., *Wide diversity of methane and short-chain alkane metabolisms in uncultured archaea.* Nature microbiology, 2019. **4**(4): p. 603-613.

26. Laso-Pérez, R., et al., *Anaerobic degradation of non-methane alkanes by "Candidatus Methanoliparia" in hydrocarbon seeps of the Gulf of Mexico.* MBio, 2019. **10**(4): p. e01814-19.

27. Lemaire, O.N. and T. Wagner, *A Structural View of Alkyl-Coenzyme M Reductases, the First Step of Alkane Anaerobic Oxidation Catalyzed by Archaea.* Biochemistry, 2022.

28. Ermler, U., et al., *Crystal structure of methyl-coenzyme M reductase: the key enzyme of biological methane formation.* Science, 1997. **278**(5342): p. 1457-1462.

29.   Costa, K.C. and J.A. Leigh, *Metabolic versatility in methanogens.* Current opinion in biotechnology, 2014. **29**: p. 70-75.

30.   Diender, M., A.J. Stams, and D.Z. Sousa, *Pathways and bioenergetics of anaerobic carbon monoxide fermentation.* Frontiers in microbiology, 2015. **6**: p. 1275.

31.   Catlett, J.L., A.M. Ortiz, and N.R. Buan, *Rerouting cellular electron flux to increase the rate of biological methane production.* Applied and environmental microbiology, 2015. **81**(19): p. 6528-6537.

32.   Aldridge, J., et al., *Anaerobic Production of Isoprene by Engineered Methanosarcina Species Archaea.* Applied and environmental microbiology, 2021. **87**(6): p. e02417-20.

Chapter 2: Insights into the biotechnological potential of methanogenic archaea

This chapter to be submitted for publication

Abstract

Methanogens are anaerobic archaea which conserve energy by producing methane. Found in nearly every anaerobic environment on earth, methanogens serve important roles in ecology as the bedrock of the global carbon cycle and in industry as a source of renewable biofuels. Environmentally, methanogens play an essential role in the reintroducing unavailable carbon to the carbon cycle by anaerobically converting low-energy, terminal metabolic degradation products such as one- and two-carbon molecules into methane which then returns to the aerobic portion of the carbon cycle. In industry, methanogens are commonly as an inexpensive source of renewable biofuels as well as serving as a vital component in the treatment of wastewater though this is only the tip of the iceberg for their metabolic potential. In this review we will discuss how methanogens' efficient central metabolism and isoprenoid membranes open the door to future biotechnology applications.

Methanogen ecology and diversity

Methanogens are single-celled organisms that conserve energy via the conversion of substrate carbon compounds into methane gas [1]. This gaseous methane then bubbles back into the aerobic world where it is consumed by methanotrophic organisms and is returned to the carbon cycle. Currently the methane produced by methanogens is of

interest due to methane's ecological impact resulting from agricultural production by livestock [2] and rice cultivation [3] as well as methane's benefits as a renewable source of natural gas [4, 5] which is a high energy fuel used for heat, electricity generation, and for transportation including for rocket engines [6, 7]. Methanogenic archaea have been identified in environments spanning the boundaries of life sustaining conditions, from acidic to alkaline (pH 3.0-10.2), thermophilic to psychrophilic (-2°C to 110°C), and including both fresh and saline aquatic environments [8]. In addition to these environments, Methanogens are found symbiotically communing in a wide range of single- and multi-cellular hosts ranging from amoebae [9] and protozoa [10] to the guts of termites [11, 12], bovine [13], and humans [14, 15]. The ability for methanogens to thrive in these wildly diverse environments is testament to their metabolic robustness. Regardless of the environment they inhabit, methanogens share a similar metabolic niche, the bioconversion of low-energy substrates into biomass and high-energy molecules at a high degree of efficiency. The average macromolecular composition of a methanogen includes 63% protein, 0.1% Fatty acid lipids, 5% isoprenoid lipids, 0.5% carbohydrates, 28% nucleic acids, and 4% metabolites and metabolic precursors [16]. The relatively high abundance of isoprenoid lipids and protein concentration make them am appealing source of difficult to synthesize lipids and molecules, something which can be further enhanced through genetic engineering. In this review we discuss how methanogen metabolism allows them to thrive under strict energetic conditions and how those special metabolic features can be utilized in biotechnology.

Expanding the Wolfe Cycle of methanogenesis

Despite a wide diversity of habitats, methanogens are united by their unique central metabolism. All known methanogens to date are strict obligate anaerobes and produce methane as an essential byproduct of metabolism [1]. As mentioned above, methanogens grow in anaerobic environments by the reduction of one carbon (C1) compounds including carbon dioxide and carbon monoxide, methanol, methylamines, and methyl sulfides as well as acetate [17-19]. It has also been demonstrated that coal can be utilized as a methanogenic substrate [20]. To grow on these energy poor substrates methanogens have adopted a highly efficient central respiratory pathway known as the Wolfe Cycle [21] (Figure 1). In the five characterized versions of this pathway substrates are reduced to methane while formate, primary alcohols/amines/thiols, or H_2 are oxidized to CO_2 [17, 22]. In most methanogens, redox cofactors associated with the Wolfe cycle are regenerated through formation of a transmembrane ion gradient which is coupled to ATP synthesis via ATP synthase [23, 24]. These reactions yield a very small amount of energy for the methanogen only amounting to between 0.5 and 2 moles of ATP per mole of substrate [17]. A result of this low energy yield is a high relative flux through respiration with over 99% of the chemistry within the cell being directly tied to the Wolfe Cycle. This focus on central respiration makes methanogens an ideal organism for the production of renewable biofuels as the vast majority of feed substrate is converted efficiently to methane.

Methanogens are involved in more than just the degradation of terminal fermentation products. In nature methanogens form syntrophic partnerships with other

microorganisms such as hydrocarbon-degrading bacteria facilitating the reintroduction of crude oil carbon into a bioavailable state [25-27]. It has recently been discovered from ecological methane accumulation and the abundance of single cell cultures attached to oil droplets in deep-sea oil seeps that methanogens are be capable of alkane oxidation independent of any other archaeal or bacterial partner [28, 29]. These alkane utilizing methanogens are not limited to short-chain alkanes; amongst these alkane degrading methanogens is *Candidatus methanoliparum* which has been shown to incorporate the degradation of long-chain hydrocarbons with methanogenesis [30]. The methanogens associated are found widely distributed [26, 28, 30], indicating that methanogens are involved in the bioconversion of crude oil to methane on a large scale and may serve a benefit to bioremediation efforts in anaerobic environments such as deep-sea sediments.

It should be noted, however, that while the Wolfe Cycle is highly conserved and exceedingly efficient, it can also be modified to better serve biotechnological goals without undermining the proficiency of methanogenic growth. By overexpressing the cytoplasmic enzyme complex heterodisulfide reductase (HdrABC), methane production in methanogens grown on methanol has been shown to produce 30% extra methane without a detectable change in growth rate compared with a non-modified strain [31]. Additionally, it is possible that the regeneration of methanogenic cofactors may be more promiscuous than initially thought [32]. If a methanogen were engineered to produce a non-native metabolite where the formation of which allows for the regeneration of ferredoxin, F420, coenzyme M or coenzyme B then production of that metabolite has the potential to increase the rate of methanogenesis while also producing the desired product [32]. Due to the tight energetic restrictions central methanogenesis is a highly streamlined

and is proposed to rely heavily on substrate channeling to minimize entropic effects [31].

This substrate channeling allows for the Wolfe Cycle to function efficiently but presents

challenges for metabolic engineers as the metabolite pools for central methanogenesis

have limited availability outside of the channeled enzyme complexes. To overcome this

metabolic obstacle metabolic engineers must choose products which draw from

metabolites which are not directly channeled or incorporate the production of their

products within the existing exchange of carbon and electrons within the Wolfe Cycle.

There are ways of making methanogens more amenable to modification and we have

complied a list of starting points for those eager to expand methanogen utilization under

novel conditions or applications (Table 1).

Anaerobic oxidation of methane and reverse methanogenesis

Given the efficiency of methanogenesis and the abundance of anaerobic

environments around the world, methanogens are distributed across every continent. Yet

of the approximately 1 billion tons of methane produced by methanogens in the wild each

year in anaerobic and microanaerobic environments, roughly half escapes into the aerobic

space of the carbon cycle [33]. The remainder of this methane is either trapped within this

anaerobic space (as gas or methane gas hydrates) or oxidized by methanotrophic archaea

and sulfate-reducing bacteria [34, 35]. Previously it was believed that the anaerobic

oxidation of methane (AOM) was possible through the symbiotic exchange of

metabolites and electrons between the methanotrophic archaea and the sulfate reducers

[36, 37]. Within this process anaerobic methane-oxidizing archaea (ANME) consisting of

methanomicrobiales (ANME-1) and methanosarcinales (ANME-2 and ANME-3) form

granular aggregates with delta-proteobacteria in which electrons are transferred from the

via multi-haem cytrochromes [38]. Metabolic modeling has suggested that iron and

sulfate can be co-substrates in AOM [39] and 16S rRNA gene-sequences for *Candidadus*

Methanoperedens correlated with increased AOM in sulfate-rich anoxic sediments

suggesting the occurrence of AOM independent of a bacterial partner[40]. In laboratory

conditions it was found that trace amounts of AOM was observed in

Methanothermobacter marburgenis [41] and *Methanosarcina acetivorans* [42] though it

was not observed that these strains were able to use methane as the major source of

carbon and energy for growth. However, by scouring the metagenomes of unculturable

ANME-1 samples from aquatic regions with high amounts of AOM, a novel gene for

methyl-coenzyme M reductase (Mcr) was discovered which facilitated AOM without the

need for a syntrophic sulfate-reducing partner [43, 44]. As every step of methanogenesis

is reversible, reverse methanogenesis is theoretically possible for any methanogen though

under most conditions these reactions are non-energy yielding [21]. When the novel

ANME-1 Mcr was introduced into *M. acetivorans* it was found that isotope labeled

methane was converted into acetate while also facilitating growth [45]. Furthermore,

methanogen strains containing this ANME-1 Mcr gene can be utilized along with a

consortia of microbes including *Geobacter sulfurreducens* to produce electricity in a

microbial fuel cell utilizing only methane as a substrate [46]. These observations indicate

that the bidirectionality of the Wolfe Cycle, particularly in *Methanosarcina spp.* enables

the potential for an alternative utilization of methanogens: the bioconversion of C1

substrates into stable to transport fuels and high-value chemicals. For example: a

Methanosarcina culture which has been engineered to produce a high-value terpenoid

product is grown using methyl compounds until stationary phase is achieved and biomass

accumulation is no longer necessary; this culture could then be induced to produce the

terpenoids utilizing potentially any C1 compound or mixtures of compounds including

CO, CO_2, or CH_4 based on substrate availability. This potential extends beyond the

production of secreted products, as the biomass of methanogens itself can be utilized as a

source of valuable lipids.

Potential for engineering the lipid membrane biosynthesis pathway as a valorization strategy

Methanogen membranes, like those found in all archaea, are distinct from those

found in bacteria and eukarya. In bacterial and eukaryotic organisms lipid membrane

structures are composed of fatty acid chains ester liked to glycerol-3-phosphate (G3P)

[47]. Archaeal lipids membranes instead utilize isoprenoid alkyl chains ether linked to

glycerol-1-phosphate (G1P) (Figure 2) [47, 48]. This fundamental differentiation in

membrane composition is the basis of the so called 'lipid divide' separating archaea from

the other two domains of life [49]. Given the high quantity and the molecular uniformity

of lipid membranes by weight, comprising on average 5% of total methanogen dry weight

[16], and the relatively high metabolic flux through the pathway, isoprenoid lipid

biosynthesis pathway is an attractive target to engineer for producing high-value

chemicals. The isoprenoid lipids used by archaea are highly adaptable and allow for

archaea to tolerate a wide range of environmental stressors. The most abundant of

archaeal lipid structures are archeol, consisting of a pair of phytanyl chains ether linked

to G1P and caldarcheol, a cyclic dimer of archeol. Caldarcheol is of particular

biotechnological interest as the cyclized tetraether lipids maintain cellular homeostasis in the presence of extreme pH and thermal stress [50, 51]. Archaeal ether linked lipids are more stable than ester linked membranes when exposed to extremes of pH and thermal conditions, and the unique monolayer structure of tetraether linked lipids imparts resistance to degradation to phospholipases [52]. These stable properties and the intrinsic monolayer formed by caldarcheol represents an enticing alternative to traditional phospholipids in liposome-based commercial applications. One such application is in the delivery of chemotherapeutic compounds via archaeal derived liposomes. It has been found that tetraether linked artificial liposomes reduce leakage of chemotherapeutic compounds by 9-fold compared to conventional eukaryotic derived liposomes, which results in a lower dose required for therapeutic effects [53]. The archaeal liposomes themselves also contribute therapeutic effects as archaeal liposomes utilized to transport vaccine components induce robust antigen specific humoral and cellular immune responses exceeding those found from traditional delivery mechanisms [54-57].

In addition to the direct application of archaeal lipids, the high metabolic flux through isoprenoid producing pathways in methanogens presents an opportunity for low-cost production of terpene compounds. Terpenes are the largest class of natural compounds and have a wide range of commercial applications. Odorant terpenes such as limonene, eucalyptol, and linalool are cornerstones for the $29B flavor and fragrance industry [58]. In addition to odorants, terpenes are often the active compound in pharmaceuticals including the anti-cancer drug paclitaxel and the antimalarial artemisinin. Hundreds of natural terpenes have shown promising bioactivity [59-63] yet are limited in application due to their availability. Many of these terpenes are currently

harvested from their native plant, fungal, and marine producers which are limited by the

endogenous expression levels which are prohibitively low [64-66] or non-renewably

synthesized from petroleum precursors. Organically produced terpenes are primarily

produced via compounds derived from one of two isoprenoid synthesis pathways, the

mevalonate (MVA) pathway and the deoxyxylose 5-phosphate (DXP) pathway [67].

These pathways in non-archaeal organisms suffer low carbon flux and depletion of

precursors towards non-target compounds [68-70]. Archaea, however, synthesize the

majority of their lipid compounds through the mevalonate pathway, accounting for a

much higher flux through that pathway [71-73]. As such there is a higher abundance of

metabolic precursors available for the synthesis of isoprenoid and terpene products

without the need to preoptimize engineered strains for substrate availability. Concerns

over the depletion of these membrane precursors have been alleviated by the synthesis of

mono-isoprene from engineered strains of *Methanosarcina acetivorans* and

Methanosarcina barkeri [32, 74]. These strains demonstrated that methanogens are able

to handle the metabolic burden of membrane substrate depletion without a decrease in

growth rate or final carrying capacity, opening the door for further isoprenoid products to

be produced (Table 2. Possible terpenoids to be produced by methanogens based on

category) The expression of genes associated with terpenoid production can also be

associated with inducible promoters to activate new pathways when cells hit stationary

phase, so that expression doesn't interfere with populating the bioreactor. One challenge

is that some terpenes require molecular oxygen for complete biosynthesis and this might

be difficult for anaerobic organisms to achieve. However, *Methanosarcina acetivorans* is

remarkably oxygen-tolerant and it is possible to further enhance through engineering or

adaptation [75, 76]. These papers indicate it is feasible to use O_2 availability as a biosynthetic inducer during the terpene fermentation process with oxygen-tolerant methanogens.

Benefits and challenges of methanogen biotechnologies

The use of methanogens in bioproduction is beneficial in a myriad of ways including ease of selection, low cost of media, and flexibility of products. Methanogens have been shown to be an excellent source of metabolically active compounds such as the Coenzyme M (CoM) which acts as a potent chemotherapy adjuvant as the drug mesna [77]. As methanogens grown in environments lacking in O_2, they are able to produce novel precursors with chirality which could later be utilized by chemists with custom oxidation steps and subsequent functionalization. In large scale industrial fermentations pure aseptic environments are difficult to maintain, and often media and growth conditions are utilized to ensure continuous selection during the fermentation [78, 79]. Methanogens circumvent this issue by growing in selective environments free of oxygen using substrates that cannot be used for the majority of common contaminating factors such as lactic acid bacteria and fungi [80, 81]. Methanogens are prototrophic organisms, able to synthesize all vitamins and cofactors required for growth from inorganic material, allowing for additional selection by limiting available vitamins and nutrients required for contaminating growth by exclusion [17, 21, 82]. While viral predation on methanogens has been observed [83] there is little evidence that these methanophage particles have a substantial effect on methanogenic digestor performance as viral titers did not correlate with a significant decrease in methane output and methanogen carrying capacity. Another

major challenge in industrial fermentations is the large amounts of fresh water required

for E. coli or yeast [84]. Methanogens however thrive in environments with high salt

concentrations, allowing for the utilization of seawater in fermentations. Non-sterile

hypersaline environments such ocean water and hydraulic fracking fluids have been

demonstrated to select for methylotrophic methanogens such as *Methanohalophilus,*

Methanohalobium, and *Methanosarcina* spp. while also presenting a high concentration

of non-competitive substrates such as methylamines [85, 86]. Methanogens are utilized

worldwide for the production of renewable biogas in non-selective environments with

high degrees of contamination such as municipal and agricultural wastewater treatment.

In these environments methanogens are exposed to a wide variety of stressors including

dramatic shifts in ammonia, osmotic shifts, and exposure to heavy metals [90]. Many

methanogens are natively capable of withstanding these stressors [87] though as stated

above, using genetic tools it is possible to stack these traits onto a single methanogen

strain to gain the maximum benefit from a single organism.

Conclusions

Methanogens are biologically important organisms with a wide-reaching impact

both in ecological and biotechnological applications. Their extremely efficient central

metabolism makes them an ideal source of renewable biofuels that can be captured

through anaerobic digestion or fermentation processes. They are able to grow

prototrophically with inexpensive feedstocks and can produce endotoxin-free protein,

carbohydrates, and valuable isoprenoid lipids. Their unique membrane composition can

be used to expand the biotechnological toolbox for the delivery of chemotherapeutics as

well as source for novel terpene compounds previously not available via conventional extraction means. By continuing to investigate the molecular, genetic, and synthetic biology potential of these unique organisms, researchers may unlock a wide range of applications from environmental and ecological management, renewable energy, agriculture, chemical manufacturing, and pharmaceutic industries.

Figures and legends:

Figure 1: The Wolfe Cycle of methanogenesis[17]

The direction of arrows represents the direction of biochemical reactions.

Reactions which are utilized in every methanogenic pathway are represented in black.

Hydrogenotrophic methanogenesis is represented in red. Methyl respiration is represented

in orange. Methylotrophic methanogenesis is represented in green. Acetoclastic

methanogenesis is represented in fuchsia. Degradation of polyaromatic hydrocarbons is

represented in dark blue [88]. Ethylene and long chain alkane reduction is represented in

purple [89]. Carboxydotrophic methanogenesis is represented in cyan. CoB-SH,

coenzyme B thiol; CoM-SH, Coenzyme M thiol; CoM-S-S-CoB, coenzyme M-coenzyme

B heterodisulfide; Fd, ferredoxin; Fd_{red}, reduced ferredoxin; H_4MPT,

tetrahydromethanopterin; MFR, methanofuran; MPh, methanophenazine; $MPhH_2$,

reduced methanophenazine. Enzymes involved in the Wolfe Cycle: a) Formyl-

methanofuran dehydrogenase (Fmd), b) Formyl-methanofuran:H_4MPT formyl transferase

(Ftr), c) Methenyl-H4MPT cyclohydrolase (Mch), d) F_{420}-dependent Methylene-H4MPT

dehydrogenase (Mtd), e) F420-dependent Methylene-H4MPT reductase (Mer), f) Methyl-

H4MPT:coenzyme M methyltransferase (Mtr), g) Methyl-coenzyme M reductase (Mcr),

g*) Atypical methyl-coenzyme M reductase (Mcr) [90], h) Electron-bifurcating

hydrogenase:heterodisulfide reductase complex (Mvh:HdrABC), i) F_{420}-reducing

hydrogenase (Frh), j) Energy-converting sodium pumping ferredoxin hydrogenase, k)

Ferredoxin reducing hydrogenase (Eha/Ech), l) Proton-translocating

methanophenazine:heterodisulfide reductase (HdrED), m) Sodium–proton antiporter

(MrpA), n) F_{420} proton-pumping methanophenazine reductase (Fpo).
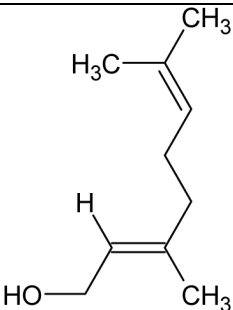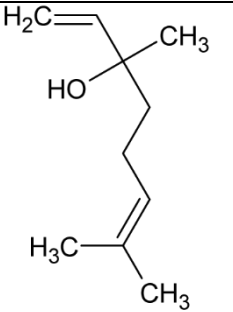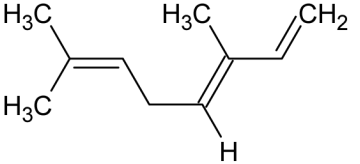
Table 1. Expanding the metabolic potential of the Wolfe Cycle
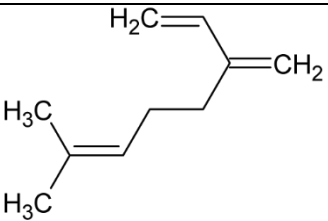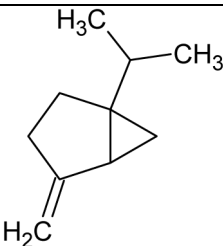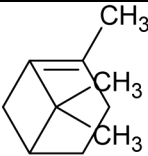
Desired Trait	Potential mechanism
Increased methanogenesis and methane production.	Overexpression of genes associated with the Wolfe Cycle. Research has shown that overexpression of redox-active cofactors such as methanophenazine relieves the metabolic bottleneck caused by cofactor regeneration and increases the production of methane [31].
Increased substrate uptake rates.	In methylotrophic methanogenesis entry point the Wolfe Cycle is limited by the substrate-specific methyltransferase whereas hydrogenotrophic methanogens rely upon membrane bound methyltransferase to conserve energy and maintain the methanogens sodium motive force[91]. By overexpressing endogenous methyltransferases and
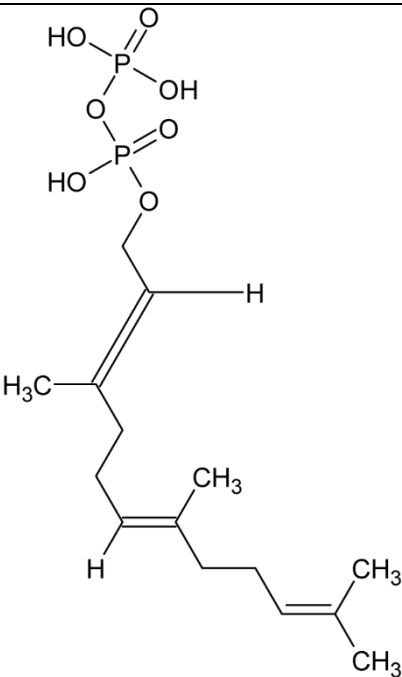
	hydrogenases more substrate carbon can enter methanogenesis.
Increased substrate diversity.	Substrate entry into the Wolfe Cycle is limited by substrate specific methyltransferases and whether the methanogen can directly utilize H_2 as an electron source. By introducing methyltransferase from different methanogens Introduction of methyltransferase genes from multiple methanogens one can expand the substrates usable to the methanogen. Additionally, the introduction of EcH hydrogenase should allow for organisms incapable of hydrogenotrophic methanogenesis to utilize H_2 and CO_2 as a carbon and energy source. By stacking these traits it is possible to maximize methanogenic efficiency in mixed substrate environments such as the treatment of waste biomass.
Increased stress resistance	All methanogens are strict anaerobes, though it has been found that *Methanosarcina* spp. are the most oxidant-tolerant [76]. Increased oxygen tolerance was observed in *Methanosarcina acetivorans* when gradually passaged with increased O2 concentrations over a course of 6 months [75]. Transcripts from adapted *Methanosarcina* suggest the over expression of superoxide dismutase, catalase, and peroxidase will confer increased aerotolerance to other
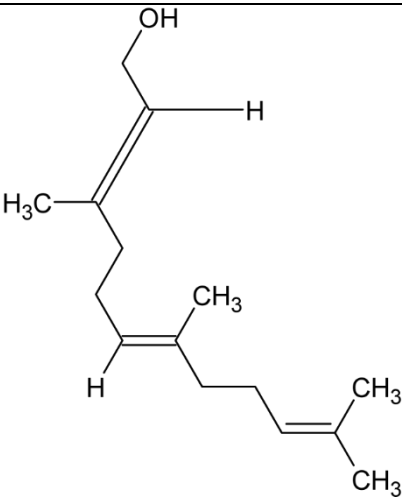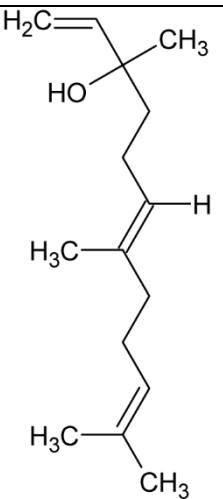
	methanogens. Cocultivation with sulfate reducing bacteria has shown to mitigate heavy metal stress in methanogenic cultures [92]. The introduction or overexpression of the betaine transporter from *Methanosarcina thermophila* TM-1 increases internal ionic balance conferring protection against osmotic stress [87]. Additionally, it has been noted that under high ammonia conditions which inhibits aceticlastic methanogenesis, the addition of magnetite reduces inhibition [93].
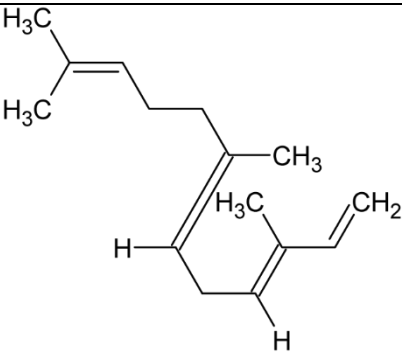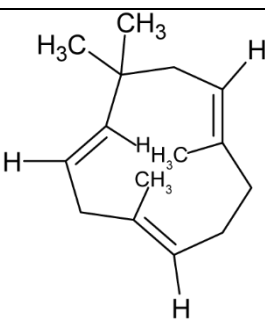
Table 2. Possible terpenoids to be produced by methanogens based on category.

Terpene name	Terpene class	Structure	Synthesis Enzyme	Substrate
Isoprene	Hemiterpene	$H_2C=$ $=CH_2$ H_3C	Isoprene synthase (4.2.3.27)	Dimethylallyl pyrophosphate
Geranyl pyrophosphate (GPP)	Monoterpene	CH_3 H_3C H CH_3 (phosphate structure)	(2E,6E)-farnesyl diphosphate synthase (2.5.1.10)	Dimethylallyl pyrophosphate
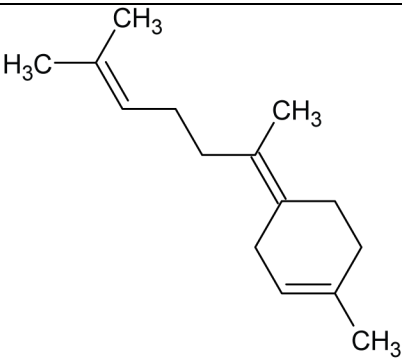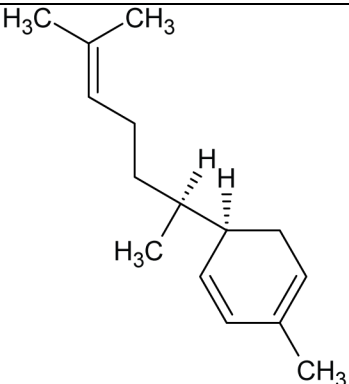
Geraniol	Monoterpene		Geraniol synthase (3.1.7.11)	Geranyl diphosphate
Linalool	Monoterpene		S-linalool synthase (4.2.3.25)	Geranyl diphosphate
Ocimene	Monoterpene		(E)-beta-ocimene synthase (4.2.3.106)	Geranyl diphosphate
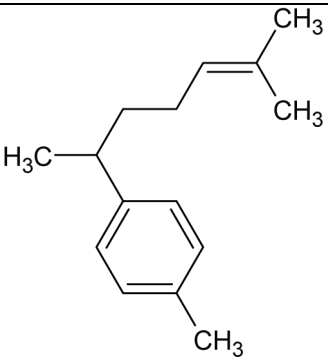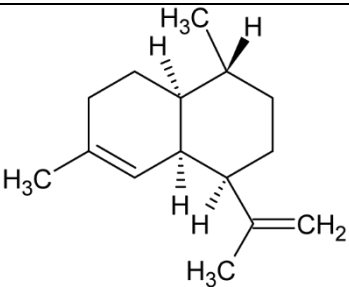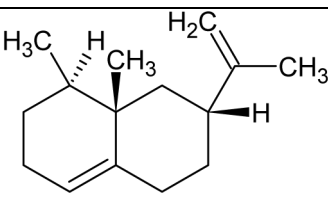
Myrcene	Monoterpene		Myrcene synthase (4.2.3.15)	Geranyl diphosphate
Sabinene	Bicyclic Monoterpenoid		(+)-sabinene synthase (4.2.3.110)	Geranyl diphosphate
Pinene	Bicyclic Monoterpenoid		Pinene synthase (4.2.3.14)	Geranyl diphosphate

Farnesyl diphosphate	Acyclic Sesquiterpenoid		Farnesyl diphosphate synthase (2.5.1.1)	Dimethylallyl diphosphate and isopentenyl diphosphate

| Farnesol | Acyclic Sesquiterpenoid | | Farnesyl diphosphatase (3.1.7.6) | Farnesyl diphosphate |
| Nerolidol | Acyclic Sesquiterpenoid | | (3S,6E)-nerolidol synthase (4.2.3.48) | Farnesyl diphosphate |

Farnesene	Acyclic Sesquiterpenoid		Alpha-farnesene synthase (4.2.3.46) and beta-farnesene synthase (4.2.3.47)	Farnesyl diphosphate
Humulene	Monocyclic Sesquiterpenoid		Alpha-humulene synthase (4.2.3.104)	Farnesyl diphosphate

Bisabolene	Monocyclic Sesquiterpenoid		Alpha-bisbolene synthase (4.2.3.38)	Farnesyl diphosphate
Zingiberene	Monocyclic Sesquiterpenoid		Zingiberene synthase (4.2.3.65)	Farnesyl diphosphate

Curcumene	Monocyclic Sesquiterpenoid		Gamma-curcumene synthase (4.2.3.94)	Farnesyl diphosphate
Amorphadiene	Bicyclic Sesquiterpenoid		Amorpha-4,11-diene synthase (4.2.3.24)	Farnesyl diphosphate
Valencene	Bicyclic Sesquiterpenoid		Valencene synthase (4.2.3.73)	Farnesyl diphosphate
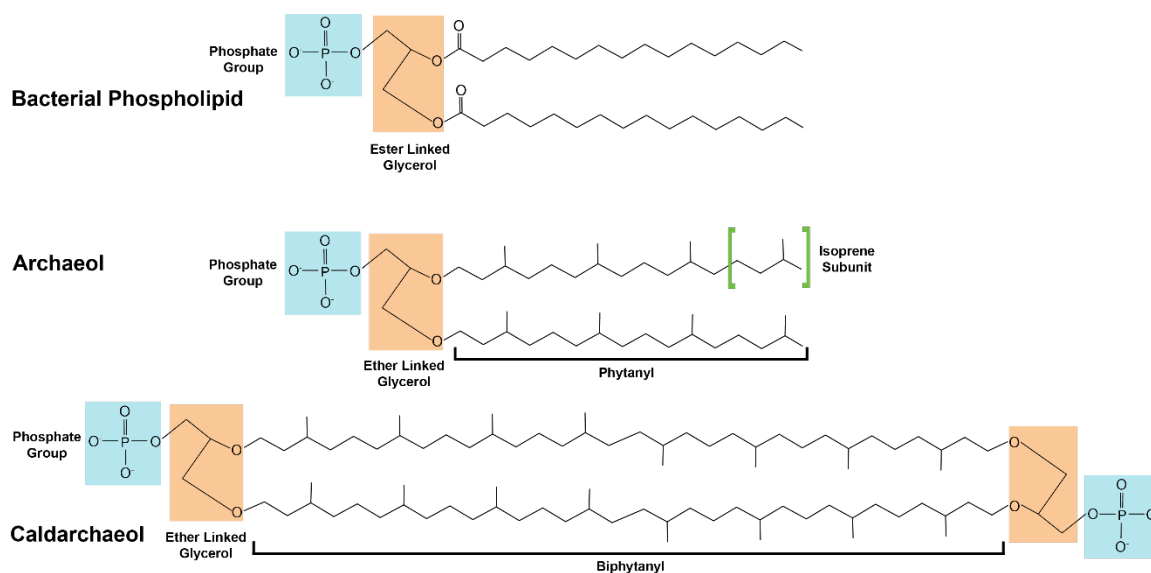
Figure 2: Comparison between lipid structures of bacterial and archaeal lipids.

Glycerol molecules are shaded in orange. Phosphate groups are shaded in cyan. The isoprenoid subunits which make up the archaeal lipids are highlighted in green brackets. Fully saturated lipids are shown; organisms may produce versions of unsaturated alkane lipids with multiple double bonds.

Table 3. Benefits and Challenges of methanogen biotechnology

Benefits	Challenges
Methanogens are some of the fastest-replicating organisms, particularly members of *Methanococcus* [94-96] and *Methanopyrus [97]* genus.	Strain differences in growth rate and carrying capacity. Growth is flux-controlled depending on substrate feed rates. Gas-phase fermentation presents similar problems as oxygenation in traditional fermentations [5, 78, 84]

Methanogens can grow on inexpensive substrates including negative value substrates such as wastewater[1, 17, 18, 23, 85, 98-100]. Methanogens already scaled up worldwide for water treatment and biogas production	Process disfavors growth of aerobic pathogens. Co-product can be water ready for discharge to aquifers and waterways.
Can be coupled directly or indirectly to electrodes for carbon capture by electrosynthesis or for electricity generation from biomass [101].	Surface-to-area, substrate solubility, and other challenges commensurate with microbial fuel cell technologies.
Oxygenation not required. Can grow on non-gas substrates. No contamination by aerobic organisms.	Methanogens require specialized culture environments to maintain anaerobicity [17, 102, 103].
Mesophilic and thermophilic strains available to tailor to the desired product and process needs	Methanogen chassis organisms may need different optimization strategies
Novel metabolic pathways being constantly discovered [17, 20, 23, 30, 86, 98, 99, 104]. Synthetic biology pathways often use methanogen genes to improve yields and reduce feedback inhibition. Bacterial synth bio and genetic strategies work in methanogens.	Methanogen biochemistry less characterized than other model organisms.

Methanogens have a high substrate to volume ratio with low accumulation of biomass relative to products [1, 17, 105].	High titers of intracellular products may be difficult to obtain unless accumulated into vacuoles or secreted extracellularly
Multiple validated genetic tools available including tools for *Methanosarcina* SPP. [106-108], *Methanococcus maripaludis [109, 110],* Methanopyrus kandleri [111], and Methanothermobacter thermautotrophicus [112]	Variability in genome copy number can present challenges when performing chromosomal modifications [32, 113].
The lack of cell wall and envelope ensures that products generated through methanogen fermentations are not contaminated with peptidoglycan or endotoxin.	

References:

1.   Ferry, J.G., *Methanogenesis: ecology, physiology, biochemistry & genetics*. 2012: Springer Science & Business Media.

2.   Johnson, K.A. and D.E. Johnson, *Methane emissions from cattle.* Journal of animal science, 1995. **73**(8): p. 2483-2492.

3.   Schütz, H., W. Seiler, and R. Conrad, *Processes involved in formation and emission of methane in rice paddies.* Biogeochemistry, 1989. **7**(1): p. 33-53.

4.   Huang, Z., et al., *Low carbon renewable natural gas production from coalbeds and implications for carbon capture and storage.* Nature communications, 2017. **8**(1): p. 1-11.

5.   Luo, G. and I. Angelidaki, *Integrated biogas upgrading and hydrogen utilization in an anaerobic reactor containing enriched hydrogenotrophic methanogenic culture.* Biotechnology and bioengineering, 2012. **109**(11): p. 2729-2736.

6.   Sheehan, S.W., *Electrochemical methane production from CO2 for orbital and interplanetary refueling.* Iscience, 2021: p. 102230.

7.   Neill, T., et al., *Practical uses of liquid methane in rocket engine applications.* Acta Astronautica, 2009. **65**(5-6): p. 696-705.

8.   Martin, W.F. and F.L. Sousa, *Early microbial evolution: the age of anaerobes.* Cold Spring Harbor perspectives in biology, 2016. **8**(2): p. a018127.

9.   Holmes, D.E., et al., *Methane production from protozoan endosymbionts following stimulation of microbial metabolism within subsurface sediments.* Frontiers in microbiology, 2014. **5**: p. 366.

10.   Stumm, C. and K. Zwart, *Symbiosis of protozoa with hydrogen-utilizing methanogens.* Microbiological Sciences, 1986. **3**(4): p. 100-105.

11.   Brune, A., *Termite guts: the world's smallest bioreactors.* Trends in Biotechnology, 1998. **16**(1): p. 16-21.

12.   Brune, A., *Methanogens in the digestive tract of termites*, in *(Endo) symbiotic methanogenic archaea*. 2018, Springer. p. 81-101.

13.   Whitford, M.F., R.M. Teather, and R.J. Forster, *Phylogenetic analysis of methanogens from the bovine rumen.* BMC microbiology, 2001. **1**(1): p. 1-5.

14.   Fricke, W.F., et al., *The genome sequence of Methanosphaera stadtmanae reveals why this human intestinal archaeon is restricted to methanol and H2 for methane formation and ATP synthesis.* Journal of bacteriology, 2006. **188**(2): p. 642-658.

15.   Rajilić-Stojanović, M., H. Smidt, and W.M. De Vos, *Diversity of the human gastrointestinal tract microbiota revisited.* Environmental microbiology, 2007. **9**(9): p. 2125-2136.

16.   Gonnerman, M.C., et al., *Genomically and biochemically accurate metabolic reconstruction of Methanosarcina barkeri Fusaro, iMG746.* Biotechnology journal, 2013. **8**(9): p. 1070-1079.

17.   Buan, N.R., *Methanogens: pushing the boundaries of biology.* Emerging Topics in Life Sciences, 2018. **2**(4): p. 629-646.

18.   Daniels, L., et al., *Carbon monoxide oxidation by methanogenic bacteria.* Journal of Bacteriology, 1977. **132**(1): p. 118-126.

19.   Rother, M. and W.W. Metcalf, *Anaerobic growth of Methanosarcina acetivorans C2A on carbon monoxide: an unusual way of life for a methanogenic archaeon.* Proceedings of the National Academy of Sciences, 2004. **101**(48): p. 16929-16934.

20.   Mayumi, D., et al., *Methane production from coal by a single methanogen.* Science, 2016. **354**(6309): p. 222-225.

21.   Thauer, R.K., *The Wolfe cycle comes full circle.* Proceedings of the National Academy of Sciences, 2012. **109**(38): p. 15084-15085.

22.   Ermler, U., et al., *Crystal structure of methyl-coenzyme M reductase: the key enzyme of biological methane formation.* Science, 1997. **278**(5342): p. 1457-1462.

23.   Costa, K.C. and J.A. Leigh, *Metabolic versatility in methanogens.* Current opinion in biotechnology, 2014. **29**: p. 70-75.

24.   Diender, M., A.J. Stams, and D.Z. Sousa, *Pathways and bioenergetics of anaerobic carbon monoxide fermentation.* Frontiers in microbiology, 2015. **6**: p. 1275.

25.   Jones, D., et al., *Crude-oil biodegradation via methanogenesis in subsurface petroleum reservoirs.* Nature, 2008. **451**(7175): p. 176-180.

26.   Zengler, K., et al., *Methane formation from long-chain alkanes by anaerobic microorganisms.* Nature, 1999. **401**(6750): p. 266-269.

27.   Dolfing, J., S.R. Larter, and I.M. Head, *Thermodynamic constraints on methanogenic crude oil biodegradation.* The ISME journal, 2008. **2**(4): p. 442-452.

28.   Laso-Pérez, R., et al., *Anaerobic degradation of non-methane alkanes by "Candidatus Methanoliparia" in hydrocarbon seeps of the Gulf of Mexico.* MBio, 2019. **10**(4): p. e01814-19.

29.   Borrel, G., et al., *Wide diversity of methane and short-chain alkane metabolisms in uncultured archaea.* Nature microbiology, 2019. **4**(4): p. 603-613.

30.   Zhou, Z., et al., *Non-syntrophic methanogenic hydrocarbon degradation by an archaeal species.* Nature, 2022. **601**(7892): p. 257-262.

31.   Catlett, J.L., A.M. Ortiz, and N.R. Buan, *Rerouting cellular electron flux to increase the rate of biological methane production.* Applied and environmental microbiology, 2015. **81**(19): p. 6528-6537.

32.   Aldridge, J., et al., *Anaerobic Production of Isoprene by Engineered Methanosarcina Species Archaea.* Applied and environmental microbiology, 2021. **87**(6): p. e02417-20.

33.   Conrad, R., *The global methane cycle: recent advances in understanding the microbial processes involved.* Environmental microbiology reports, 2009. **1**(5): p. 285-292.

34.   Knittel, K. and A. Boetius, *Anaerobic oxidation of methane: progress with an unknown process.* Annual review of microbiology, 2009. **63**: p. 311-334.

35.   Thauer, R.K., *Anaerobic oxidation of methane with sulfate: on the reversibility of the reactions that are catalyzed by enzymes also involved in methanogenesis from CO2.* Current opinion in microbiology, 2011. **14**(3): p. 292-299.

36.	Alperin, M.J. and T.M. Hoehler, *Anaerobic methane oxidation by archaea/sulfate-reducing bacteria aggregates: 1. Thermodynamic and physical constraints.* American Journal of Science, 2009. **309**(10): p. 869-957.

37.	Summers, Z.M., et al., *Direct exchange of electrons within aggregates of an evolved syntrophic coculture of anaerobic bacteria.* Science, 2010. **330**(6009): p. 1413-1415.

38.	McGlynn, S.E., et al., *Single cell activity reveals direct electron transfer in methanotrophic consortia.* Nature, 2015. **526**(7574): p. 531-535.

39.	Riedinger, N., et al., *An inorganic geochemical argument for coupled anaerobic oxidation of methane and iron reduction in marine sediments.* Geobiology, 2014. **12**(2): p. 172-181.

40.	Su, G., et al., *Manganese/iron-supported sulfate-dependent anaerobic oxidation of methane by archaea in lake sediments.* Limnology and Oceanography, 2020. **65**(4): p. 863-875.

41.	Scheller, S., et al., *The key nickel enzyme of methanogenesis catalyses the anaerobic oxidation of methane.* Nature, 2010. **465**(7298): p. 606-608.

42.	Moran, J.J., et al., *Trace methane oxidation studied in several Euryarchaeota under diverse conditions.* Archaea, 2005. **1**(5): p. 303-309.

43.	Shima, S., et al., *Structure of a methyl-coenzyme M reductase from Black Sea mats that oxidize methane anaerobically.* Nature, 2012. **481**(7379): p. 98-101.

44.	Meyerdierks, A., et al., *Metagenome and mRNA expression analyses of anaerobic methanotrophic archaea of the ANME-1 group.* Environmental microbiology, 2010. **12**(2): p. 422-439.

45.   Soo, V.W., et al., *Reversing methanogenesis to capture methane for liquid biofuel precursors.* Microbial cell factories, 2016. **15**(1): p. 1-14.

46.   McAnulty, M.J., et al., *Electricity from methane by reversing methanogenesis.* Nature communications, 2017. **8**(1): p. 1-8.

47.   Koga, Y. and H. Morii, *Biosynthesis of ether-type polar lipids in archaea and evolutionary considerations.* Microbiology and Molecular Biology Reviews, 2007. **71**(1): p. 97-120.

48.   Koga, Y., *Thermal adaptation of the archaeal and bacterial lipid membranes.* Archaea, 2012. **2012**.

49.   Villanueva, L., et al., *Bridging the membrane lipid divide: bacteria of the FCB group superphylum have the potential to synthesize archaeal ether lipids.* The ISME journal, 2021. **15**(1): p. 168-182.

50.   Siliakus, M.F., J. van der Oost, and S.W. Kengen, *Adaptations of archaeal and bacterial membranes to variations in temperature, pH and pressure.* Extremophiles, 2017. **21**(4): p. 651-670.

51.   Boyd, E., et al., *The role of tetraether lipid composition in the adaptation of thermophilic archaea to acidity.* Frontiers in microbiology, 2013. **4**: p. 62.

52.   Jacquemet, A., et al., *Archaeal tetraether bipolar lipids: structures, functions and applications.* Biochimie, 2009. **91**(6): p. 711-717.

53.   Leriche, G., et al., *Characterization of drug encapsulation and retention in archaea-inspired tetraether liposomes.* Organic & biomolecular chemistry, 2017. **15**(10): p. 2157-2162.

54.   Patel, G.B. and W. Chen, *Archaeal lipid mucosal vaccine adjuvant and delivery system.* Expert review of vaccines, 2010. **9**(4): p. 431-440.

55.   Haq, K., Y. Jia, and L. Krishnan, *Archaeal lipid vaccine adjuvants for induction of cell-mediated immunity.* Expert review of vaccines, 2016. **15**(12): p. 1557-1566.

56.   Conlan, J.W., et al., *Immunization of mice with lipopeptide antigens encapsulated in novel liposomes prepared from the polar lipids of various Archaeobacteria elicits rapid and prolonged specific protective immunity against infection with the facultative intracellular pathogen, Listeria monocytogenes.* Vaccine, 2001. **19**(25-26): p. 3509-3517.

57.   Landi, A., et al., *Superior immunogenicity of HCV envelope glycoproteins when adjuvanted with cyclic-di-AMP, a STING activator or archaeosomes.* Vaccine, 2017. **35**(50): p. 6949-6956.

58.   Markets, M.a., *Flavors & Fragrances Market by Ingredients (Natural, Synthetic), End use (Beverage, Savory & Snacks, Bakery, Dairy Products, Confectionery, Consumer Products, Fine Fragrances), and Region (Asia Pacific, North America, Europe) - Global Forecast to 2026.* 2021.

59.   Ajikumar, P.K., et al., *Terpenoids: Opportunities for biosynthesis of natural product drugs using engineered microorganisms.* Molecular Pharmaceutics, 2008. **5**(2): p. 167-190.

60.   Friedman, M., P.R. Henika, and R.E. Mandrell, *Bactericidal activities of plant essential oils and some of their isolated constituents against Campylobacter*

jejuni, Escherichia coli, Listeria monocytogenes, and Salmonella enterica. Journal of Food Protection, 2002. **65**(10): p. 1545-1560.

61.   Gould, M.N., *Cancer chemoprevention and therapy by monoterpenes.* Environmental Health Perspectives, 1997. **105**: p. 977-979.

62.   Paduch, R., et al., *Terpenes: substances useful in human healthcare.* Archivum Immunologiae Et Therapiae Experimentalis, 2007. **55**(5): p. 315-327.

63.   Sgadari, C., et al., *Mechanism of paclitaxel activity in Kaposi's sarcoma.* Journal of Immunology, 2000. **165**(1): p. 509-517.

64.   Long, B.H., et al., *Eleutherobin, a novel cytotoxic agent that induces tubulin polymerization, is similar to paclitaxel (Taxol (R)).* Cancer Research, 1998. **58**(6): p. 1111-1115.

65.   Newman, D.J. and G.M. Cragg, *Marine natural products and related compounds in clinical and advanced preclinical trials.* Journal of Natural Products, 2004. **67**(8): p. 1216-1238.

66.   Sills, A.K., et al., *Squalamine inhibits angiogenesis and solid tumor growth in vivo and perturbs embryonic vasculature.* Cancer Research, 1998. **58**(13): p. 2784-2792.

67.   Lange, B.M., et al., *Isoprenoid biosynthesis: the evolution of two ancient and distinct pathways across genomes.* Proceedings of the National Academy of Sciences, 2000. **97**(24): p. 13172-13177.

68.   Vranova, E., D. Coman, and W. Gruissem, *Structure and dynamics of the isoprenoid pathway network.* Mol Plant, 2012. **5**(2): p. 318-33.

69.   McGarvey, D.J. and R. Croteau, *Terpenoid metabolism.* Plant Cell, 1995. **7**(7): p. 1015-26.

70.   Rodriguez-Concepcion, M. and A. Boronat, *Elucidation of the methylerythritol phosphate pathway for isoprenoid biosynthesis in bacteria and plastids. A metabolic milestone achieved through genomics.* Plant Physiol, 2002. **130**(3): p. 1079-89.

71.   Boucher, Y., M. Kamekura, and W.F. Doolittle, *Origins and evolution of isoprenoid lipid biosynthesis in archaea.* Mol Microbiol, 2004. **52**(2): p. 515-27.

72.   Jain, S., A. Caforio, and A.J. Driessen, *Biosynthesis of archaeal membrane ether lipids.* Front Microbiol, 2014. **5**: p. 641.

73.   Villanueva, L., J.S. Damste, and S. Schouten, *A re-evaluation of the archaeal membrane lipid biosynthetic pathway.* Nat Rev Microbiol, 2014. **12**(6): p. 438-48.

74.   Carr, S., J. Aldridge, and N.R. Buan, *Isoprene Production from Municipal Wastewater Biosolids by Engineered Archaeon Methanosarcina acetivorans.* Applied Sciences, 2021. **11**(8): p. 3342.

75.   Jasso-Chávez, R., et al., *Air-adapted Methanosarcina acetivorans shows high methane production and develops resistance against oxygen stress.* PLoS One, 2015. **10**(2): p. e0117331.

76.   Horne, A.J. and D.J. Lessner, *Assessment of the oxidant tolerance of Methanosarcina acetivorans.* FEMS microbiology letters, 2013. **343**(1): p. 13-19.

77.   Shaw, I. and M. Graham, *Mesna—a short review.* Cancer treatment reviews, 1987. **14**(2): p. 67-86.

78.   Mosier, N.S. and M.R. Ladisch, *Modern biotechnology: connecting innovations in microbiology and biochemistry to engineering fundamentals*. 2011: John Wiley & Sons.

79.   Doran, P.M., *Bioprocess Engineering Principles. Waltham, MA*. 2013, USA: Elsevier Ltda.

80.   Skinner, K.A. and T.D. Leathers, *Bacterial contaminants of fuel ethanol production.* Journal of Industrial Microbiology and Biotechnology, 2004. **31**(9): p. 401-408.

81.   Beckner, M., M.L. Ivey, and T.G. Phister, *Microbial contamination of fuel ethanol fermentations.* Letters in applied microbiology, 2011. **53**(4): p. 387-394.

82.   Patil, U.K. and K. Muskan, *Essentials of biotechnology*. 2009: IK International Pvt Ltd.

83.   Park, M.-O., H. Ikenaga, and K. Watanabe, *Phage diversity in a methanogenic digester.* Microbial ecology, 2007. **53**(1): p. 98-103.

84.   Chen, G.-Q., *New challenges and opportunities for industrial biotechnology.* Microbial Cell Factories, 2012. **11**(1): p. 1-3.

85.   McGenity, T.J. and D.Y. Sorokin, *Methanogens and methanogenesis in hypersaline environments.* Handbook of hydrocarbon and lipid microbiology, 2010: p. 665-680.

86.   Guan, Y., et al., *Diversity of methanogens and sulfate-reducing bacteria in the interfaces of five deep-sea anoxic brines of the Red Sea.* Research in microbiology, 2015. **166**(9): p. 688-699.

87.   Macario, E.C.d. and A.J. Macario, *Molecular biology of stress genes in methanogens: potential for bioreactor technology.* Biomethanation I, 2003: p. 95-150.

88.   Siegert, M., et al., *Accelerated methanogenesis from aliphatic and aromatic hydrocarbons under iron-and sulfate-reducing conditions.* FEMS microbiology letters, 2011. **315**(1): p. 6-16.

89.   Lemaire, O.N. and T. Wagner, *A Structural View of Alkyl-Coenzyme M Reductases, the First Step of Alkane Anaerobic Oxidation Catalyzed by Archaea.* Biochemistry, 2022.

90.   Wang, Y., et al., *Expanding anaerobic alkane metabolism in the domain of Archaea.* Nature microbiology, 2019. **4**(4): p. 595-602.

91.   Kurth, J.M., H.J. Op den Camp, and C.U. Welte, *Several ways one goal—methanogenesis from unconventional substrates.* Applied Microbiology and Biotechnology, 2020. **104**(16): p. 6839-6854.

92.   Paulo, L.M., A.J. Stams, and D.Z. Sousa, *Methanogens, sulphate and heavy metals: a complex system.* Reviews in Environmental Science and Bio/Technology, 2015. **14**(4): p. 537-553.

93.   Wang, C., et al., *Tolerance of aceticlastic methanogenesis enhanced by magnetite under the condition of ammonia stress.* ACS Sustainable Chemistry & Engineering, 2020. **8**(3): p. 1417-1426.

94.   Jones, W.J., M. Paynter, and R. Gupta, *Characterization of Methanococcus maripaludis sp. nov., a new methanogen isolated from salt marsh sediment.* Archives of microbiology, 1983. **135**(2): p. 91-97.

95.   Goyal, N., Z. Zhou, and I.A. Karimi, *Metabolic processes of Methanococcus maripaludis and potential applications.* Microbial cell factories, 2016. **15**(1): p. 1-19.

96.   Long, F., et al., *A flexible system for cultivation of Methanococcus and other formate-utilizing methanogens.* Archaea, 2017. **2017**.

97.   Takai, K., et al., *Cell proliferation at 122 C and isotopically heavy CH4 production by a hyperthermophilic methanogen under high-pressure cultivation.* Proceedings of the National Academy of Sciences, 2008. **105**(31): p. 10949-10954.

98.   Borrel, G., P.S. Adam, and S. Gribaldo, *Methanogenesis and the Wood–Ljungdahl pathway: an ancient, versatile, and fragile association.* Genome biology and evolution, 2016. **8**(6): p. 1706-1711.

99.   Chadwick, G.L., et al., *Comparative genomics reveals electron transfer and syntrophic mechanisms differentiating methanotrophic and methanogenic archaea.* PLoS biology, 2022. **20**(1): p. e3001508.

100.   Schiraldi, C., M. Giuliano, and M. De Rosa, *Perspectives on biotechnological applications of archaea.* Archaea, 2002. **1**(2): p. 75-86.

101.   Ragab, A., et al., *Effects of set cathode potentials on microbial electrosynthesis system performance and biocathode methanogen function at a metatranscriptional level.* Scientific reports, 2020. **10**(1): p. 1-15.

102.   Balch, W., et al., *Methanogens: reevaluation of a unique biological group.* Microbiological reviews, 1979. **43**(2): p. 260.

103. Rouviere, P.E. and R. Wolfe, *Novel biochemistry of methanogenesis.* Journal of Biological Chemistry, 1988. **263**(17): p. 7913-7916.

104. Yan, Z. and J.G. Ferry, *Electron bifurcation and confurcation in methanogenesis and reverse methanogenesis.* Frontiers in microbiology, 2018. **9**: p. 1322.

105. Thauer, R.K., et al., *Methanogenic archaea: ecologically relevant differences in energy conservation.* Nature Reviews Microbiology, 2008. **6**(8): p. 579-591.

106. Buan, N., G. Kulkarni, and W. Metcalf, *Genetic methods for Methanosarcina species*, in *Methods in enzymology*. 2011, Elsevier. p. 23-42.

107. Metcalf, W.W., et al., *A genetic system for Archaea of the genus Methanosarcina: liposome-mediated transformation and construction of shuttle vectors.* Proceedings of the National Academy of Sciences, 1997. **94**(6): p. 2626-2631.

108. Nayak, D.D. and W.W. Metcalf, *Cas9-mediated genome editing in the methanogenic archaeon Methanosarcina acetivorans.* Proceedings of the National Academy of Sciences, 2017. **114**(11): p. 2976-2981.

109. Blank, C.E., P.S. Kessler, and J.A. Leigh, *Genetics in methanogens: transposon insertion mutagenesis of a Methanococcus maripaludis nifH gene.* Journal of bacteriology, 1995. **177**(20): p. 5773-5777.

110. Bao, J. and S. Scheller, *Efficient CRISPR/Cas12a-based genome editing toolbox for metabolic engineering in Methanococcus maripaludis.* bioRxiv, 2021.

111.   Sarmiento, F.B., J.A. Leigh, and W.B. Whitman, *Genetic systems for hydrogenotrophic methanogens*, in *Methods in enzymology*. 2011, Elsevier. p. 43-73.

112.   Fink, C., et al., *A shuttle-vector system allows heterologous gene expression in the thermophilic methanogen Methanothermobacter thermautotrophicus ΔH.* Mbio, 2021. **12**(6): p. e02766-21.

113.   Hildenbrand, C., et al., *Genome copy numbers and gene conversion in methanogenic archaea.* Journal of bacteriology, 2011. **193**(3): p. 734-743.

Chapter 3: Anaerobic Production of Isoprene by Engineered Methanosarcina Species Archaea

This chapter represents the contents of: Jared Aldrige, Sean Carr, Karrie A. Weber, and Nicole R. Buan. "Anaerobic production of isoprene by engineered *Methanosarcina* species archaea." Applied and environmental microbiology 87, no. 6 (2021): e02417-20. DOI:

Author contributions: Conceptualization, N.R.B.; methodology, S.C., J.A., and N.R.B.; formal analysis, S.C., J.A., and N.R.B.; investigation, S.C. and J.A.; resources, N.R.B.; data curation, S.C. and J.A.; writing—original draft preparation, S.C. and N.R.B.; writing—review and editing, S.C. and N.R.B.; visualization, S.C., J.A., and N.R.B.; supervision, N.R.B.; project administration, N.R.B.; funding acquisition, N.R.B.

Abstract

Isoprene is a valuable petrochemical used for a wide variety of consumer goods, such as adhesives and synthetic rubber. We were able to achieve a high yield of renewable isoprene by taking advantage of the naturally high-flux mevalonate lipid synthesis pathway in anaerobic methane-producing archaea (methanogens). Our study illustrates that by genetically manipulating *Methanosarcina* species methanogens, it is possible to create organisms that grow by producing the hemiterpene isoprene. Mass balance measurements show that engineered methanogens direct up to 4% of total carbon flux to isoprene, demonstrating that methanogens produce higher isoprene yields than engineered yeast, bacteria, or cyanobacteria, and from inexpensive feedstocks.

Expression of isoprene synthase resulted in increased biomass and changes in gene expression that indicate that isoprene synthesis depletes membrane precursors and redirects electron flux, enabling isoprene to be a major metabolic product. Our results demonstrate that methanogens are a promising engineering chassis for renewable isoprene synthesis.

Introduction

Isoprene (2-methyl-1,3-butadiene, C_5H_8) is a valuable chemical used to synthesize synthetic rubber, styrene-isoprene-styrene (SIS block) copolymer adhesives, flavorings, cosmetics, and pharmaceuticals. Approximately 800,000 tons of isoprene is refined from petroleum annually, in which over 95% of it is used to produce *cis*-1,4-polyisoprene (synthetic rubber) (1). The global market for isoprene, including natural and synthetic polyisoprene rubber, is estimated at 1.3 metric tons per year, at a value approaching $4.3 billion (2). Cost-effective, high-yield synthesis of renewable isoprene from biomass feedstocks has the potential to supplant the need for petroleum-derived isoprene and would contribute to reducing use of fossil fuels. monomer or isoprenoid lipids can be naturally synthesized by various species of plants and microbes (3–5). It is estimated some plant species channel up to 10% of total fixed carbon into isoprene, which transpires through photosynthetic tissues (6).

To obtain industrial quantities of renewable isoprene, synthetic biologists have introduced the isoprene synthase *ispS* gene from plants into microbial host organisms such as *Escherichia coli* (3, 7), *Saccharomyces* yeast (8, 9), and *Synechocystis* cyanobacteria (10). Synthesis of isoprene by engineered microbes or algae is

advantageous over natural plant isoprene synthesis because microbes can be grown in enclosed bioreactors that facilitate isoprene recovery from the gas phase. Because the isoprene monomer has a low vapor point (35°C) and evaporates rapidly at room temperature, it can be easily captured from the gas phase of a microbial culture. While efforts to engineer isoprene monomer synthesis using microbes have been successful at small scales, there are remaining issues with cost of production and yield optimization (11). Three factors limit industrial-scale renewable isoprene technologies: scale-up development costs, production costs, and metabolic flux of the chassis organism. We hypothesized that using methane-producing archaea as a chassis could simultaneously solve all three of these limiting factors.

Methane-producing archaea (methanogens) are strict anaerobes that use gaseous or liquid C_1 substrates or acetate to grow, converting 60 to 99% of C to pure methane gas (12). Technologies for growing methanogens at industrial scale are already well established (13). Methanogens are currently used in large-scale anaerobic digesters worldwide, where waste biomass is used to produce methane-containing biogas that is recovered, upgraded, and compressed to be used to generate electricity and transportation fuel. Production costs for methanogen-based technologies are also very low. When cultivated in anaerobic digesters at large scale, methanogens do not require light or aeration, and substrates for methanogenesis (CO, CO_2, methanol, acetate, etc.) are inexpensive and abundant. *Methanosarcina* species have been coaxed to grow on other substrates (14), to synthesize bioproducts such as lactate in the reverse methanotrophic direction (15), and to increase tolerance to oxygen exposure (16, 17). Hydrogenotrophic *Methanococcus* strains have also been engineered to produce geraniol, a monoterpene

derived from the mevalonate pathway for use as a fragrance (Table 1). Combined with an expanding list of available genetic tools, methanogens are emerging as viable chassis for bio-product synthesis from inexpensive feedstocks. Due to the low feedstock cost, high yield, and existing anaerobic digestion infrastructure, methanogens have the potential to be an efficient and adaptable platform for renewable isoprene synthesis.

The substrate for the isoprene synthase enzyme, IspS, is dimethylallyl pyrophosphate (DMAPP), an isomer of isopentenyl diphosphate (IPP) (3). IPP/DMAPP is synthesized by one of two known biochemical pathways, the 2-C-methyl-D-erythritol 4-phosphate/1-deoxy-D-xylulose 5-phosphate (MEP/DOXP) pathway or the mevalonate pathway (Fig. 1). The two pathways differ in starting substrates (the branch point from central metabolism), enzyme steps, substrate intermediates, and energetic requirements, particularly due to a variation in the conversion of mevalonate to IPP. The MEP/ DOXP pathway is primarily used by bacteria, while the mevalonate pathway is used by eukaryotes and archaea. The MEP/DOXP pathway uses 8 enzymes, 2 NADPH, 2 CTP, ATP, and reduced ferredoxin (2 e–) to produce DMAPP from pyruvate. The mevalonate pathway used by eukaryotes and archaea requires 2 or 3 ATP and 2 NADPH (18–21). Using the MEP/DOXP pathway results in a substrate pool IPP:DMAPP ratio of 5:1, and thus isoprene synthesis using this pathway also necessitates increased activity of isopentenyl diphosphate isomerase *idi* (22). The mevalonate pathway uses seven or eight enzymes to synthesize DMAPP from acetyl-CoA and results in a more favorable IPP: DMAPP ratio of 3:7. It has been found in previous attempts to produce isoprenoids at an industrial scale that the mevalonate pathway produces superior yields (23). The yeast *Saccharomyces cerevisiae* has been engineered to synthesize isoprene; unfortunately,

isoprene yields were low because eukaryote enzymes are feedback-inhibited (24, 25).

Thus, efforts to increase flux through the mevalonate pathway to increase isoprene yields

by manipulating intracellular substrate pools are unsuccessful unless archaeal enzymes,

which are resistant to feedback inhibition, are used (26–28). Methanogens, in contrast,

already grow on inexpensive feedstocks (CO_2, CO, C_1 compounds, acetate) that are 3 to

20x less expensive than glucose, do not require illumination or aeration, and naturally

direct 5% of biomass to isoprenoid lipid synthesis (Table S1 in the supplemental material)

(29). We surmised that so long as they are still able to synthesize isoprenoid lipid

membranes for growth, methanogens may be able to produce renewable isoprene in high

yields due to their inherently high metabolic flux through the archaeal mevalonate

pathway (Fig. 1). The purpose of our study was to test whether *Methanosarcina* can be

used to synthesize isoprene from C_1 substrates and acetate.

Methods

Anaerobic techniques

Anaerobic procedures were performed in a custom B-type Coy anaerobic chamber

(Coy Labs, Grass Lake, MI). Internal environment of the chamber is maintained at 5%

H_2/20% CO_2/75% N_2 (6 3%) (Matheson Gas, Lincoln, NE). Cells incubated outside the

anaerobic chamber are contained in glass Balch tubes secured with butyl rubber stoppers

(Belco Glass, Vineland, NJ) and aluminum crimps (Wheaton, Millville, NJ).

Methanogen cell culture

Cells listed in Table 4 were grown in anaerobic high-salt (HS) medium (200 mM

NaCl, 45 mM $NaHCO_3$, 13 mM KCl, 54 mM $MgCl_2 \cdot 6H_2O$, 2 mM $CaCl_2 \cdot 2H_2O$, 2 mM

0.1% resazurin [w v21], 5 mM KH_2PO_4, 19 mM NH_4Cl, 2.8 mM cysteine·HCl, 0.1 mM

$Na_2S·9H_2O$, trace elements, vitamin solution) (47) supplemented with a carbon and

energy source (methanol, 125 mM; trimethylamine, 50 mM; sodium acetate, 120 mM)

and 2 mg liter^{-1} puromycin as needed (48, 49). 3-(N-morpholino)propanesulfonic acid

(MOPS) high-salt medium (MHS) was created by substituting 45 mM $NaHCO_3$ with 50

mM MOPs buffer (50). Cells in liquid medium were incubated at 35°C without shaking.

For growth on solid medium, 1.4% agar was added to HS medium. All chemicals and

reagents were sourced from Millipore Sigma (St. Louis, MO) or Thermo Fisher Scientific

(Waltham, MA).

Cloning and genetic techniques

Methods for genetic manipulation of *M. acetivorans* have been described

previously (51). All plasmids and primers shown in Table 4 were designed using

VectorNTI software (Thermo Fisher Scientific, Waltham MA). PCR primers were

synthesized by Integrated DNA Technologies (IDT, Coralville, IA). All plasmids were

verified by sequencing (Eurofins, Louisville, KY). Plasmid pNB730 was used as a parent

vector (31). Key features of pNB730 include: (i) pUC *ori* for highcopy replication in *E.

coli*; (ii) φC31 phage recombinase *att* site for chromosomal insertion of the vector into the

host genome; (iii) resistance to ampicillin for selection during amplification in

Escherichia coli; and (iv) puromycin resistance for selection in *Methanosarcina* spp. The

cDNA sequence of *ispS* was obtained from NCBI (locus BAD98243, gi: 63108310) from

the isoprene-producing poplar plant, *Populus alba* (30). The *P. alba ispS* gene was codon-

optimized for translation in archaea and inverted repeats were removed to create sNB19,

which was commercially synthesized by Life Technologies Corporation (Grand Island,

NY). PCR amplification of synthetic genes designed with predicted chloroplast localization signal intact or truncated (*ispS* and *ispS*$^{\Delta 1\text{-}13}$) was achieved using the primers listed in Table 4 with Phusion Flash PCR Master Mix as a proofreading DNA polymerase (Thermo Fisher Scientific, Waltham, MA). DNA purification was accomplished using Promega Wizard SV Gel and PCR clean-up kits (Madison, WI). Fast Digest restriction enzymes (BamHI and Ndel) were purchased from Thermo Fisher Scientific (Waltham, MA). DNA fragments were assembled using the sequence and ligation-independent cloning (SLIC) protocol previously described (52). The synthesized *ispS* genes were expressed from the constitutive methyl-CoM reductase promoter (Pmcr) at the pNB730 multiple cloning site. Electroporated *E. coli* cells were plated on lysis broth (LB) agarose plates with 100 mg liter^{-1} ampicillin and colonies were selected after overnight growth at 37°C (53). Plasmids were screened by PCR as described and sequenced (31). Plasmids were transfected into *Methanosarcina* spp. cells according to established procedures using Roche DOTAP liposomal transfection reagent (Roche Diagnostics Corporation, Indianapolis, IN) (48, 51). Cells transfected with pNB730 lacking *ispS* were used as a vector-only control.

Quantitative PCR (qPCR) was used to quantify integrated gene copies of *ispS* in the population relative to the unique *rpoA1* gene found on each chromosome. Cells were grown in HS + MeOH medium until late exponential (optical density at 600 nm [OD$_{600}$] = 0.8) and harvested by vacuum filtration followed by lysis using TRI reagent (Sigma-Aldrich, St. Louis, MO) according to the manufacturer's instructions. cDNA was synthesized with random hexamers (Promega, Madison, WI) using GoTaq 2-step RT-qPCR system (Promega, Madison, WI) and the *ispS* transcript was confirmed by qPCR

using primers oNB735 and oNB736, listed in Table 4.

Cellular growth measurements

Cell growth rate was determined by measuring culture optical density at 600 nm using a Spectronic D spectrophotometer (Thermo Fisher Scientific, Waltham, MA). Biomass measurements for each strain were obtained as previously described (37).

Pyrophosphate assay

M. acetivorans cell extracts were assayed for isopentenyl pyrophosphate pyrophosphatase activity using EnzChek pyrophosphate assay kit (Molecular Probes, Eugene, OR). Briefly, cells were harvested at late exponential phase of growth from a 100 ml culture by centrifugation in a Thermo Fisher Scientific Sorvall Legend XTR centrifuge using a TX-750 swinging bucket rotor with 50 ml conical tube adapters at 4,000 x g for 5 min at room temperature. Cell pellets were washed twice using 1 ml of 0.4 M NaCl to remove spent culture medium. After resuspension, cells were lysed using 9 ml ddH$_2$O and centrifuged at 10,000 x g in a Thermo Fisher Scientific Sorvall Legend Micro21 rotor to pellet cell debris. The resulting supernatant was transferred to a fresh microcentrifuge tube and kept on ice. Cell lysate was used to test for enzymatic activity of IspS by following the protocol described by the manufacturer using dimethylallyl diphosphate purchased from Sigma-Aldrich (St. Louis, MO) as the substrate for the reaction. The reaction was monitored spectrophotometrically at 360 nm on a Jenway 7305 spectrophotometer (Burlington, NJ).

Methane production assay

Methane in culture headspace was measured by gas chromatography using a flame ionization detector (GC-FID) as previously described (54). Briefly, 10-ml cultures were

grown to stationary phase. After growth, 100 μl of headspace was captured using a gastight Hamilton syringe and transferred to an empty crimped 2 ml autosampler serum vial (Wheaton, Millville, NJ). Vial contents were analyzed by flame ionization using a custom Agilent 7890A gas chromatography (GC) system. The GC is equipped with an autosampler for consistent sample injection and utilized a GS CarbonPLOT column (Agilent Technologies) at 145°C for separation of volatile metabolites. Quantification of methane was achieved by comparison to a methane standard curve (Matheson, Lincoln, NE) run in parallel with experimental samples.

Isoprene production assay

The same GC-FID system as above was deployed to quantify isoprene (55). *M. acetivorans* strains were grown in 10 ml cultures with a 1 ml paraffin oil overlay. Once grown to stationary phase, the oil was harvested and transferred to a 2 ml stoppered and crimped autosampler vial. The GC-FID method for isoprene quantification was as follows: 160°C for 35 min, ramp to 200°C at 75°C/min for 20 min, ramp to 275°C at 75°C/min for 20 min, 275°C for 5 min, and ramp to 160°C at 75°C/min to equilibrate the system for the next run. Isoprene quantification was achieved using a standard of known volumes of isoprene injected into 1 ml of paraffin oil in a 2 ml autosampler vial.

Mass balance measurements

M. acetivorans was grown to early stationary phase in 100 ml cultures. Cultures were centrifuged and concentrated to 10 ml in MHS medium. Cells were washed twice with MHS and resuspended in 10 ml MHS. Then, 0.250 ml of resuspended cells was transferred to sterile, anaerobic autosampler vials, after which 0.250 ml of 2x MeOH MHS was added to the autosampler vials, which were then stoppered and crimped. The

headspaces of the autosampler vials were flushed with N_2 to remove residual CO_2.

Prepared samples were incubated for 36 h at 35°C. After incubation, remaining methanol

in spent medium was analyzed by GC-FID and the methanol peak area was compared to

standard curves generated by serial dilutions of HS MeOH medium. CO_2 and CH_4 in the

headspace were quantified using a thermal conductivity detector (GC-TCD). Peak areas

of headspace gases were compared to standard curves generated for each gas using

methane and CO_2 reference standards (Airgas, Randor, PA, and Matheson Gas, Lincoln,

NE).

qRT-PCR methods

Cultures of *att:ispS*[+] and control strains were grown anaerobically in triplicate in

HS 1 MeOH until exponential phase (OD_{600} of 0.56 to 0.74). Cells were anaerobically

concentrated in a clinical centrifuge (5,000 x g) and RNA isolation was performed using

TRI reagent (Invitrogen) as per the manufacturer's protocol. DNase treatment was

performed using TURBO DNase (Invitrogen) and DNA digestion was confirmed by lack

of PCR amplification after 35 cycles using primers oNB733 and oNB734. The cDNA was

synthesized using GoTaq 2-step RT-qPCR system (Promega, Madison, WI) with random

hexamers and cDNA integrity was verified via agarose gel. qPCR was performed using

the primers in Table 4 and GoTaq qPCR Master Mix with SYBR Green I (Promega,

Madison, WI) on a Mastercycler RealPlex (2) thermocycler (Eppendorf). Data were

obtained from three biological replicates and five technical replicates each (n = 15).

Threshold cycle (C_T) values from qPCR were normalized to the expression of *rpoA1*, the

DNA-dependent RNA polymerase found in a single copy in *M. acetivorans* (38) and

transcript abundance of each gene was compared using the $2^{(-\Delta\Delta C_T)}$ method as

described (56, 57).

Data availability

Plasmids, strains, and growth and assay data that support the findings of this study are available from the corresponding author (N.R.B.) upon reasonable request. The sequence for sNB19 was submitted to GenBank (MW295460) but not released prior to publication; it is expected to be released shortly. This sequence may also be found in the supplemental material.

Results

Creation and characterization of *Methanosarcina acetivorans ispS*$^+$ strains

In plants, the isoprene monomer is synthesized by cleavage of the C-O bond of dimethylallyl pyrophosphate (DMAPP) to produce isoprene monomer and pyrophosphate by the enzyme isoprene synthase (IspS) (3). To generate isoprene-synthesizing methanogens, we cloned the codon-optimized *ispS* gene from poplar (Populus alba) into the *Methanosarcina* spp. overexpression suicide vector pNB730 (Figure 2a) (30, 31). Once transfected into cells, the resulting plasmid pJA2 integrates into the chromosome, resulting in constitutive overexpression of synthetic *ispS* from the methyl coenzyme M reductase (*mcr*) promoter, P_{mcrB} (Figure 2a) (32). Integration of pJA2 was confirmed by PCR, and transcription of *ispS* mRNA was validated by reverse transcriptase-PCR (RT- PCR) of an 88-bp fragment of the *ispS* cDNA transcript (Figure 2b). A vector-only control (*att:pNB730*) strain was also created by integrating pNB730 onto the *M. acetivorans* chromosome. These results indicate successful integration of pJA2 onto the chromosome and transcription of *ispS* in *M. acetivorans*.

Gene integration and transcription alone is not necessarily sufficient to ensure an enzyme will be translated, folded, and maintain stable biochemical activity in a new host cell. *P. alba* IspS is most enzymatically active at 40°C and has a high K_m for DMAPP (30). To determine if the newly designed, synthetic *ispS* was translated and maintained enzyme activity in methanogen cells grown at 35°C, the cell extract was assayed for DMAPP pyrophosphatase activity (Figure 2c). Cells expressing *ispS* had a 2-fold higher release of PPi from DMAPP activity versus vector-only control (*att:pNB730*) cells, suggesting IspS is enzymatically active in methanogen cells. Isoprene synthesis by methanol-grown cells was confirmed by gas chromatography using flame ionization and mass spectrometry (Figure 2d and e). These data suggest the synthetic *ispS* gene was transcribed, translated, and folded into an active enzyme that could access the intracellular DMAPP pool in growing *M. acetivorans* cells at 35°C to yield the end product isoprene.

M. acetivorans att:ispS⁺ strains were cultured and physiologically characterized to determine if *ispS* expression had an effect on growth of the organism (Table S2). Because methanogens synthesize cell membrane lipids entirely from DMAPP (Figure 1d) (4, 29, 33), it was initially expected that high constitutive expression of *ispS* from P_{mcrB} could decrease viability or may even be lethal. However, when grown on methanol, there was no detectable difference in methane produced (Figure 2e) or in population doubling time (Figure 2g), thus demonstrating that *ispS* expression does not result in decreased cell viability.

Some possible explanations for tolerance of high *ispS* expression by *M. acetivorans* include substrate channeling (such that DMAPP is preferentially funneled

to membrane synthesis and only excess intracellular DMAPP pools are available to

IspS), the high K_m of IspS (34), or autotitration of gene copies. Previous work has

shown that methanogens vary the number of copies of the entire chromosome

determined by growth phase and type of growth substrate, with chromosomal copies

ranging from 3 to 18 (35). We hypothesized that this variance could possibly modulate

ispS gene copy number and therefore expression levels by homologous recombination at

the site of pJA2 integration. To test this hypothesis, the stability of the *ispS* gene in the

culture population was assessed by serial passaging of *ispS*⁺ strains with and without

puromycin antibiotic selection. If expression of *ispS* caused a decrease in reproductive

fitness, serial passaging in the absence of antibiotic selection should have selected for

fewer copies of the *ispS* gene in the total population, which could be detected using

quantitative PCR (qPCR) of *ispS* versus an unlinked essential housekeeping gene, such

as *rpoA1*. The *rpoA1* gene encodes the sole DNA-dependent RNA polymerase gene on

the chromosome and can be used as a reference gene in a qPCR assay. By comparing

ispS gene copy number to copies of the chromosomal reference gene *rpoA1*, we could

calculate the average number of *ispS* genes per chromosome and per cell. If expression

of *ispS* was neither beneficial nor detrimental under the culturing conditions, we would

have expected no change in the *ispS:rpoA1* ratio. With constant antibiotic pressure, *M.

acetivorans* strains transformed with pJA2 were found to have an average of 0.57 copies

of *ispS* per chromosome after 20 generations (Table 2). The *ispS:rpoA1* ratio was

relatively unchanged at 0.56 after 140 generations. Without antibiotic selection, the

ispS:rpoA1 ratios were 0.59 at 20 generations and 0.53 at 140 generations. We next

tested whether we could drive an increase in *ispS:rpoA1* ratio through homologous

recombination by selecting for increased expression of the linked puromycin resistance cassette; however, these efforts were unsuccessful and the *ispS:rpoA1* ratio remained unchanged. These data suggest pJA2 is stably integrated onto the chromosome. Additional experiments are needed to further explore the effects of gene dosage and gene expression on isoprene production.

Mass balance of isoprene synthesis from methanol

The primary metabolic products of methylotrophic methanogenesis by *M. acetivorans* are methane, CO_2, and biomass. Mass balance experiments were used to measure the molar carbon partitioning between control and *ispS*$^+$ strains to determine if isoprene was derived from the methane, CO_2, or biomass pools (Table S3). Mass balance experiments showed both control and *ispS*$^+$ strains consumed 100% of the substrate methanol and produced nearly equivalent amounts of methane (73.0 ± 2.2 and 72.8 ± 3.8, $P = 0.0191$, respectively, for a 0.2% C flux difference). However, the *ispS*$^+$ strain shows 3.7% less CO_2 flux than the control strain ($P = 0.0001$) but 6.7% more biomass C according to dry weight ($P = 0.0041$). The *ispS*$^+$ strain directed 3.8% of total C to isoprene. The yields of methane were not significantly different for control or *ispS*$^+$ strains on bicarbonate-buffered medium versus MOPS-buffered medium (Table S3). These results show cells benefit with increased biomass synthesis when carbon is siphoned from the oxidative branch of the methylotrophic methanogenesis pathway to produce isoprene (Figure 2h).

Isoprene synthesis affects transcription of Mcr, mevalonate, and TCA enzymes

Isoprene synthesis would be expected to reduce the intracellular pool of DMAPP that normally feeds into membrane synthesis. Therefore, as a result of isoprene

synthesis, we would expect the *ispS⁺* strain to upregulate expression of mevalonate pathway genes that supply DMAPP/IPP to the lipid synthesis pathway (Fig. S1). In addition, if isoprene synthesis is affecting electron flux through the electron transport system, we would expect to observe downregulation of one or more genes in the tricarboxylic acid (TCA) or methanogenesis cycles that are responsible for maintaining redox balance in the cell (Fig. 1). Compared to the control strain, the *M. acetivorans att::ispS⁺* strain was found to have a slight decrease in 3-hydroxy-3-methylglutaryl-CoA (HMG-CoA) synthase transcripts (1.5-fold) compared to the control strain and increased mRNA abundance for genes downstream of HMG-CoA synthase. These changes in mRNA levels suggest the cell is reacting to a depletion of downstream metabolite pools that includes DMAPP (Table 3). We also observed that methyl coenzyme M reductase (*mcrB*), pyruvate carboxylase, and malate dehydrogenase were upregulated, while fumarate hydratase was significantly downregulated. These results suggest the cell is sensing an imbalance between methanogenesis, biomass synthesis, and redox-dependent reactions and supports the hypothesis that electron flux is decreased through the rate-limiting terminal electron acceptor CoM-CoB heterodisulfide and the membrane electron carrier methanophenazine, which is critical for ATP synthesis (36, 37). Together, these results suggest that isoprene synthesis may relieve known kinetic bottlenecks in CoM-CoB and methanophenazine redox balance, thereby contributing to increased biomass. Future experiments using mutant strains could provide further evidence of this process.

Isoprene production utilizing other carbon sources

Isoprene production and *ispS⁺* strain physiology were assessed on additional

carbon sources trimethylamine (TMA) and acetate to determine if isoprene yields changed depending on growth substrate (Fig. 3). When growing on methanol or TMA, *M. acetivorans* uses the methylotrophic methanogenesis pathway, while when growing on acetate uses the acetoclastic pathway. The methylotrophic and acetoclastic methanogenesis pathways differ with respect to intracellular carbon and electron fluxes, which could have an impact on isoprene yields. Cells grown on TMA and acetate had similar DMAPP pyrophosphatase activity and isoprene yields as methanol-grown cells (Fig. 3, Table S2). Endpoint methane production by *ispS+* strains was 10% lower than control strains when grown on TMA, despite the fact that methanol and TMA are both metabolized by the methylotrophic methanogenesis pathway (Table S2). Similar to methanol-grown cells, TMA- and acetate-grown *ispS$^+$* strains had population doubling times that were the same as control strains (Table S2). These data show engineered *M. acetivorans* can produce high quantities of isoprene from a variety of inexpensive carbon sources and production is independent of whether the methylotrophic or acetoclastic methanogenesis pathway is used by the cell.

Isoprene synthesis by engineered *Methanosarcina barkeri*

Methanosarcina acetivorans is a versatile organism capable of growth on the widest range of methanogenic substrates, including C_1 chemicals (carbon monoxide, methanol, methylamines, methylsulfides, etc.) and acetate (38). *Methanosarcina barkeri*, a related methanogen, can grow on C_1 compounds and acetate similar to *M. acetivorans*, except it has maintained the ability to use H_2 as an electron donor via the hydrogenotrophic (reducing carbon dioxide to methane) or methyl respiration (reducing methanol or other C_1 compounds to methane) methanogenesis pathways. To expand the

possible feedstocks for isoprene synthesis and to determine whether the different electron transport system configuration found in *M. barkeri* affects isoprene yields, we transformed *M. barkeri* with the pJA2 plasmid.

After confirmation of successful integration of pJA2 onto the chromosome, biochemical tests were used to confirm isoprene production and its effect on growth of the organism (Table S4). Similar to *M. acetivorans*, the methanol-grown *M. barkeri* $ispS^+$ strain had increased DMAPP pyrophosphatase levels (136% ± 0.4%) compared to the parental strain (100% ± 0.2%), indicating the introduced *ispS* gene was translated into active enzyme in methanogen whole-cell lysate. *M. barkeri* $ispS^+$ strains had identical growth rates as control strains; however, methane yields were 18% less on methanol and 10% less on $H_2 + CO_2$ versus control strains, similar to what was observed with TMA-grown *M. acetivorans* (Figure 4a). Isoprene yield with *M. barkeri* was 3.8% of the isoprene produced by *M. acetivorans* during growth on methanol. Isoprene yield on $H_2 + CO_2$ was 2.4% of the *M. acetivorans* yield on methanol (Figure 4b), and roughly equivalent to the reported yield of geraniol diterpene by *Methanococcus maripaludis* (Table 1, Table S4) (39).

Differences in isoprene yield between these methanogens likely results from expression of hydrogenases in *M. barkeri* and *M. maripaludis*. Hydrogenases are essential in the hydrogenotrophic methanogenesis pathway (40) and are necessary for conserving energy through hydrogen cycling in *M. barkeri* (41). As a result of hydrogenase expression, redox balancing in *M. barkeri* kinetically favors hydrogen synthesis rather than acetyl-CoA and DMAPP synthesis. *M. acetivorans*, which does not use hydrogen cycling for energy conservation, is poised to donate electrons to CoM-

CoB heterodisulfide reductase or to acetyl-CoA synthesis (42). Previous work has shown that further decreasing flux through the CoM-CoB terminal electron acceptor in *M. acetivorans* results in increased biomass synthesis and increased metabolic efficiency (37). The degree of similarity in substrate channeling and redox balance mechanisms between *M. acetivorans* and *M. barkeri* is an ongoing area of research, but it is clear that isoprene optimization will require tailored metabolic engineering approaches depending on whether methanogens are capable of hydrogenotrophic growth. Our results indicate that while *M. acetivorans* produces higher yields than hydrogenotrophic methanogens, both *M. acetivorans* and *M. bakeri* can be engineered to produce isoprene from various inexpensive feedstocks without significantly sacrificing growth kinetics or biomass yields.

Discussion

Our results confirm the hypothesis that archaea, and *Methanosarcina* spp. in particular, can be engineered to synthesize high yields of isoprene. Under batch-growth conditions using methanol as a substrate, *M. acetivorans* was able to produce 6×10^6 times more isoprene than the bacterium *Clostridium ljungdahlii*, and 179 times more isoprene than the autotrophic cyanobacterium Synechocystis. The high carbon fluxes we measured (4% total C) and the observation of increased biomass (Figure 2h) suggest that in *M. acetivorans ispS*$^+$ strains, isoprene is an abundant metabolic product that benefits cells. Furthermore, the engineered strains showed no detectable changes in population doubling rate, maximum culture optical density, and methane production compared to a vector-only control strain. Mass balance data indicated a 16% decrease in

CO_2 production, suggesting that C for isoprene was derived from the oxidative branch of the methylotrophic methanogenesis pathway. The data support the conclusion that *M. acetivorans* and *M. barkeri ispS*$^+$ strains have become "isoprenogens," i.e., methanogens capable of growing by synthesizing mixed products of isoprene and methane. Importantly, the isoprene yields and 4% total C flux we observed were obtained by expression of a single terpene synthase without extensive pathway optimization.

Can we push isoprene yields further? Other investigators using *S. cerevisiae* and *E. coli* chassis were challenged by unstable expression and low activity of terpene synthases, low substrate pathway fluxes, and enzyme feedback inhibition that had to be overcome through biochemical and metabolic engineering. Optimization of these factors and use of inducible promoters has the potential to further increase isoprene yield using *Methanosarcina* spp. The results of genetic selection experiments, shown in Table 2, suggest that 4% flux seems to be an upper limit that still provides enough isoprenoid lipid synthesis for central metabolism and maintaining redox balance at wild-type growth rates. However, by identifying metabolic bottlenecks and addressing these with additional mutations, such as using an engineered IspS enzyme with a lower K_m (43), it is possible that yields may be increased.

Methanogens survive on the very edge of thermodynamic favorability, producing approximately 0.3 ATP per mole of carbon substrate utilized (44). This lean metabolism creates a high flux of carbon with an exceedingly small fraction of overall carbon being utilized for biomass, all of which is coupled to the rate-limiting reactions of methanogenesis. As such, the growth of methanogens can be predicted

predominantly from the energetics of substrate utilization. In a steady-state culture, methylotrophic methanogenesis can be modeled based on the mass balance equation:

$4CH_3OH \rightarrow 1CO_2 + 3CH_4 + 2H_2O$ ($\Delta G° = -84.25$ kJ Cmol^{-1}). Assuming all mevalonate pathway flux is devoted to isoprene synthesis at the expense of CO_2 or membrane lipid synthesis in a nonreplicating culture, up to 75% of C could be directed to isoprene synthesis from methylotrophic substrates according to the mass balance equation:

$40CH_3OH \rightarrow 9CH_4 + 6C_5H_8 + 38H_2O$ ($\Delta G°= -5.2$ kJ Cmol^{-1}). Based on current understanding of metabolism in methanogens, up to 85.7% of substrate carbon could be used to synthesize isoprene using hydrogenotrophic methanogens ($35CO_2 + 104H_2 \rightarrow 5CH_4 + 6C_5H_8 + 70H_2O$, $\Delta G° = -9.9$ kJ Cmol^{-1}) and up to 71.4% at near equilibrium from acetoclastic methanogens ($7CH_3CO_2H \rightarrow 2C_5H_8 + 4CO_2 + 6H_2O$, $\Delta G° = -16.6$ kJ Cmol^{-1}). While growing cells must divert some C flux to lipid synthesis, as long as cells can couple additional isoprene synthesis to generation of a transmembrane ion gradient, they will be able to conserve energy via ATP synthesis. Recent studies have shown that *E. coli* and *S. cerevisiae* strains were able to significantly increase isoprene yields utilizing nonreplicating cells in fed-batch fermentation (Table 1) (45, 46). The data reported here for *Methanosarcina* spp. were obtained from batch-grown cultures to facilitate mass balance measurements and likely represent an underestimate compared to the isoprene yield that could be obtained from larger-scale fed-batch or chemostat bioreactors.

The lack of change in growth rate of isoprene-producing *Methanosarcina* species strains, as well as the decrease in CO_2 production, are consistent with the interpretation that isoprene synthesis does not negatively affect the cell's ability to

conserve energy. In methanogens, the methanogenesis pathway is linked to biosynthesis by the carbon monoxide dehydrogenase/acetyl-CoA synthase (CODH/ACS) complex, which facilitates growth and ATP generation by the regeneration of the cofactor ferredoxin (Fdx) and the synthesis of acetyl-CoA (36). We speculate that by providing the ability to synthesize an alternative metabolic by-product, isoprene, the cell can overcome the kinetic bottleneck caused by reduced Fdx and high acetyl-CoA pools. Further investigation is needed to test this hypothesis and to clarify how the introduction of isoprene synthase may have altered metabolism in *M. acetivorans* and *M. barkeri*.

Acknowledgements

References

1.	Kim JH, Wang C, Jang HJ, Cha MS, Park JE, Jo SY, Choi ES, Kim SW. 2016. Isoprene production by *Escherichia coli* through the exogenous mevalonate pathway with reduced formation of fermentation byproducts. Microb Cell Fact 15:214. https://doi.org/10.1186/s12934-016-0612-6.

2.	International Rubber Study Group. Rubber statistical bulletin. 2012. International Rubber Study Group. http://www.rubberstudy.com/reports.

3.	Miller B, Oschinski C, Zimmer W. 2001. First isolation of an isoprene synthase

gene from poplar and successful expression of the gene in *Escherichia coli*. Planta 213:483–487. https://doi.org/10.1007/s004250100557.

4.   Matsumi R, Atomi H, Driessen AJM, van der Oost J. 2011. Isoprenoid biosynthesis in Archaea—biochemical and evolutionary implications. Res Microbiol 162:39–52. https://doi.org/10.1016/j.resmic.2010.10.003.

5.   Wagner WP, Helmig D, Fall R. 2000. Isoprene biosynthesis in *Bacillus subtilis* via the methylerythritol phosphate pathway. J Nat Prod 63:37–40. https://doi.org/10.1021/np990286p.

6.   Sharkey TD, Yeh S. 2001. Isoprene emission from plants. Annu Rev Plant Physiol Plant Mol Biol 52:407–436. https://doi.org/10.1146/annurev.arplant .52.1.407.

7.   Yang JM, Xian M, Su SZ, Zhao G, Nie QJ, Jiang XL, Zheng YN, Liu W. 2012. Enhancing production of bio-isoprene using hybrid MVA pathway and isoprene synthase in *E. coli*. PLoS One 7:e33509. https://doi.org/10.1371/ journal.pone.0033509.

8.   Lv XM, Xie WP, Lu WQ, Guo F, Gu JL, Yu HW, Ye LD. 2014. Enhanced isoprene biosynthesis in *Saccharomyces cerevisiae* by engineering of the native acetyl-CoA and mevalonic acid pathways with a push-pull-restrain strategy. J Biotechnol 186:128–136. https://doi.org/10.1016/j.jbiotec.2014 .06.024.

9.   Hong SY, Zurbriggen AS, Melis A. 2012. Isoprene hydrocarbons production upon heterologous transformation of *Saccharomyces cerevisiae*. J Appl Microbiol 113:52–65. https://doi.org/10.1111/j.1365-2672.2012.05319.x.

10.   Lindberg P, Park S, Melis A. 2010. Engineering a platform for photosyn- thetic

isoprene production in cyanobacteria, using *Synechocystis* as the model organism. Metab Eng 12:70–79. https://doi.org/10.1016/j.ymben .2009.10.001.

11.   Meadows AL, Hawkins KM, Tsegaye Y, Antipov E, Kim Y, Raetz L, Dahl RH, Tai A, Mahatdejkul-Meadows T, Xu L, Zhao L, Dasika MS, Murarka A, Lenihan J, Eng D, Leng JS, Liu CL, Wenger JW, Jiang H, Chao L, Westfall P, Lai J, Ganesan S, Jackson P, Mans R, Platt D, Reeves CD, Saija PR, Wichmann G, Holmes VF, Benjamin K, Hill PW, Gardner TS, Tsong AE. 2016. Rewriting yeast central carbon metabolism for industrial isoprenoid production. Nature 537:694–697. https://doi.org/10.1038/nature19769.

12.   Ferry JG. 2012. Methanogenesis: ecology, physiology, biochemistry & genetics. Springer Science1Business Media, Berlin, Germany.

13.   Shen YW, Linville JL, Urgun-Demirtas M, Mintz MM, Snyder SW. 2015. An overview of biogas production and utilization at full-scale wastewater treatment plants (WWTPs) in the United States: challenges and opportunities towards energy-neutral WWTPs. Renew Sust Energ Rev 50:346–362. https://doi.org/10.1016/j.rser.2015.04.129.

14.   Lessner DJ, Lhu L, Wahal CS, Ferry JG. 2010. An engineered methanogenic pathway derived from the domains Bacteria and Archaea. mBio 1:e00243- 10. https://doi.org/10.1128/mBio.00243-10.

15.   McAnulty MJ, Poosarla VG, Li J, Soo VW, Zhu F, Wood TK. 2017. Metabolic engineering of *Methanosarcina acetivorans* for lactate production from methane. Biotechnol Bioeng 114:852–861. https://doi.org/10.1002/bit.26208.

16.   Jennings ME, Schaff CW, Horne AJ, Lessner FH, Lessner DJ. 2014. Expression

of a bacterial catalase in a strictly anaerobic methanogen significantly increases tolerance to hydrogen peroxide but not oxygen. Microbiology (Reading) 160:270–278. https://doi.org/10.1099/mic.0.070763-0.

17.   Jasso-Chavez R, Santiago-Martinez MG, Lira-Silva E, Pineda E, Zepeda-Rodriguez A, Belmont-Diaz J, Encalada R, Saavedra E, Moreno-Sanchez R. 2015. Air-adapted *Methanosarcina acetivorans* shows high methane pro- duction and develops resistance against oxygen stress. PLoS One 10: e0117331. https://doi.org/10.1371/journal.pone.0117331.

18.   Goldstein JL, Brown MS. 1990. Regulation of the mevalonate pathway. Nature 343:425–430. https://doi.org/10.1038/343425a0.

19.   Vinokur JM, Korman TP, Cao Z, Bowie JU. 2014. Evidence of a novel mevalonate pathway in archaea. Biochemistry 53:4161–4168. https://doi.org/10 .1021/bi500566q.

20.   Hayakawa H, Motoyama K, Sobue F, Ito T, Kawaide H, Yoshimura T, Hemmi H. 2018. Modified mevalonate pathway of the archaeon *Aeropyrum pernix* proceeds via trans-anhydromevalonate 5-phosphate. Proc Natl Acad Sci U S A 115:10034–10039. https://doi.org/10.1073/pnas.1809154115.

21.   Yoshida R, Yoshimura T, Hemmi H. 2020. Reconstruction of the "archaeal" mevalonate pathway from the methanogenic archaeon Methanosarcina mazei in *Escherichia coli* cells. Appl Environ Microbiol 86:e02889-19. https://doi.org/10.1128/AEM.02889-19.

22.   Heuston S, Begley M, Gahan CGM, Hill C. 2012. Isoprenoid biosynthesis in bacterial pathogens. Microbiology (Reading) 158:1389–1401. https://doi.org/

10.1099/mic.0.051599-0.

23.   Zhao L, Chang W-c, Xiao Y, Liu H-w, Liu P. 2013. Methylerythritol phosphate

pathway of isoprenoid biosynthesis. Annu Rev Biochem 82:497–530. https://

doi.org/10.1146/annurev-biochem-052010-100934.

24.   Gray JC, Kekwick RGO. 1972. Inhibition of plant mevalonate kinase preparations

by prenyl pyrophosphates. Biochim Biophys Acta 279:290–296. https://

doi.org/10.1016/0304-4165(72)90145-6.

25.   Fu Z, Voynova NE, Herdendorf TJ, Miziorko HM, Kim J-JP. 2008. Biochemical

and structural basis for feedback inhibition of mevalonate kinase and isoprenoid

metabolism. Biochemistry 47:3715–3724. https://doi.org/10

.1021/bi7024386.

26.   Huang KX, Scott AI, Bennett GN. 1999. Overexpression, purification, and

characterization of the thermostable mevalonate kinase from *Methanococcus jannaschii*.

Protein Expr Purif 17:33–40. https://doi.org/10.1006/ prep.1999.1106.

27.   Kazieva E, Yamamoto Y, Tajima Y, Yokoyama K, Katashkina J, Nishio Y. 2017.

Characterization of feedback-resistant mevalonate kinases from the methanogenic

archaeons *Methanosaeta concilii* and *Methanocella paludicola*. Microbiology (Reading)

163:1283–1291. https://doi.org/10.1099/mic

.0.000510.

28.   Liu CL, Bi HR, Bai Z, Fan LH, Tan TW. 2019. Engineering and manipulation of

a mevalonate pathway in *Escherichia coli* for isoprene production. Appl Microbiol

Biotechnol 103:239–250. https://doi.org/10.1007/s00253-018

-9472-9.

29.   Feist AM, Scholten JC, Palsson BO, Brockman FJ, Ideker T. 2006. Modeling methanogenesis with a genome-scale metabolic reconstruction of *Methanosarcina barkeri*. Mol Syst Biol 2:2006.0004. https://doi.org/10.1038/ msb4100046.

30.   Sasaki K, Ohara K, Yazaki K. 2005. Gene expression and characterization of isoprene synthase from Populus alba. FEBS Lett 579:2514–2518. https:// doi.org/10.1016/j.febslet.2005.03.066.

31.   Shea MT, Walter ME, Duszenko N, Ducluzeau AL, Aldridge J, King SK, Buan NR. 2016. pNEB193-derived suicide plasmids for gene deletion and protein expression in the methane-producing archaeon, *Methanosarcina acetivorans*. Plasmid 84–85:27–35. https://doi.org/10.1016/j.plasmid.2016.02 .003.

32.   Guss AM, Rother M, Zhang JK, Kulkarni G, Metcalf WW. 2008. New methods for tightly regulated gene expression and highly efficient chromosomal integration of cloned genes for Methanosarcina species. Archaea 2:193–203. https://doi.org/10.1155/2008/534081.

33.   Sprott GD. 1992. Structures of archaebacterial membrane lipids. J Bioenerg Biomembr 24:555–566. https://doi.org/10.1007/BF00762348.

34.   Schnitzler JP, Zimmer I, Bachl A, Arend M, Fromm J, Fischbach RJ. 2005. Biochemical properties of isoprene synthase in poplar (Populus x canescens). Planta 222:777–786. https://doi.org/10.1007/s00425-005-0022-1.

35.   Hildenbrand C, Stock T, Lange C, Rother M, Soppa J. 2011. Genome copy numbers and gene conversion in methanogenic archaea. J Bacteriol 193:734–743. https://doi.org/10.1128/JB.01016-10.

36.   Buan NR, Metcalf WW. 2010. Methanogenesis by *Methanosarcina acetivorans* involves two structurally and functionally distinct classes of heterodisulfide reductase. Mol Microbiol 75:843–853. https://doi.org/10.1111/j .1365-2958.2009.06990.x.

37.   Catlett JL, Ortiz AM, Buan NR. 2015. Rerouting cellular electron flux to increase the rate of biological methane production. Appl Environ Microbiol 81:6528–6537. https://doi.org/10.1128/AEM.01162-15.

38.   Galagan JE, Nusbaum C, Roy A, Endrizzi MG, Macdonald P, FitzHugh W, Calvo S, Engels R, Smirnov S, Atnoor D, Brown A, Allen N, Naylor J, Stange- Thomann N, DeArellano K, Johnson R, Linton L, McEwan P, McKernan K, Talamas J, Tirrell A, Ye W, Zimmer A, Barber RD, Cann I, Graham DE, Grahame DA, Guss AM, Hedderich R, Ingram-Smith C, Kuettner HC, Krzycki JA, Leigh JA, Li W, Liu J, Mukhopadhyay B, Reeve JN, Smith K, Springer TA, Umayam LA, White O, White RH, Conway de Macario E, Ferry JG, Jarrell KF, Jing H, Macario AJL, Paulsen I, Pritchett M, Sowers KR, et al. 2002. The genome of *M. acetivorans* reveals extensive metabolic and physiological diversity. Genome Res 12:532–542., https://doi.org/10.1101/ gr.223902.

39.   Lyu Z, Jain R, Smith P, Fetchko T, Yan Y, Whitman WB. 2016. Engineering the autotroph Methanococcus maripaludis for geraniol production. ACS Synth Biol 5:577– 581. https://doi.org/10.1021/acssynbio.5b00267.

40.   Buan NR. 2018. Methanogens: pushing the boundaries of biology. Emerging Topics in Life Sciences 2:629–646. https://doi.org/10.1042/etls20180031.

41.   Kulkarni G, Mand TD, Metcalf WW. 2018. Energy conservation via hydrogen cycling in the methanogenic archaeon Methanosarcina barkeri. mBio 9:e01256-18.

https://doi.org/10.1128/mBio.01256-18.

42.   Lieber DJ, Catlett J, Madayiputhiya N, Nandakumar R, Lopez MM, Metcalf WW, Buan NR. 2014. A multienzyme complex channels substrates and electrons through acetyl-CoA and methane biosynthesis pathways in Methanosarcina. PLoS One 9:e107563. https://doi.org/10.1371/journal .pone.0107563.

43.   Bott RR, Cervin MA, Kellis JT, McAuliffe JC, Miasnikov A, Peres CM, Rife CL, Wells DH, Weyler W, Whited GM. 2008. Isoprene synthase variants for improved microbial production of isoprene. US patent US20100003716A1. https://patents.google.com/patent/US20100003716A1/en.

44.   Thauer RK, Kaster A-K, Seedorf H, Buckel W, Hedderich R. 2008. Methanogenic archaea: ecologically relevant differences in energy conservation. Nat Rev Microbiol 6:579–591. https://doi.org/10.1038/nrmicro1931.

45.   Yang C, Gao X, Jiang Y, Sun B, Gao F, Yang S. 2016. Synergy between methylerythritol phosphate pathway and mevalonate pathway for isoprene production in *Escherichia coli*. Metab Eng 37:79–91. https://doi.org/ 10.1016/j.ymben.2016.05.003.

46.   Yao Z, Zhou P, Su B, Su S, Ye L, Yu H. 2018. Enhanced isoprene production by reconstruction of metabolic balance between strengthened precursor supply and improved isoprene synthase in *Saccharomyces cerevisiae*. ACS Synth Biol 7:2308–2316. https://doi.org/10.1021/acssynbio.8b00289.

47.   Sowers KR, Boone JE, Gunsalus RP. 1993. Disaggregation of Methanosarcina spp. and growth as single cells at elevated osmolarity. Appl Environ Microbiol 59:3832–3839. https://doi.org/10.1128/AEM.59.11.3832-3839.1993.

48.   Metcalf WW, Zhang JK, Apolinario E, Sowers KR, Wolfe RS. 1997. A genetic system for Archaea of the genus Methanosarcina: liposome-mediated trans- formation and construction of shuttle vectors. Proc Natl Acad Sci U S A 94:2626–2631. https://doi.org/10.1073/pnas.94.6.2626.

49.   Zhang JK, White AK, Kuettner HC, Boccazzi P, Metcalf WW. 2002. Directed mutagenesis and plasmid-based complementation in the methanogenic archaeon *Methanosarcina acetivorans* C2A demonstrated by genetic analysis of proline biosynthesis. J Bacteriol 184:1449–1454. https://doi.org/10 .1128/jb.184.5.1449-1454.2002.

50.   Welander PV, Metcalf WW. 2008. Mutagenesis of the C_1 oxidation pathway in Methanosarcina barkeri: new insights into the Mtr/Mer bypass pathway. J Bacteriol 190:1928–1936. https://doi.org/10.1128/JB.01424-07.

51.   Buan N, Kulkarni G, Metcalf W. 2011. Genetic methods for methanosarcina species. Methods Enzymol 494:23–42. https://doi.org/10.1016/B978-0-12 -385112-3.00002-0.

52.   Li MZ, Elledge SJ. 2007. Harnessing homologous recombination in vitro to generate recombinant DNA via SLIC. Nat Methods 4:251–256. https://doi .org/10.1038/nmeth1010.

53.   Bertani G. 1951. Studies on lysogenesis. I. The mode of phage liberation by lysogenic *Escherichia coli*. J Bacteriol 62:293–300. https://doi.org/10 .1128/JB.62.3.293-300.1951.

54.   Aldridge JT, Catlett JL, Smith ML, Buan NR. 2016. Methods for detecting microbial methane production and consumption by gas chromatography. Bio Protoc

6:e1779. https://doi.org/10.21769/bioprotoc.1779.

55.   Aldridge J, Carr S, Weber KA, Buan NR. 2018. Production of bioisoprene from wastewater. Report no. NTRY6R14/4822. The Water Research Foundation, Denver, CO. https://www.waterrf.org/research/projects/production-bioisoprene-wastewater.

56.   Bose A, Kulkarni G, Metcalf WW. 2009. Regulation of putative methyl-sulphide methyltransferases in *Methanosarcina acetivorans* C2A. Mol Microbiol 74:227–238. https://doi.org/10.1111/j.1365-2958.2009.06864.x.

57.   Rao X, Huang X, Zhou Z, Lin X. 2013. An improvement of the 2^(-delta delta CT) method for quantitative real-time polymerase chain reaction data analysis. Biostat Bioinforma Biomath 3:71–85.

58.   Egan AJ, Vollmer W. 2013. The physiology of bacterial cell division. Ann N Y Acad Sci 1277:8–28. https://doi.org/10.1111/j.1749-6632.2012.06818.x.

59.   Yamada EA, Sgarbieri VC. 2005. Yeast (*Saccharomyces cerevisiae*) protein concentrate: preparation, chemical composition, and nutritional and functional properties. J Agric Food Chem 53:3931–3936. https://doi.org/ 10.1021/jf0400821.

60.   Diner BA, Fan J, Scotcher MC, Wells DH, Whited GM. 2017. Synthesis of heterologous mevalonic acid pathway enzymes in Clostridium ljungdahlii for the conversion of fructose and of syngas to mevalonate and isoprene. Appl Environ Microbiol 84:e01723-17. https://doi.org/10.1128/AEM.01723-17.

61.   Pade N, Erdmann S, Enke H, Dethloff F, Duhring U, Georg J, Wambutt J, Kopka J, Hess WR, Zimmermann R, Kramer D, Hagemann M. 2016. Insights into isoprene production using the cyanobacterium Synechocystis sp. PCC 6803. Biotechnol Biofuels 9:89. https://doi.org/10.1186/s13068-016-0503-4.
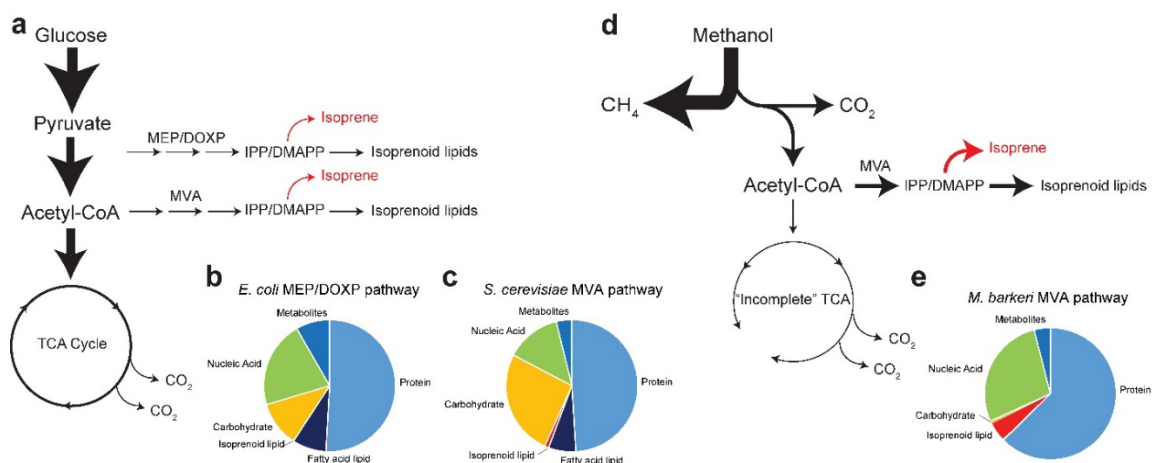
Figure 1. Isoprenoid biosynthesis pathways and macromolecular compositions of representative bacteria, eukarya, and archaea. (a) Isoprene is synthesized from isopentenyl pyrophosphate/dimethylallyl pyrophosphate (IPP/DMAPP) derived from glucose via the methylerythritol phosphate/deoxy xylulose phosphate (MEP/DOXP) pathway in bacteria or mevalonate (MVA) pathway in eukarya. (b and c) Relative amounts of macromolecules in E. coli bacterium (58) and S. cerevisiae yeast (59), respectively. (d) Isoprenoid lipids are synthesized from IPP/DMAPP by the archaeal MVA pathway in methanogens. (e) Isoprenoid lipids in methanogens comprise 5% of biomass dry weight (29). Arrow sizes and line widths depict published carbon fluxes through each pathway. One or more genes are required for most organisms to produce isoprene monomer (red arrows). See Table S1 for macromolecular composition values shown in panels b, c, and e.
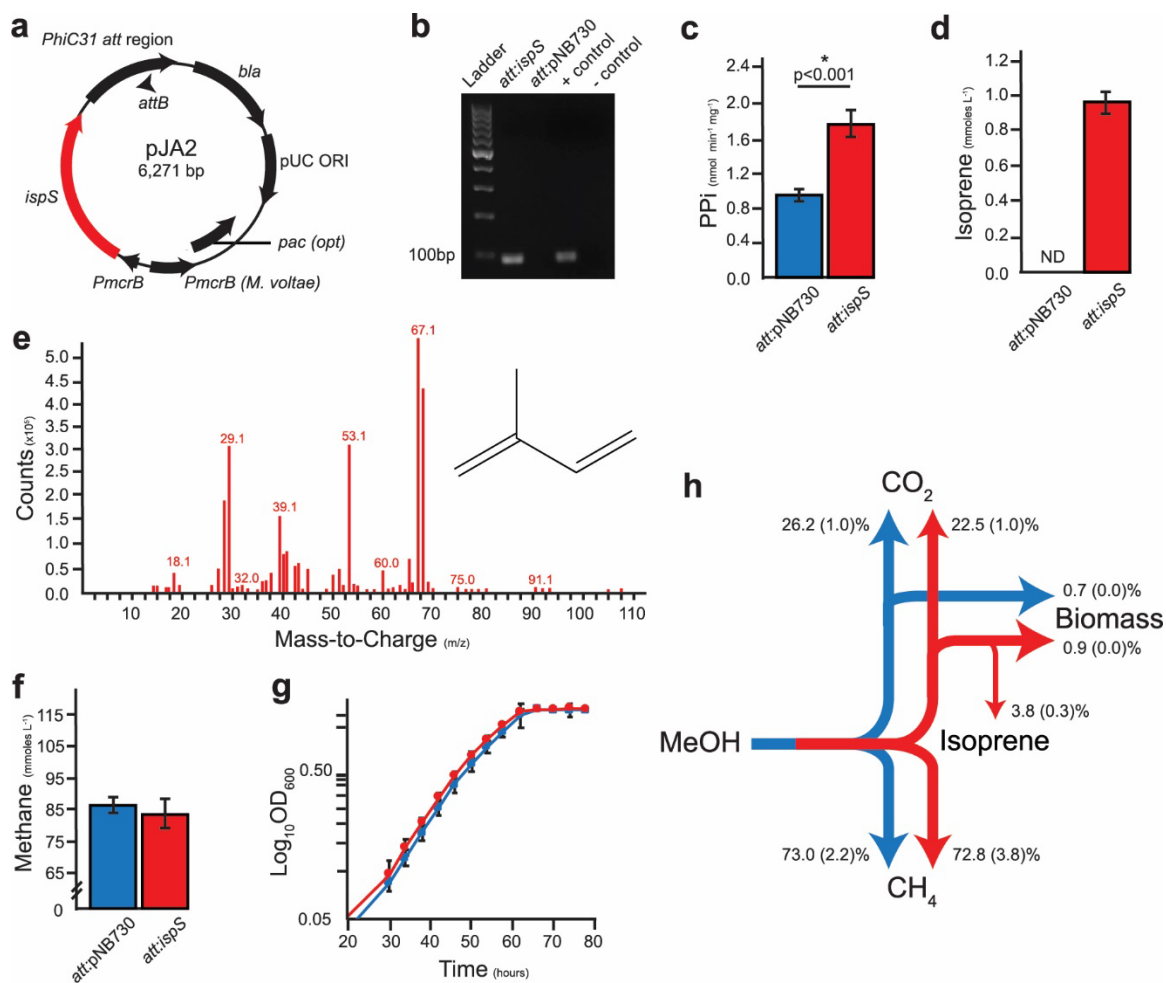
Figure 2. Strain construction and validation of isoprene production from methanol. (a) Plasmid

map of pJA2 for constitutive expression of isoprene synthase IspS in Methanosarcina spp. (b)

Validation of *ispS* transcription by RT-qPCR. Plasmid DNA from pJA2 was used as

a positive control, while genomic DNA from the parent strain NB34 was used as a negative

control. (c) Dimethylallyl pyrophosphate pyrophosphatase activity in cell extracts. (d) Isoprene

production measured by gas chromatography. (e) Validation of isoprene production by mass

spectrometry. (f) Endpoint methane production. (g) Growth curve of *att*:pNB730 and *att:ispS*

strains. (h) Mass balance of *M. acetivorans att*:pNB730 (blue) and *att:ispS* (red) strains showing

percent molar carbon fluxes. Standard deviations are shown in parentheses. Blue bars,

att:pNB730 strain; red bars, *att:ispS* strain. Data presented in panels c, d, f, and h were obtained

from quadruplicate biological and triplicate technical replicates (n = 12). Data presented in panel

e were from a double-blinded experiment. Data from panel g were from five biological replicates.
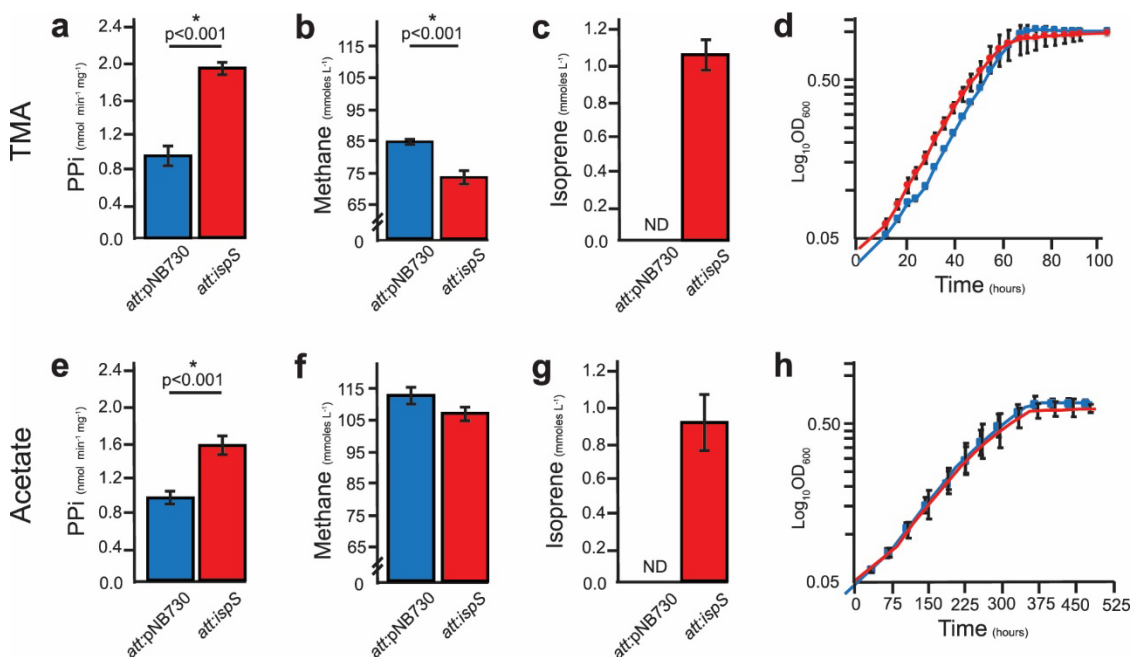
Figure 3. Characterization of ispS1 strains grown on trimethylamine (TMA) or acetate substrates.

(a and e) Dimethylallyl pyrophosphate pyrophosphatase activity in cell extracts. (b and f)

Endpoint methane production. (c and g) Isoprene production measured by gas chromatography. (d

and h) Growth curves of *att*:pNB730 and *att:ispS* strains. Blue bars, *att*:pNB730 strain; red bars,

att:ispS strain. Data presented in panels a to c and e to g were obtained from quadruplicate

biological and triplicate technical replicates (n =12). Data in panels d and h were from five

biological replicates.
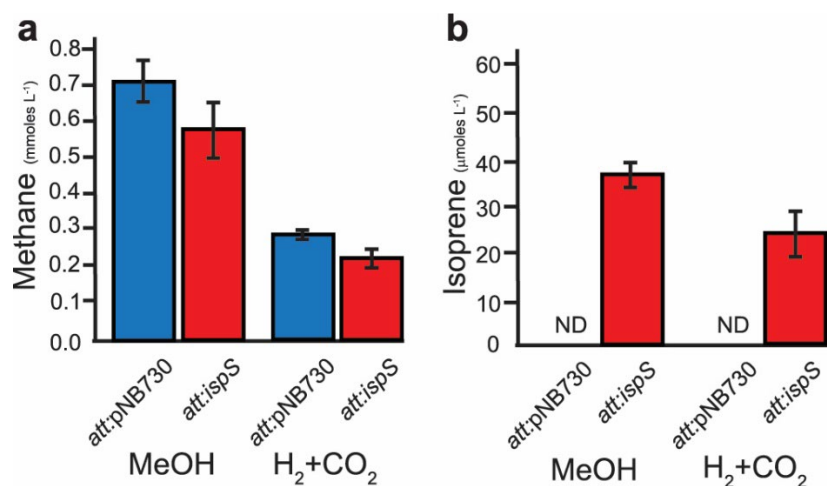
Figure 4. Demonstration of isoprene production by Methanosarcina barkeri. (a) Endpoint methane assays for M. barkeri *att*:pNB730 and *att:ispS* strains. (b) Isoprene production by M. barkeri *att*:pNB730 and att:ispS strains as measured by gas chromatography. Blue, *att*:pNB730 strains; red, *att:ispS* strains. Data for panels a and b were obtained from quadruplicate biological and triplicate technical replicates (n = 12).

Table 1. Comparison of isoprene and terpenoid yields in engineered bacteria and archaea.

Organism	Yield	Condition	Citation
Batch culture yields[a]			
Clostridium ljungdahlii[b]	0.00001	MES-Fructose, batch	[60]
Synechocyctis[b]	0.336	Light+CO_2, batch	[61]
Methanococcus maripaludis[c]	2.8	H_2+CO_2, batch (geraniol)	[39]
Methanococcus maripaludis[c]	4.6	Formate, batch (geraniol)	[39]
Methanosarcina acetivorans	67.2	Methanol, batch	[This study]
Fed-batch yields[d]			
Escherichia coli	24.0	0.1-2% glucose, fed-batch	[45]
Saccharomyces cerevisiae[e]	11.9	25g/L initial glucose, fed-batch	[46]

a. Batch culture yields in mg mol^{-1} g^{-1} dry weight.
b. Strains contain two or more mutations to enhance isoprene production.
c. Values are for the terpene geraniol.
d. Fed-batch fermentation yields in g/L.
e. The rate of feed solution and final concentration of glucose utilized were not reported.

Table 2. Gene copies per cell

Gene	Puromycin[a]	Generation (days)						P-value
		20 (7)	Std Dev	56 (19)	Std Dev	140 (47)	Std Dev	
rpoA1	-	16	0	16	0	16	0	1
IspS	-	9.39	0.10	8.32	0.51	8.52	0.53	0.545
ratio	-	0.59		0.56		0.53		
rpoA1	+	16	0	16	0	16	0	1
IspS	+	9.19	0.34	9.51	0.23	8.91	0.18	0.548
ratio	+	0.57		0.59		0.56		

a. Without antibiotic selection (-), with constant antibiotic selection (+).
Values were obtained from biological and technical triplicates (n=9).

Table 3. Relative transcript abundance between *att:ispS* and *att:pNB730* strains of *M. acetivorans*.[a]

Pathway	Gene	Fold Change	p-value
Mevalonate pathway	HMG-CoA synthase	0.66	0.001271
	HMG-CoA reductase	1.49	0.045242
	Mevalonate kinase	1.31	0.004854
	Isopentenyl phosphate kinase	1.88	0.117332
	Isopentenyl diphosphate delta-isomerase	2.26	0.011509
TCA Pathway[b]	Pyruvate synthase	0.80	0.211017
	Pyruvate carboxylase	1.96	0.000206
	Malate dehydrogenase	1.68	0.007657
	Fumarate hydratase	0.21	1.53E-05
Methanogenesis	Methyl coenzyme M reductase B (*mcrB*)	1.55	0.000121

a. Values were obtained from triplicate biological and 5 technical replicates (n=15).
b. All annotated TCA cycle enzymes in *M. acetivorans*. Methanogens have an incomplete TCA cycle.

Table 4: Strains, plasmids, and primers used in this study

Strain, Plasmid, or Primer	Description	Purpose	Source
Methanosarcina acetivorans **C2A**			
394	D*hpt::w*C31 *int, att*:pJA2	Isoprene production (*att:ispS*)	This study
452	D*hpt::w*C31 *int, att*:pNB730	Vector-only control (*att:*pNB730)	This study
Methanosarcina barkeri			
396	D*hpt::w*C31 *int, att*:pJA2	Isoprene production	This study
459	Dhpt::*w*C31 *int, att:*pNB730	Vector-only control (*att:*pNB730)	(31)
Escherichia coli			
3	F9*proA*¹*B*¹ *lacI*�q D*(lacZ)M15 zzf::Tn10 (TetR)/fhuA2*D*(argF-lacZ)* U169 phoA glnV44 U80D*(lacZ)M15 gyrA96 recA1 endA1 thi-1 hsdR17*	Cloning and plasmid propagation	New England Biolabs
134	F9 *proA*¹*B*¹ *lacI*�q D*(lacZ)M15 zzf::Tn10 (TetR)/fhuA2*D*(argF-lacZ)* U169 phoA glnV44 U80D*(lacZ)M15 gyrA96 recA1 endA1 thi-1 hsdR17*/pNB730	Production of pNB730 plasmid	(31)
453	F9 *proA*¹*B*¹ *lacI*�q D*(lacZ)M15 zzf::Tn10 (TetR)/fhuA2*D*(argF-lacZ)* U169 phoA glnV44 U80D*(lacZ)M15 gyrA96 recA1 endA1 thi-1 hsdR17*/ pJA2	Expression of *ispS* in *M. acetivorans*	(55)
Plasmids			
pNB730	pUC ori bla PmcrB pac(opt) w C31 attB	*Methanosarcina* spp. integration and expression vector	(31)
pJA2	pNB730 *ispS*^D1213	Integration of *ispS* into genome for constitutive expression of isoprene synthase	(55)
Primers and DNA strings			
sNB19	GenBank accession no. MW295460 (see the supplemental material)	Synthetic optimized *Populus alba ispS* (isoprene synthase)	This study
oNB568	ATTAAGGAGGAAATTCATATGTCCGTTTCCACCGAA AATGT	*ispS*^D1213 DNA string amplification and cloning, fwd	(55)
oNB576	CGAGGGCCCAAGCTTGGATCCTCATCTTTCAAAAGG AAGAATAG	DNA string amplification and cloning, rev	(55)
oNB729	CATATGCCTGACGACCTCATTA	RNA polymerase, *rpoA1* qRT fwd housekeeping gene	This study
oNB730	GAATTTGATTTCGAGCTGTTCC	RNA polymerase, *rpoA1* qRT rev housekeeping gene	This study
oNB733	GTTTACAAAAGTAGCTGCAAGGGTA	Methyl-coenzyme M reductase, *mcrB* qRT fwd	This study
oNB734	ATACAAATTCTACAAGGCAAACGAC	Methyl-coenzyme M reductase, *mcrB* qRT rev	This study
oNB735	GGATTCGATGCAGTTACCAAA	*ispS* qPCR primer, fwd	This study
oNB736	TGCTTCCTGGCTAACTTCAAA	*ispS* qPCR primer, rev	This study
oNB930	CCGTGCCTGATGTCGACGAA	HMG-CoA synthase fwd	This study
oNB931	TGGAGGGATCTACGCCGCTT	HMG-CoA synthase rev	This study
oNB932	GCCGGCCTTCTGAAAGTAAACG	HMGR fwd	This study
oNB933	TCCGCGGTTTACACTGGCAA	HMGR rev	This study
oNB934	CCCGTGTGCGGGTGGAATTA	Mevalonate kinase fwd	This study
oNB935	ACCACTGCGGAGATATAAGGATGT	Mevalonate kinase rev	This study
oNB936	GAGGCAGCGCCATTACCGAT	Isopentenyl phosphate kinase fwd	This study
oNB937	GCCTGAAACTTCCCGCGCAA	Isopentenyl phosphate kinase rev	This study
oNB938	CAGCCAGAGAGCCGCAATCG	Isopentenyl-diphosphate *d*-isomerase fwd	This study
oNB939	CCGTAGACAAAGGCGTTCGGA	Isopentenyl-diphosphate *d*-isomerase rev	This study

oNB940	GCTCATGCACGAGGTGCTCT	Pyruvate synthase fwd	This study
oNB941	GCACTGACTGCCCTGTTTGC	Pyruvate synthase rev	This study
oNB942	TCATGCGTGCCTGCAGAGAG	Pyruvate carboxylase fwd	This study
oNB943	GCCTCATCGGCATACTTGGCA	Pyruvate carboxylase rev	This study
oNB944	CCGAACTGGAACCTGGCGAA	Malate dehydrogenase fwd	This study
oNB945	TGCCTGCATGAGGTCAAGGG	Malate dehydrogenase rev	This study
oNB946	TCCTCGACCTGCCTATCGGT	Fumarate hydratase fwd	This study
oNB947	GGTCGGCTGGAACCTCAACC	Fumarate hydratase rev	This study

Figure S1: Relative transcript abundance in *att:ispS*+ strains. Genes in red were assayed by RT-qPCR. Circles represent changes in gene expression as determined using the -ΔΔCt method versus control strain. Green circles, upregulated genes; red circles, downregulated genes; gray circles, not statistically significant (p>0.01). Numbers represent average fold change from three biological replicates with five technical replicates each (n=15). Question marks represent unknown mechanisms. ADP, adenosine diphosphate; AMPD, anhydromevalonate phosphate decarboxylase; ATP, adenosine triphosphate; *atoB*, acetyl-CoA acetyltransferase; CoA, coenzyme A; Fdx(ox), oxidized ferredoxin; Fdx(red), reduced ferredoxin; *fumA*, fumarate hydratase; HMGR, hydroxymethylglutaryl-CoA reductase; HMGS; hydroxymethylglutaryl-CoA

synthase; *idi*, isopentenyl diphosphate isomerase; *ipk*, isopenetyl phosphate kinase; *ispS*, isoprene

synthase *mcrB*, methyl-coenzyme M reductase; MDH, malate dehydrogenase; MK, mevalonate

kinase; MP, methanophenazine; MPH$_2$, reduced methanophenazine; PMDh, phosphomevalonate

dehydratase; Pi, inorganic phosphate; PPi, pyrophosphate; *porB*, pyruvate synthase; *pycA*,

pyruvate carboxylase.

Table S1: Macromolecular composition by % dry weight.			
Macromolecule class	***E. coli*[1]**	***S. cerevisiae*[2]**	***M. barkeri* [3]**
Protein	50.90	44.90	62.97
Fatty acid lipid	8.33	12.29	0.10
Isoprenoid lipid	0.05	Not reported	5.00
Carbohydrate	11.11	29.58	0.50
Nucleic Acid	21.29	8.88	27.99
Metabolites	8.33	4.35	4.00

Table S2: *M. acetivorans* strains grown in HS medium.						
	MeOH		**TMA**		**Acetate**	
Doubling time[a]	**Hours**	**Std dev**	**Hours**	**Std dev**	**Hours**	**Std dev**
att:pNB730	9.57	0.36	11.8	0.31	44.0	2.80
att:ispS	9.01	0.42	13.0	1.92	46.6	2.64
p	0.770		0.472		1.00	
CH$_4$[b]	**mmoles L^{-1}**	**Std dev**	**mmoles L^{-1}**	**Std dev**	**mmoles L^{-1}**	**Std dev**
att:pNB730	83.18	2.53	82.34	0.75	111.07	3.24
att:ispS	79.44	2.76	73.54	3.54	107.71	3.03
p	0.0610		0.0006		0.0593	
Isoprene[b]	**mmoles L^{-1}**	**Std dev**	**mmoles L^{-1}**	**Std dev**	**mmoles L^{-1}**	**Std dev**
att:pNB730	ND		ND		ND	
att:ispS	0.954	0.236	1.020	0.239	0.933	0.271
a. Data were obtained from five biological replicates (n=5).						
b. Data were obtained from quadruplicate biological replicates and triplicate technical replicates (n=12).						
ND, Not detected.						

Table S3: *M. acetivorans* mass balance on MOPS buffered MeOH medium.[a]

Strain	CH_4[b] mmoles L^{-1} (%C)[d]	Std dev	CO_2[b] mmoles L^{-1} (%C)[d]	Std dev	Isoprene[b] mmoles L^{-1} (%C)[d]	Std dev	Biomass[c] g/L (%C)[d]	Std dev
Theoretical	90 (74.4)		30 (24.8)		0		0.9 (0.7)	
att:pNB730	84.10 (73.0)	2.48 (2.2)	30.1 (26.2)	1.16 (1.0)	ND		0.904 (0.7)	0.040 (0.0)
att:ispS	81.00 (72.8)	4.21 (3.8)	25.0 (22.5)	1.06 (1.0)	0.855 (3.8)	0.073 (0.3)	0.965 (0.9)	0.043 (0.0)
p	0.0191		0.0001				0.0041	

a. Calculated from 125 mmoles MeOH.
b. Data were obtained from quadruplicate biological replicates and triplicate technical replicates (n=12).
c. Data were obtained from ten biological replicates (n=10). Estimated as CHO (mwt=29).
d. Calculated using the equation $\%C = (C/\sum C) \cdot 100$
ND, Not detected.

Table S4: *M. barkeri* strains grown in HS medium.

	MeOH[a]		H_2+CO_2[b]	
Doubling time[c]				
Strain	**Hours**	**Std dev**	**Hours**	**Std dev**
att:pNB730	8.95	0.232	NT	
att:ispS	9.33	0.299	NT	
p	0.061			
CH4 production [d]				
Strain	**Δmoles L^{-1}**	**Std dev**	**Δmoles L^{-1}**	**Std dev**
att:pNB730	715.13	22.067	289.53	12.54
att:ispS	583.98	32.20	263.67	20.39
p	0.0001		0.0011	
Isoprene production[d]				
Strain	**Δmoles L^{-1}**	**Std dev**	**Δmoles L^{-1}**	**Std dev**
att:pNB730	ND		ND	
att:ispS	36.0	2.02	23.2	3.56

a. Calculated from 125 mmoles MeOH.
b. H2:CO2 80%:20% every 12h at 15 psi.
c. Data were obtained from five biological replicates (n=5).
d. Data were obtained from quadruplicate biological replicates and triplicate technical replicates (n=12).
ND, Not detected. NT, Not tested.

Supplementary References

1   Egan, A. J. & Vollmer, W. The physiology of bacterial cell division. *Ann N Y Acad Sci* **1277**, 8-28, doi:10.1111/j.1749-6632.2012.06818.x (2013).

2   Yamada, E. A. & Sgarbieri, V. C. Yeast (*Saccharomyces cerevisiae*) protein concentrate: preparation, chemical composition, and nutritional and functional properties. *J Agric Food Chem* **53**, 3931-3936, doi:10.1021/jf0400821 (2005).

3   Feist, A. M., Scholten, J. C., Palsson, B. O., Brockman, F. J. & Ideker, T. Modeling methanogenesis with a genome-scale metabolic reconstruction of *Methanosarcina barkeri*. *Mol Syst Biol* **2**, 2006 0004, doi:msb4100046 (2006).

Chapter 4: Isoprene Production from Municipal Wastewater Biosolids by Engineered Archaeon *Methanosarcina acetivorans*

This chapter represents the contents of: Sean Carr, Jared Aldridge, and Nicole R. Buan. "Isoprene production from municipal wastewater biosolids by engineered archaeon Methanosarcina acetivorans." *Applied Sciences* 11, no. 8 (2021): 3342.

Author contributions: Conceptualization, N.R.B.; methodology, S.C., J.A., and N.R.B.; formal analysis, S.C., J.A., and N.R.B.; investigation, S.C. and J.A.; resources, N.R.B.; data curation, S.C. and J.A.; writing—original draft preparation, S.C. and N.R.B.; writing—review and editing, S.C., J.A., and N.R.B.; visualization, S.C., J.A., and N.R.B.; supervision, N.R.B.; project administration, N.R.B.; funding acquisition, N.R.B.

Abstract

Wastewater biosolids are a promising feedstock for production of value-added renewable chemicals. Methane-producing archaea (methanogens) are already used to produce renewable biogas via the anaerobic treatment of wastewater. The ability of methanogens to efficiently convert dissolved organic carbon into methane makes them an appealing potential platform for biorefining using metabolic engineering. We have engineered a strain of the methanogen Methanosarcina acetivorans to produce the volatile hemiterpene isoprene in addition to methane. The engineered strain was adapted to grow in municipal wastewater through cultivation in a synthetic wastewater medium. When

introduced to municipal wastewater the engineered methanogens were able to compete with the indigenous microorganisms and produce 0.97 mM of isoprene (65.9 ± 21.3 g per m3 of effluent). The production of isoprene in wastewater appears to be dependent on the quantity of available methanogenic substrate produced during upstream digestion by heterotrophic fermenters. This shows that with minimal adaptation it is possible to drop-in engineered methanogens to existing wastewater environments and attain value-added products in addition to the processing of wastewater. This shows the potential for utilizing methanogens as a platform for low-cost production of renewable materials without expensive feedstocks or the need to build or adapt existing facilities.

Introduction

Methane-producing archaea (methanogens) are obligate anaerobes which inhabit a keystone niche in the global carbon cycle, utilizing the endpoint degradation products of complex organic material and liberating otherwise inaccessible carbon [1–4]. Their unique metabolism and their potential to utilize a wide array of plentiful substrates make methanogens a subject of particular interest in industrial applications such as wastewater treatment [5–7], and the production of value-added products (Figure 1) [8,9]. Methanogens are used worldwide to reduce dissolved organic carbon in effluent as part of the wastewater treatment process. Wastewater treatment is a multistage process which is highly variant depending on the substrate being treated, though the end goal is largely the same: the detoxification of water by degrading complex biomass and pollutants before reintroducing the effluent into the water cycle. For the purpose of this study, we focused on the anaerobic digestion of municipal wastewater which primarily aims to remove dissolved carbon and suspended solids from a city's water supply.

Municipal wastewater treatment generally occurs in three distinct stages based upon the aerobicity of the wastewater and the activity of microorganisms involved in the multistage process. In the first stage, aerobic microorganisms breakdown complex biomass into simpler organic material [10]. The deconvoluted material is further anaerobically digested by a second consortia of microbes into one- or two-carbon compounds and organic acids. These one- and two-carbon compounds are utilized by methanogens to complete the decomposition process [6,11]. In addition to removing polluting organic carbon from the water, anaerobic digestion has the added benefit of producing methane which is often captured as renewable biogas [11–14]. Due to the low energetic potential of methanogenic feedstocks, methanogens utilize a highly efficient central metabolism which greatly favors the production of methane over biomass and heat. Anaerobic treatment of wastewater results in 95% conversion of the initial substrate into available biogas with 5% being utilized for microbial biomass [15,16]. We hypothesized that the highly efficient metabolism of methanogens may have potential to produce high yields of other value-added products in addition to methane.

Isoprene (2-methyl-1,3-butadiene) is the primary component of natural rubber and an important chemical precursor utilized in the production of synthetic rubber as well as adhesives, flavorings, cosmetics, and pharmaceuticals. Traditionally, isoprene is harvested from natural rubber from tree sap or produced industrially through the thermal cracking of petroleum. By producing renewable isoprene via engineered microbes, it could be possible to reduce the need to rely on the harvesting of plant biomass or the mining of fossil fuels. Recently our laboratory demonstrated that the methanogen Methanosarcina acetivorans can be engineered to efficiently produce bioisoprene as a

methane coproduct under laboratory conditions [9]. The gene for isoprene synthase, ispS, was stably inserted into the chromosome of M. acetivorans (att::ispS) and the production of isoprene as well as methane was confirmed via gas chromatography. The production of isoprene showed no detrimental effect on growth rate or metabolic efficiency of the engineered strains compared with a vector-only control. We surmised that without an obvious decrease in fitness it may be possible to drop-in these engineered methanogens into an existing anaerobic wastewater treatment consortium to produce bioisoprene. However, any inoculated methanogens would have to compete for substrate with wild methanogens in the mixed microbial community of the anaerobic digester. M. acetivorans has the largest genome of any characterized methanogen as well as the widest range of substrate utilization, allowing for growth from methanol, methyl-amines, carbon monoxide, and acetate [17,18]. We postulated that this metabolic flexibility would allow for our engineered strains to compete with the endogenous methanogens present in municipal wastewater resulting in an increase in methane production as well as the production of bioisoprene. The detection of isoprene in wastewater inoculated with our engineered strains with and without the supplementation of additional feed substrate supports our hypothesis.

Materials and Methods

Anaerobic Techniques

Anaerobic procedures were performed in a custom B-type Coy anaerobic chamber (Coy Labs, Grass Lake, MI, USA). The chamber was maintained at 35 °C with an atmosphere of 5% H_2/20% CO_2/75% N_2 (±3%) (Matheson Gas, Lincoln, NE, USA). The Methanosarcina acetivorans strains used in this study are the isoprene-producing strain NB394 (Δhpt::φC31 int, att:pJA2) and the vector-only control NB452 (Δhpt::φC31 int, att:pNB730) [9]. Strains were cultured in anaerobic high-salt (HS) medium (200 mM NaCl, 45 mM $NaHCO_3$, 13 mM KCl, 54 mM $MgCl_2·6H_2O$, 2 mM $CaCl_2·2H_2O$, 2 μM 0.1% resazurin (w v−1), 5 mM KH_2PO_4, 19 mM NH_4Cl, 2.8 mM cysteine·HCl, 0.1 mM $Na_2S·9H_2O$, trace elements, vitamin solution) [19] supplemented with a carbon and energy source (methanol, 125 mM; trimethylamine, 50 mM; sodium acetate, 120 mM) and 2 mg L−1 puromycin as needed [20,21]. Cells were incubated at 35 °C outside of anaerobic chamber in glass Balch tubes secured with butyl rubber stoppers (Belco Glass, Vineland, NJ, USA) and aluminum crimps (Wheaton, Millville, NJ, USA).

Synthetic Wastewater

Anaerobic synthetic wastewater (SWW) medium was developed to adapt cells from laboratory conditions to growth on municipal wastewater [22]. Chemical composition of SWW medium is based on OECD guidelines for testing of chemicals [23]. SWW is composed from 28 mg L−1 peptone, 100 mg L−1 meat extract, 100 mg L−1 urea, 161 μM KH_2PO_4, 120 μM NaCl, 27 μM $CaCl_2·2H_2O$, 8.7 μM $MgCl_2·6H_2O$, 0.23% agarose (w v−1), and 3% evaporated milk (w v−1), supplemented with a carbon

and energy source: 125 mM of methanol, 50 mM of trimethylamine, or 120 mM of sodium acetate.

Methane Production Assay

Methane in culture headspace was measured by gas chromatography using a flame ionization detector (GC-FID) as previously described [24]. Briefly, 10 mL cultures were grown to stationary phase. After growth, 100 µL of headspace was captured using a gastight Hamilton syringe and transferred to an empty crimped 2 mL autosampler serum vial (Wheaton, Millville, NJ, USA). Vial contents were analyzed by flame ionization using a custom Agilent 7890A Gas Chromatography System (Agilent Technologies, Santa Clara, CA, USA, 2010). The GC was equipped with an autosampler for consistent sample injection and utilized a GS CarbonPLOT column (Agilent Technologies, Santa Clara, CA, USA) at 145 °C for separation of volatile metabolites. Quantification of methane was achieved by comparison to a methane standard curve (Matheson, Lincoln, NE, USA) ran in parallel with experimental samples.

Isoprene Production Assay

The same GC-FID system as above was deployed to quantify isoprene [22]. M. acetivorans strains were grown in 10 mL cultures with 1 mL paraffin oil overlay in Balch tubes. Once grown to stationary phase, the oil was harvested and transferred to a 2 mL stoppered and crimped autosampler vial. The GC-FID method for isoprene quantification was as follows: 160 °C for 35 min, ramp to 200 °C at 75 °C/min for 20 min, ramp to 275 °C at 75 °C/min for 20 min, 275 °C for 5 min, ramp to 160 °C at 75 °C/min to equilibrate the system for the next run. Isoprene quantification was achieved using a standard of known volumes of isoprene injected into 1 mL of paraffin oil in a 2 mL autosampler vial.

Municipal Wastewater Handling

Municipal wastewater sludge was collected from the City of Lincoln Teresa Street Water Resource Recovery Facility (Lincoln, NE, USA) [22]. Two different sludges were collected anaerobically: one after primary anaerobic digestion, and another after secondary anaerobic digestion and settling (before dewatering, disinfection, and discharge). Aliquots (~50 g) were transferred to serum bottles and methanol (5 µL g−1) was added as appropriate. Sludge samples were inoculated with 10% (w/v) SWW starter cultures and incubated at 35 °C without shaking. Methane and isoprene synthesis were measured as described above except 10 mL paraffin oil overlay was added. Isoprene was detectable but not accurately measurable in the headspace when paraffin oil was omitted. Sludge was not autoclaved until experiments were completed.

Results

Adapting Methanosarcina acetivorans to Growth in Wastewater

A challenge when introducing a laboratory methanogen strain to a wastewater environment is their sensitivity to changes in osmolarity. M. acetivorans was originally isolated from marine sediment and grows best under high-salt conditions (400 mM NaCl). When introduced directly to a comparatively low solute environment such as wastewater M. acetivorans rapidly lyses. To counteract this phenomenon, strains had to first be adapted to growth in synthetic wastewater (SWW), a complex growth medium containing mixed carbohydrates, lipids, and proteins that mimics the composition of wastewater digester solids [23]. Cultures of M. acetivorans were gradually adapted by supplementing our high-salt (HS) media with 10% (v/v) of synthetic wastewater every 24

h until the media reached a ratio of 50:50 HS:SWW (8 days; final NaCl concentration was 100.06 mM). At this point the methanogens were passaged into SWW supplemented with MeOH and confirmed to grow without lysis via autofluorescence (Figure 2).

Measurement of Methane and Isoprene Production on Wastewater

Once growth was achieved in SWW, cells were transferred to wastewater biosolids pre- and postdigest effluent (before and after second-stage anaerobic digestion) from the Teresa Street Water Resource Recovery Facility in Lincoln, NE (Figure 3). Microcosms with and without methanol supplementation were incubated for 5 days at 35 °C, after which time methane and isoprene yields were quantified (Table 1). Methane was detected from predigest effluent whether or not methanol was added, indicating that substrates for methanogens (both wild and engineered strains) were present in the effluent (Figure 4).

Methane yield was higher in the postdigest effluent than the predigest effluent, which was anticipated because wild methanogens are enriched during the anaerobic digestion treatment step. When methanol was added to SWW, pre- or postdigester effluent the methane yields were comparable to methane yields when isolated strains are grown in defined medium [9]. No methane was detected when samples were heat-killed by autoclaving microcosms before inoculating with engineered M. acetivorans, suggesting active fermentation by the digester microbial community is necessary to produce substrate unless the microcosm is supplemented with methanol. Isoprene was not detected from predigest effluent microcosms or when wastewater was heat-killed by autoclaving. Isoprene production was observed in postdigest effluent microcosms with and without addition of methanol (Figure 4). With methanol supplementation, isoprene

yields were equivalent to SWW cultures, which was similar to the isoprene yield achieved by isolated strains grown in defined medium [9]. Based on these data we estimate up to $0.77 \pm 0.25\%$ of dissolved organic carbon in postdigest effluent was recovered as isoprene (Table 1). These data suggest engineered M. acetivorans can compete with wild methanogens in anaerobic digesters and isoprene can be detected in biogas from municipal waste. In pure batch culture the M. acetivorans ispS+ strain produces 0.89 mmol isoprene per mol methanol per gram of cells [9], which is 180× the yield of engineered Synechocystis cyanobacteria growing on CO_2 [25]. In comparison, E. coli and Saccharomyces have been engineered to produce 352 and 175 mM isoprene, respectively, from glucose under fed-batch conditions [26,27]. It is unknown whether any of these engineered strains can synthesize isoprene from digester effluent as has been demonstrated by M. acetivorans in this work. Additional studies are needed to develop a commercially viable process that optimizes isoprene recovery from wastewater digester biogas streams.

Discussion

Our results confirm the hypothesis that engineered Methanosarcina acetivorans can survive in municipal wastewater and produce isoprene at detectable levels. Methane production was greater in wastewater biosolids which had undergone anaerobic digestion compared with those samples grown in preanaerobic digestion biosolids. While there is an incidental enrichment process during fermentation over time, the majority of microbes found in municipal wastewater are known bacterial gut symbionts such as Proteobacteria, Firmicutes, and Bacteroides [28], as well as a diverse collection of methanogens

including Methanomicrobiales, Methanosarcinales, Methanobacteriales, and Methanobrevibacter spp. [29–31]. It has been well documented that these organisms exchange nutrients via syntrophy both in the gut and during wastewater treatment [32–35] and methanogen growth is dependent on metabolic byproducts of upstream microbial metabolism. The increase in methane production observed in samples grown in wastewater postanaerobic digestate suggests the engineered M. acetivorans ispS+ strains may be capable of participating in syntrophic relationships with other microbes in the digestate.

After four days of incubation at 35 °C methane was detected though no isoprene production was identified in samples grown in preanaerobic digested effluent, indicating that there may not be enough freely available methanogenic substrates for the engineered strains to compete with the existing microbial population. However, the postdigester effluent inoculated with our isoprene-producing M. acetivorans incubated under the same culture conditions yielded detectable bioisoprene (0.144 ± 0.273 mM). When this postdigest effluent was supplemented with 125 mM of MeOH the yield was increased to 0.968 ± 0.144 mM. This indicates that isoprene production from wastewater is primarily determined by the available substrate rather than environmental stressors. These results demonstrate that engineered methanogens are viable as a drop-in additive to wastewater treatment, and that the rate limiting factor for isoprene production is the rate at which the syntrophic microbial community can produce metabolites necessary for methanogen growth. By stimulating the microbial community, higher titers of bioisoprene production may be achieved.

Methanogens are a compelling source of renewable bioproducts due to their high substrate to product ratio efficiency. Here, we have demonstrated that with minor adaptation, it is possible to drop-in engineered methanogens to existing wastewater environments and attain value-added products in addition to the processing of wastewater. Due to existing capabilities for methane capture, many wastewater treatment facilities are already equipped with the infrastructure necessary for the capture of gaseous products such as isoprene. Separation of isoprene from biogas would require additional investment in biogas refining. However, isoprene separation from biogas streams is expected to be compatible with existing biogas upgrading technologies that are used to separate CO_2 and enrich methane content to produce renewable natural gas. Our results suggest there may be promising potential for utilizing methanogens as a platform for low-cost production of synthetic materials without expensive feedstocks or extensive modification of existing renewable natural gas facilities.

Acknowledgements

has disclosed a significant financial interest in RollingCircle Biotech, LLC and Molecular Trait Evolution, LLC.

References

1. Zinder, S.H. Physiological ecology of methanogens. In Methanogenesis; Springer: Boston, MA, 1993; pp. 128–206. doi: 10.1007/978-1-4615-2391-8_4.

2. Thauer, R.K.; Kaster, A.-K.; Seedorf, H.; Buckel, W.; Hedderich, R. Methanogenic archaea: Ecologically relevant differences in energy conservation. Nat. Rev. Microbiol. 2008, 6, 579–591.

3. Conrad, R. Microbial ecology of methanogens and methanotrophs. Adv. Agron. 2007, 96, 1–63.

4. Lyu, Z.; Shao, N.; Akinyemi, T.; Whitman, W.B. Methanogenesis. Curr. Biol. 2018, 28, R727–R732.

5. Schiraldi, C.; Giuliano, M.; De Rosa, M. Perspectives on biotechnological applications of archaea. Archaea 2002, 1, 75–86.

6. Tabatabaei, M.; Rahim, R.A.; Abdullah, N.; Wright, A.-D.G.; Shirai, Y.; Sakai, K.; Sulaiman, A.; Hassan, M.A. Importance of the methanogenic archaea populations in anaerobic wastewater treatments. Process Biochem. 2010, 45, 1214–1225, doi:10.1016/j.procbio.2010.05.017.

7. Chen, S.; Cheng, H.; Liu, J.; Hazen, T.C.; Huang, V.; He, Q. Unexpected competitiveness of Methanosaeta populations at elevated acetate concentrations in methanogenic treatment of animal wastewater. Appl. Microbiol. Biotechnol. 2017, 101, 1729–1738.

8.   Ferry, J.G.; Maranas, C.D.; Wood, T.K. Methane-to-Acetate Pathway for Producing Liquid Biofuels and Biorenewables. US20150147791A1, 28 May 2015.

9.   Aldridge, J.; Carr, S.; Weber, K.A.; Buan, N.R. Anaerobic production of isoprene by engineered Methanosarcina spp. archaea. Appl. Environ. Microbiol. 2021, doi:10.1128/AEM.02417-20.

10.   Elalami, D.; Carrere, H.; Monlau, F.; Abdelouahdi, K.; Oukarroum, A.; Barakat, A. Pretreatment and co-digestion of wastewater sludge for biogas production: Recent research advances and trends. Renew. Sustain. Energy Rev. 2019, 114, 109287.

11.   Vítězová, M.; Kohoutová, A.; Vítěz, T.; Hanišáková, N.; Kushkevych, I. Methanogenic Microorganisms in Industrial Wastewater Anaerobic Treatment. Processes 2020, 8, 1546.

12.   Lettinga, G. Anaerobic digestion and wastewater treatment systems. Antonie van Leeuwenhoek 1995, 67, 3–28.

13.   Sekiguchi, Y.; Kamagata, Y.; Harada, H. Recent advances in methane fermentation technology. Curr. Opin. Biotechnol. 2001, 12, 277–282.

14.   McCarty, P.L.; Bae, J.; Kim, J. Domestic wastewater treatment as a net energy producer—Can this be achieved? Environ. Sci. Technol. 2011, doi:10.1021/es2014264.

15.   Van Lier, J.B.; Mahmoud, N.; Zeeman, G. Anaerobic wastewater treatment. In Biological Wastewater Treatment: Principles, Modelling and Design; IWA Publishing: London, UK, 2008; pp. 415–456.

16.   Dionisi, D. Biological Wastewater Treatment Processes: Mass and Heat Balances; CRC Press: Boca Raton, FL, USA, 2017.

17. Galagan, J.E.; Nusbaum, C.; Roy, A.; Endrizzi, M.G.; Macdonald, P.; FitzHugh, W.; Calvo, S.; Engels, R.; Smirnov, S.; Atnoor, D. The genome of M. acetivorans reveals extensive metabolic and physiological diversity. Genome Res. 2002, 12, 532–542.

18. Ferry, J.G. Methanosarcina acetivorans: A Model for Mechanistic Understanding of Aceticlastic and Reverse Methanogenesis. Front. Microbiol. 2020, 11, 1806.

19. Sowers, K.R.; Boone, J.E.; Gunsalus, R.P. Disaggregation of Methanosarcina spp. and Growth as Single Cells at Elevated Osmolarity. Appl. Environ. Microbiol. 1993, 59, 3832–3839.

20. Metcalf, W.W.; Zhang, J.K.; Apolinario, E.; Sowers, K.R.; Wolfe, R.S. A genetic system for Archaea of the genus Methanosarcina: Liposome-mediated transformation and construction of shuttle vectors. Proc. Natl. Acad. Sci. USA 1997, 94, 2626–2631.

21. Zhang, J.K.; White, A.K.; Kuettner, H.C.; Boccazzi, P.; Metcalf, W.W. Directed mutagenesis and plasmid-based complementation in the methanogenic archaeon Methanosarcina acetivorans C2A demonstrated by genetic analysis of proline biosynthesis. J. Bacteriol. 2002, 184, 1449–1454.

22. Aldridge, J.; Carr, S.; Weber, K.A.; Buan, N.R. Production of Bioisoprene from Wastewater; NTRY6R14/4822; The Water Research Foundation: Denver, CO, USA, 2018.

23. OECD. Test No. 314: Simulation Tests to Assess the Biodegradability of Chemicals Discharged in Wastewater; OECD: Paris, France, 2008.

24. Aldridge, J.T.; Catlett, J.L.; Smith, M.L.; Buan, N.R. Methods for Detecting Microbial Methane Production and Consumption by Gas Chromatography. Bio Protoc. 2016, 6, e1779.

25.   Pade, N.; Erdmann, S.; Enke, H.; Dethloff, F.; Duhring, U.; Georg, J.; Wambutt, J.; Kopka, J.; Hess, W.R.; Zimmermann, R.; et al. Insights into isoprene production using the cyanobacterium Synechocystis sp. PCC 6803. Biotechnol. Biofuels 2016, 9, 89, doi:10.1186/s13068-016-0503-4.

26.   Yang, C.; Gao, X.; Jiang, Y.; Sun, B.; Gao, F.; Yang, S. Synergy between methylerythritol phosphate pathway and mevalonate pathway for isoprene production in Escherichia coli. Metab. Eng. 2016, 37, 79–91, doi:10.1016/j.ymben.2016.05.003.

27.   Yao, Z.; Zhou, P.; Su, B.; Su, S.; Ye, L.; Yu, H. Enhanced Isoprene Production by Reconstruction of Metabolic Balance between Strengthened Precursor Supply and Improved Isoprene Synthase in Saccharomyces cerevisiae. ACS Synth. Biol. 2018, 7, 2308–2316, doi:10.1021/acssynbio.8b00289.

28.   Cabezas, A.; de Araujo, J.C.; Callejas, C.; Galès, A.; Hamelin, J.; Marone, A.; Sousa, D.Z.; Trably, E.; Etchebehere, C. How to use molecular biology tools for the study of the anaerobic digestion process? Rev. Environ. Sci. Bio/Technol. 2015, 14, 555–593.

29.   Weiss, A.; Jérôme, V.; Freitag, R.; Mayer, H.K. Diversity of the resident microbiota in a thermophilic municipal biogas plant. Appl. Microbiol. Biotechnol. 2008, 81, 163–173.

30.   Karakashev, D.; Batstone, D.J.; Angelidaki, I. Influence of environmental conditions on methanogenic compositions in anaerobic biogas reactors. Appl. Environ. Microbiol. 2005, 71, 331–338.

31.   Ozgun, H.; Tao, Y.; Ersahin, M.E.; Zhou, Z.; Gimenez, J.B.; Spanjers, H.; van Lier, J.B. Impact of temperature on feed-flow characteristics and filtration performance

of an upflow anaerobic sludge blanket coupled ultrafiltration membrane treating municipal wastewater. Water Res. 2015, 83, 71–83.

32.   Catlett, J.L.; Catazaro, J.; Cashman, M.; Carr, S.; Powers, R.; Cohen, M.B.; Buan, N.R. Metabolic Feedback Inhibition Influences Metabolite Secretion by the Human Gut Symbiont Bacteroides thetaiotaomicron. mSystems 2020, 5, doi:10.1128/mSystems.00252-20.

33.   McInerney, M.J.; Sieber, J.R.; Gunsalus, R.P. Microbial syntrophy: Ecosystem-level biochemical cooperation. Microbe Mag. 2011, 6, 479–485.

34.   Sieber, J.R.; McInerney, M.J.; Gunsalus, R.P. Genomic insights into syntrophy: The paradigm for anaerobic metabolic cooperation. Annu. Rev. Microbiol. 2012, 66, 429–452.

35.   Worm, P.; Koehorst, J.J.; Visser, M.; Sedano-Núñez, V.T.; Schaap, P.J.; Plugge, C.M.; Sousa, D.Z.; Stams, A.J. A genomic view on syntrophic versus non-syntrophic lifestyle in anaerobic fatty acid degrading communities. Biochim. Biophys. Acta BBA Bioenerg. 2014, 1837, 2004–2016.
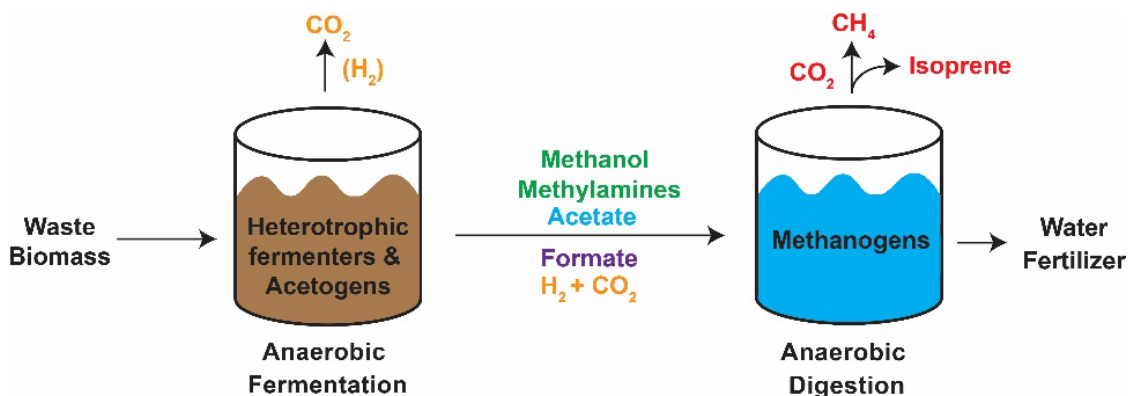
Figure 1. Schematic representation of anaerobic digestion of waste biomass at the Theresa Street Water Resource Recovery facility in Lincoln, NE. After aerobic incubation, waste biomass is anaerobically digested in a two-step process. First, the complex biomolecules are degraded through heterotrophic fermentation to less complex substrates for methanogenic growth in the second stage. In the methanogenic bioreactor dissolved organic carbon is converted to biogas that can be recouped as a biofuel. Introduction of isoprene-synthesizing methanogens (e.g., strain NB 394 in which plasmid pJA2 expressing isoprene synthase is integrated onto the chromosome) to the second stage digester has potential to produce renewable isoprene in the captured biogas.

(**a**) (**b**)
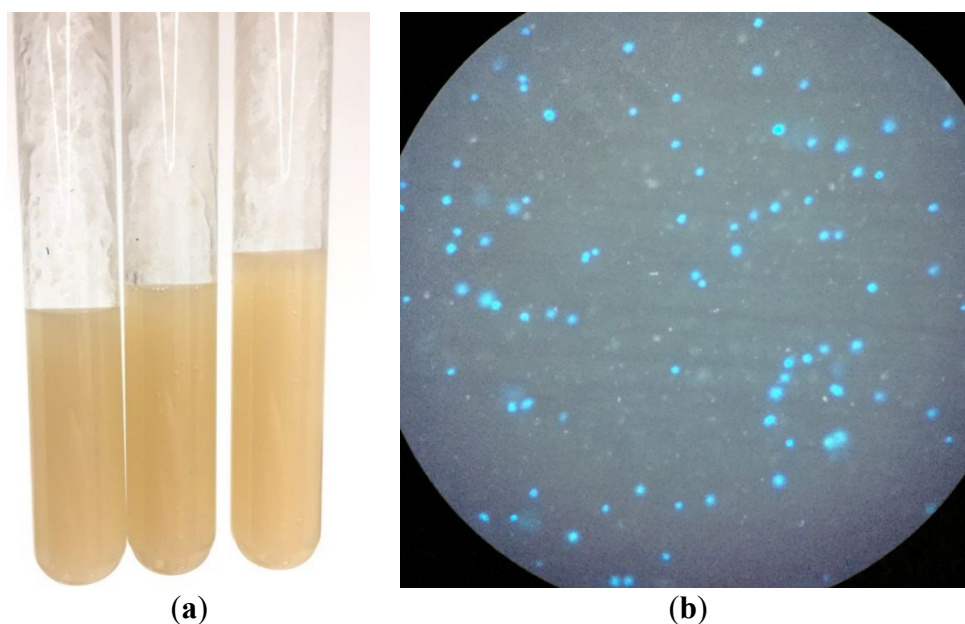
Figure 2. Engineered methanogens adapted to synthetic wastewater. (a) Inoculated synthetic wastewater (SWW) in anaerobic Balch tubes. (b) Confirmation of live engineered methanogens in SWW under 400× optical magnification. Viable methanogens are irregular cocci (0.5–1 μm diameter) that fluoresce blue through a DAPI filter when UV illuminated.

Figure 3. Municipal wastewater collected from the Theresa Street Water Resource Recovery Facility in Lincoln, Nebraska. (Left) Organic solids before anaerobic digestion. (Right) Organic solids after anaerobic digestion.

Table 1. Methane and isoprene production on wastewater biosolids.

		Synthetic Waste Water		Predigest Effluent		Postdigest Effluent	
		CH$_4$[a] Production					
Substrate	**Strain [b]**	**mmol L^{-1}**	**Std Dev**	**mmol L^{-1}**	**Std Dev**	**mmol L^{-1}**	**Std Dev**
MeOH [c]	*att:*VOC	84.64	6.19	80.98	7.34	89.87	2.94
	att:ispS	83.89	8.32	80.22	9.42	87.63	6.98
None	*att:*VOC	NT		33.85	1.64	31.36	12.30
	att:ispS	NT		26.36	2.74	54.82	4.57
Heat killed	*att:*VOC	ND		ND		ND	
	att:ispS	ND		ND		ND	
		Isoprene[a] Production					
Substrate	**Strain**	**mmol L^{-1}**	**Std Dev**	**mmol L^{-1}**	**Std Dev**	**mmol L^{-1}**	**Std Dev**
MeOH [c]	*att:*VOC	ND		ND		ND	
	att:ispS	0.972	0.301	ND		0.968	0.312
None	*att:*VOC	NT		ND		ND	
	att:ispS	NT		ND		0.144	0.273
Heat killed	*att:*VOC	ND		ND		ND	
	att:ispS	ND		ND		ND	

[a] Data were obtained from triplicate biological replicates and triplicate technical replicates (n = 9);
[b] *att:*VOC, parent strain in which vector only negative control (plasmid pNB730) was integrated onto the chromosome. *att:ispS*, strain in which plasmid pJA2 expressing isoprene synthase was integrated onto the chromosome;
[c] calculated from 125 mmol MeOH (e.g., 250 μL 100% MeOH added to 50 g digester solids) as described in the Materials and Methods (Section 2.5).
NT, Not tested. ND, Not detected.
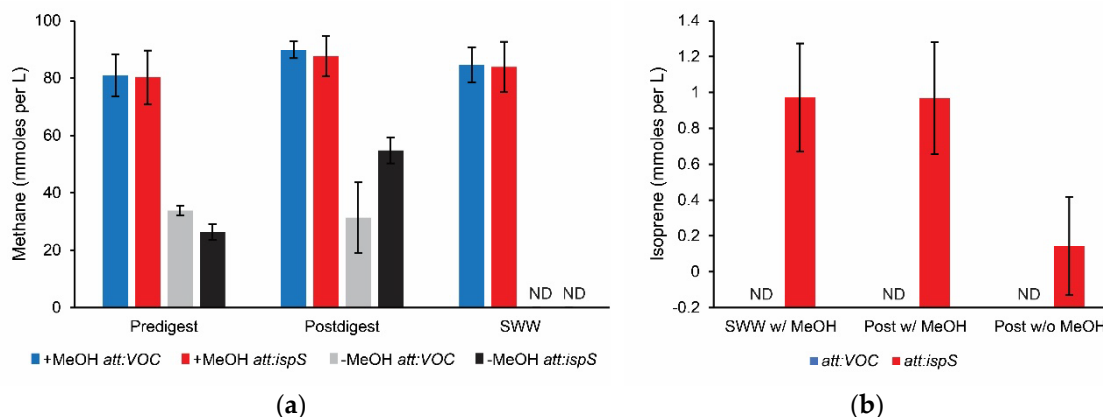
Figure 4. Methane and isoprene production from waste biosolids. Endpoint methane assays after *M. acetivorans* strains were added to unsterilized wastewater biosolids digestate or synthetic wastewater (SWW) amended with methanol. (**a**) Methane production by isoprene-producing *M. acetivorans* (*att:ispS*) and vector only control (*att:*VOC) strains added to predigest effluent, postdigest effluent, or SWW with (w/MeOH) and without (w/o MeOH) added methanol. (**b**) Isoprene production by *M. acetivorans att:*VOC and *att:ispS* strains added to SWW or postdigest effluent amended with methanol and postdigest effluent without added substrates. Blue, *att:*VOC strain in which empty vector pNB730 is integrated onto the chromosome. Red, *att:ispS* strain in which plasmid pJA2 expressing isoprene synthase is integrated onto the chromosome. All data were obtained from triplicate biological and technical replicates (n = 9).

Chapter 5: Expression of isoprene synthase in *Methanosarcina acetivorans* reveals energetic adaptations and links to amino acid biosynthesis.

This chapter to be submitted for publication

Abstract

Methane-producing archaea (methanogens) are a promising platform for biorefining due to their efficient central metabolism and use of inexpensive substrates. We engineered a strain of the methanogen *Methanosarcina acetivorans* to produce the volatile hemiterpene isoprene in addition to methane. Characterization of the engineered methanogen against a vector-only control showed no significant variation in growth rate, carrying capacity, or methane production despite the additional energetic burden and depletion of DMAPP, an essential lipid precursor. Differential expression analysis of the isoprene producing methanogens showed shifts in genes associated with membrane permeability and cellular energy conservation. A decrease was observed in genes associated with the uptake of sodium as well as C1 transporting cofactors while the proteins associated with the metabolic transition of purines between nucleotide and amino acid synthesis was upregulated. We propose this shift supports our hypothesis that the production of isoprene in *Methanosarcina acetivorans* is not treated as an increased burden but rather treated as a respiratory byproduct.

Introduction

      Methanogens, anaerobic methane producing archaea, are key organisms in the global carbon cycle and are predicted to play a major role in global carbon cycle and play a major role in climate change[1-3]. One of the most defining features of methanogens beyond the production of methane as a byproduct of their central respiration is their ability to efficiently grow utilizing low energy substrates as their primary carbon and energy source[4, 5]. In order to subsist on these low energy substrates, methanogens utilize a highly efficient central respiration strategy known as the Wolfe Cycle [1, 5, 6]. In the Wolfe Cycle, methanogenic substrates are reduced to methane and oxidized to carbon dioxide, driving the establishment of a chemiosmotic gradient through the coupling of cofactor regeneration with the transportation of H^+ and Na^+ ions which is harnessed for ATP synthesis (Figure 1) [1, 5, 7-9]. This cycle produces only a fraction of an ATP for each substrate molecule entering the pathway, which results in respiration reactions making up over 99% of the biochemistry carried out within the methanogen[4]. From a biotechnical standpoint, this is appealing as the emphasis on respiration over biomass accumulation drives a high substrate:product ratio so long as the desired product does not interfere with methanogenic homeostasis. Recently our laboratory examined the effects of introducing the gene for isoprene synthase, IspS, to observe how *Methanosarcina spp.* reacted to the energetic burden of producing a non-native metabolite [10, 11]. As isoprene is synthesized via the consumption of dimethylallyl pyrophosphate (DMAPP), the precursor to archaeal membrane biosynthesis, it was assumed that the production of isoprene would result in decreased growth rate or diminished biomass accumulation. However, it was observed that the isoprene producing strains did not show any significant decrease in growth rate, rather there was an increase in total biomass accumulation and a ~20% decrease in CO_2 production. This stoichiometric decrease in CO_2 production related to the 4% total substrate carbon being diverted towards isoprene production lead us to postulate that the production of isoprene is being linked to methanogenesis as a respiratory byproduct

rather than a secondary metabolite, fulfilling the metabolic purpose of CO_2 respiration in the regeneration of methanogenic cofactors, namely ferredoxin. To further understand how this phenotype is achieved and how the cells react to this new pathway, we performed transcriptomic analysis on the isoprene producing strains against a vector only control.

Methods

Strains and anaerobic culturing techniques. Anaerobic procedures were performed in a B-type Coy anaerobic chamber (Coy Labs, Grass Lake, MI). The internal gas composition of the anaerobic chamber is maintained at 5% H_2 / 20% CO_2 / 75% N_2 ($\pm$ 3%). An isoprene producing strain, NB394 (Δhpt::φC31 *int, att*:pJA2), and an isogenic vector only control strain, NB452 (Δhpt::φC31 *int, att*:pNB730) were grown in triplicate in high salt (HS) media supplemented with methanol as a carbon and energy source [200 mM NaCl, 45 mM NaHCO$_3$, 13 mM KCl, 54 mM MgCl$_2$•6H$_2$O, 2 mM CaCl$_2$•2H$_2$O, 2 μM 0.1% resazurin (w v^{-1}), 5 mM KH$_2$PO$_4$, 19 mM NH$_4$Cl, 2.8 mM cysteine•HCl, 0.1 mM Na$_2$S•9H$_2$O, trace elements, vitamin solution, 125mM methanol] as previously described [12]. Cells were inoculated in the anaerobic chamber and incubated outside of the chamber in glass Balch tubes sealed with butyl rubber stoppers (Belco Glass, Vinelane, NJ) at 35° until late exponential phase (OD$_{600}$ 7.0-8.0).

RNA Sequencing

The cells were harvested with TRI Reagent™ (Invitrogen™) according to the manufacturers' protocol. RNA quantity and purity were measured via Nanodrop before transportation to GeneWiz for sequencing (Table 1). RNA integrity was assayed via agarose gel and revealed no significant degradation or contamination (Figure 2). The RNA was treated with DNase before ribosomal RNA depletion using Ribo-Zero Plus rRNA Depletion kit (Illumina) according to the standard protocol. The treated RNA was sequenced on an Illumina HiSeq

providing paired-end 2x150bp sequencing (Azenta Life Sciences, South Plainfield, NJ). The samples produced 396,282,199 reads with a mean quality score of 38.3 and 92% of the reads being ≥30. With help from the UNL Bioinformatics core facility, reads were mapped against the canonical genome of *Methanosarcina acetivorans* C2A (GCA_000007345) using Bowtie2 as described by Owens et al. [13] resulting in a coverage of 97.32%. It should be noted that the genome of C2A contains slight variations from the parental strain used to create these strains (NB34) including the addition of a phage integration (φC31*)* site and recombinase expression cassette where the plasmids integrated [14]. Differential expression analysis was carried out using DESeq2 with a significance cutoff of <P=0.05 [15].

Results

The RNA sequences mapped against the *M. acetivorans* C2A genome revealed 4914 protein coding genes. Differential expression analysis was performed using DEseq2 revealing 55 significant differentially expressed genes (Figure 3, Table 2) and 73 significantly differentially expressed non-coding RNAs. The most highly upregulated genes were those associated with the tryptophan biosynthesis pathway (Figure 4).

Filtering out any genes with a differential expression of less than 2-fold and factoring a 5% false discovery rate, the pool of differentially expressed genes were narrowed down to the top 14 most significantly expressed (Figure 5, Table 3). Many of the genes previously identified as differentially expressed via qRT-PCR previous [10] did not meet the significance cutoff. This could have been a result of variations in preparation or a biproduct of selecting only a handful of select genes rather than surveying the entire transcriptome. Among the most downregulated genes in isoprene producing methanogens were the genes encoding for an aldolase associated with the production of methanopterin (figure 6), an important methanogenic cofactor which facilitates the

C1 transportation from substrates through the reduction to a methyl group as well as genes associated with the import of sodium and a Zn^{2+}/Mn^{2+} permease. The Zn^{2+}/Mn^{2+} permease is part of a larger metal transport operon promoted by a metal dependent transcriptional regulator. A decrease in the production of these enzymes would result in a less permeable cellular membrane and restrict the flow of the Na^+ ions to import through the membrane bound ATPase. Additionally downregulated was an uncharacterized MA1715-like protein which contains domains required for optimum growth in methanogens with sulfide as the sole sulfur source.

Genes upregulated in isoprene producing *M. acetivorans* included several proteins of unknown function. An inorganic pyrophosphatase was upregulated not as part of any known operon as well as a molybdopterin synthase associated with molybdenum cofactor biosynthesis. An operon containing the initiation factor IF-2 as well a DNA binding protein and 5-formaminoimidazole-4-carboxamide-1-(beta)-D-ribofuranosyl 5'-monophosphate synthetase was upregulated indicating an increase in ribosomal recruitment for the translation of mRNA. The upregulation of PurP (GeneID 1475582) is of particular interest as this gene is considered a signature gene of archaea [16]. Increased expression of PurP is significant as it is responsible for the branching point in purine biosynthesis between amino acid biosynthesis and the IMP and subsequently AMP, ADP, and ATP. Increased expression of PurP would correlate with increased energetic flexibility, allowing for the diverting of carbon and nitrogen from amino acid biosynthesis to energy as required by the cell. It would be worthwhile to assay whether this increase in expression correlates to increased enzymatic activity utilizing the Bratton-Marshall assay [17] in isoprene producing cells as an increase in metabolic flexibility could be relevant for future trait stacking experiments.

Discussion

Central methanogenesis is a highly efficient respiratory pathway with very little energetic latitude for change. Of the 4914 protein coding genes identified only a small percentage of these were found to be differentially expressed in *Methanosarcina acetivorans* strains producing bioisoprene. This indicates that isoprene biosynthesis does not have a major impact in the overall functioning of the organism, elicit a stress response, or interfere with central methanogenesis. With the expression of IspS and the production of isoprene we expected either a decrease in growth rate as a response to the depletion of dimethylallyl pyrophosphate (DMAPP) the precursor to isoprenoid lipid formation in archaea or a diminished final carrying capacity as a result of carbon destined for cellular division was diverted towards a non-usable volatile compound. However, phenotyping and metabolic flux analysis revealed no significant variation in growth rate or carrying capacity [10]. Flux balance analysis revealed 4% of substrate carbon being allocated towards the production of isoprene and a 20% decrease in CO_2 production. This stoichiometric shift in flux indicates the carbon which would otherwise be directed towards the oxidation of methyl substrates towards CO_2 is instead being diverted towards isoprene production. The energetic limitations and highly consistent nature of methanogenesis suggest that without the reducing equivalents generated through the oxidation of methyl substrates the generation of methane would not be possible [6, 18]. However, no decrease in methane production was observed in methane producing *Methanosarcina acetivorans*. This left us with the hypothesis that the production of isoprene was serving the metabolic function of the oxidation of methyl substrates to CO_2.

Given the energetic limitations of methanogenesis, when analyzing the differential expression of genes between isoprene producing *M. acetivorans* and a vector only control we were cognizant of the expression of stress response genes. The response of methanogenic archaea towards various stressors has been documented including those in response to heat, oxygen, pH,

osmotic shift, nutritional variation, heavy metals, and antibiotic stressors [19, 20]. If the expression of isoprene synthase and the production of isoprene depleted metabolite pools we would have seen an increase in expression of the genes associated upstream of those metabolites to increase their abundance and to relieve the metabolic bottleneck. No genes associated with either the mevalonate pathway or lipid biosynthesis was observed. In bacteria which have been engineered express a heterologous mevalonate pathway toxicity was observed as a result of the accumulation of diphosphates [21]. The generation of excess PPi did not seem to generate any cytotoxic response though the increased expression of the inorganic diphosphatase does reflect the cell utilizing the available free diphosphate generated as a result of the conversion of DMAPP to isoprene. There was no detected protein stress response such as an increase in the expression of chaperone proteins including Hsp70, Hsp60, or Hsp40 as well as no increase in genes associated general stress reduction [22, 23], or most importantly starvation [24]. If the synthesis of isoprene is an energetic burden to the cell we would expect to see an increase in genes associated with the ATP synthesis to make up for the deficit. This response would have elicited an increase in genes associated with the incomplete TCA cycle found in methanogens [25, 26] or have facilitated an upregulation of genes associated with central methanogenesis to generate the required reducing equivalents to stimulate the required to generate ATP through membrane found ATPases [5, 6]. We did not observe any significant upregulation in any of those genes. We did observe a significant decrease in the expression of an aldolase associated with the biosynthesis of methanopterin [27] and the sodium symporter PutP. The decrease in expression of genes associated with the chemiosmotic gradient responsible for the regeneration of methanogenic cofactors as well as ATP biosynthesis further supports our previous assessment that the production of isoprene is treated by the cell as an alternative respiratory pathway. Both methanopterin and PutP are involved in the utilization of ferredoxin (Fd) whose regeneration drives the methanogen's membrane bound ATPase.

The change in expression for redox carriers and an increase in genes associated with purine and amino acid biosynthesis as a result of a product of the Mevalonate pathway is interesting. All chemistry in a methanogen is tied back to methanogenesis via either redox carriers or ATP generation[4]. A key component in this pathway is the regeneration of redox carrier ferredoxin from its reduced to its oxidized state through the utilization of the enzyme complex Rnf [6, 18, 28]. The energy required for the reaction is driven by the export of Na^+ ions which would have been affected by the downregulation of PutP, reducing Na^+ concentration in the cell. We have theorized that the synthesis of isoprene is able to fulfil the role of regenerating ferredoxin during the Mg^{2+} assisted phosphatase reaction which forms isoprene (Figure 7). This would also explain the decrease the expression of the Zn^{2+} and Mn^{2+} permease found in *M. acetivorans* which would decrease the metallic ions cell-wide.

The increase in expression of genes associated with the metabolic routing of purine backbones between nucleotide and amino acid synthesis is interesting as it could allow for more flexibility between energy production and amino acid biosynthesis. Of all of the genes associated with amino acid synthesis, the increase in tryptophan biosynthesis is curious as the TRP pathway is an important regulator in nitrogen utilization in the cell and indicates the potential for further genetic engineering in that pathway. Tryptophan is the most energetically costly of the amino acids to produce and is tightly regulated in most organisms, often with regulation imposed upon multiple levels [29-31]. In methanogens, the biosynthesis of tryptophan appears to be regulated both from a transcriptional level but also through the interactions with small RNAs [32, 33]. That these engineered methanogens appear to be enhancing expression of tryptophan biosynthetic genes could indicate the pushing of carbon towards this branch of metabolism. Although methanogens do not natively produce terpenes, this indicates that further engineering could be utilized to produce higher ordered terpenes while sidestepping the sequestration of metabolic precursors necessary for membrane biosynthesis. This is promising as an increase in flux through

the tryptophan biosynthetic pathway could lead to higher metabolite pools for (3-indolyl)-glycerol phosphate, opening the door to the biosynthesis of indole diterpene alkaloids alongside terpenoid backbones generated through a modified mevalonate pathway.

It should be noted that changes in abundance of transcripts most likely corresponds to changes in protein levels, the magnitude of the correlation is often variable and difficult to predict [34, 35]. Further investigations into the direct shift in protein abundance is required to validate these results as well as an in-depth analysis of the small non-coding RNAs found to be significantly varied in isoprene producing methanogens.

Conclusions: Isoprene production in the engineered methanogen *M. acetivorans* showed unexpected variation in genes associated with membrane permeability and energy conservation. The lack of change in growth-phenotype as well as no significant increase in genes associated with stress response indicates the cell is not treating the production of isoprene as a burden. Shifts in energy conservation mechanisms such as an increase in the metabolic router between amino acid and nucleotide biosynthesis indicate an increased flexibility between energy production and biomass accumulation. The limitation of multiple ion channels suggests a restriction of sodium uptake to the energy producing ATPase which could denote an alternative method for increasing energetic efficiency. The varied response from multiple, seemingly distantly related pathways further emphasizes the importance of systems level analysis in organisms with novel introduced metabolic pathways.

Figures and tables
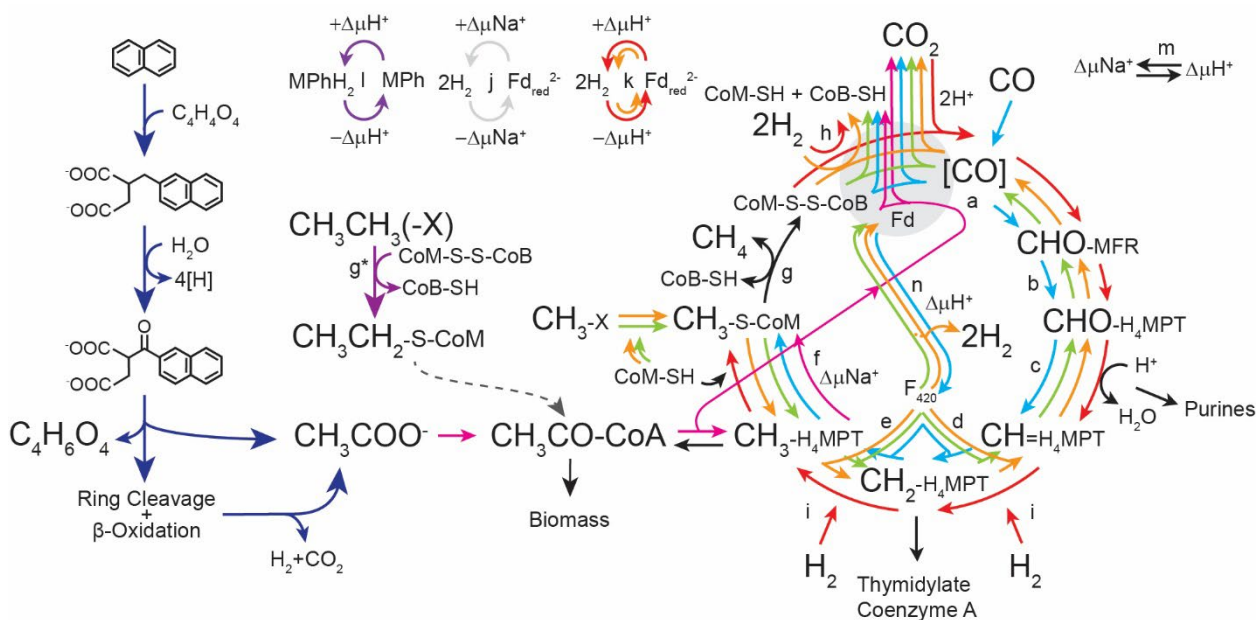
Figure 1: The Wolfe Cycle of methanogenesis[4]

The direction of arrows represents the direction of biochemical reactions. Reactions which are

utilized in every methanogenic pathway are represented in black. Hydrogenotrophic

methanogenesis is represented in red. Methyl respiration is represented in orange. Methylotrophic

methanogenesis is represented in green. Acetoclastic methanogenesis is represented in fuchsia.

Degradation of polyaromatic hydrocarbons is represented in dark blue [36]. Ethylene and long

chain alkane reduction is represented in purple [37]. Carboxydotrophic methanogenesis is

represented in cyan. CoB-SH, coenzyme B thiol; CoM-SH, Coenzyme M thiol; CoM-S-S-CoB,

coenzyme M-coenzyme B heterodisulfide; Fd, ferredoxin; Fd_{red}, reduced ferredoxin; H_4MPT,

tetrahydromethanopterin; MFR, methanofuran; MPh, methanophenazine; $MPhH_2$, reduced

methanophenazine. Enzymes involved in the Wolfe Cycle: a) Formyl-methanofuran

dehydrogenase (Fmd), b) Formyl-methanofuran:H_4MPT formyl transferase (Ftr), c) Methenyl-

H_4MPT cyclohydrolase (Mch), d) F_{420}-dependent Methylene-H_4MPT dehydrogenase (Mtd), e)

F420-dependent Methylene-H_4MPT reductase (Mer), f) Methyl-H_4MPT:coenzyme M

methyltransferase (Mtr), g) Methyl-coenzyme M reductase (Mcr), g*) Atypical methyl-coenzyme

M reductase (Mcr) [38], h) Electron-bifurcating hydrogenase:heterodisulfide reductase complex

(Mvh:HdrABC), i) F_{420}-reducing hydrogenase (Frh), j) Energy-converting sodium pumping

ferredoxin hydrogenase, k) Ferredoxin reducing hydrogenase (Eha/Ech), l) Proton-translocating

methanophenazine:heterodisulfide reductase (HdrED), m) Sodium–proton antiporter (MrpA), n)

F_{420} proton-pumping methanophenazine reductase (Fpo).

Table 1. Yield and purity of RNA samples assessed via NanoDrop spectrophotometer.

Sample Name	Harvest Yield (NG/uL)	260/280	260/230
Iso1	2861.42	2.01	2.18
Iso2	678.99	2.04	1.98
Iso3	2357.49	2.02	2.20
Voc1	3241.45	2.03	2.14
Voc2	3406.78	2.01	2.08
Voc3	2744.50	2.16	2.16
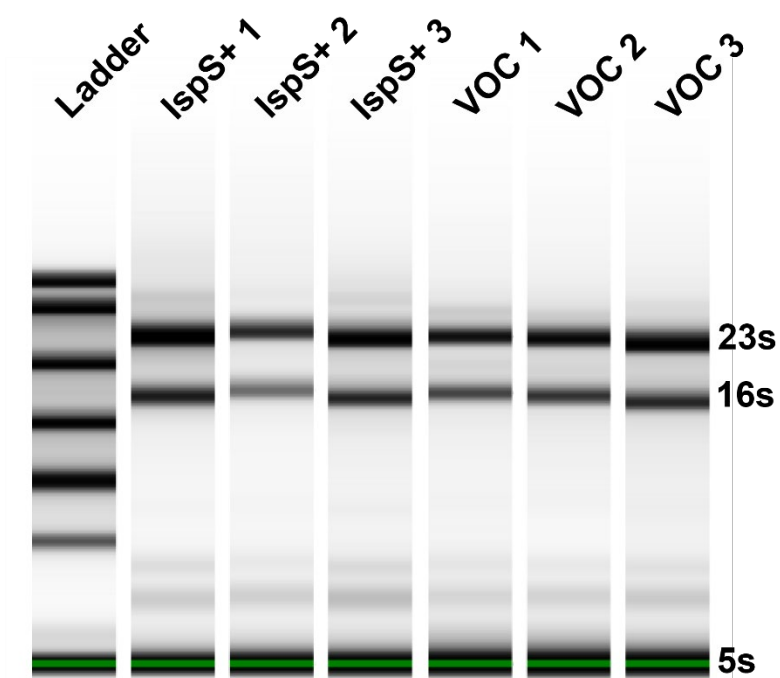
Figure 2. Confirmation of RNA integrity prior to cDNA synthesis. Total RNA from isoprene producing strains (*att:ispS*) and a vector only control (VOC) strains were harvested via TRI Reagent and run on an agarose gel. The presence of defined 23s, 16s, and 5s bands without smearing indicates high quality RNA without any significant degradation.
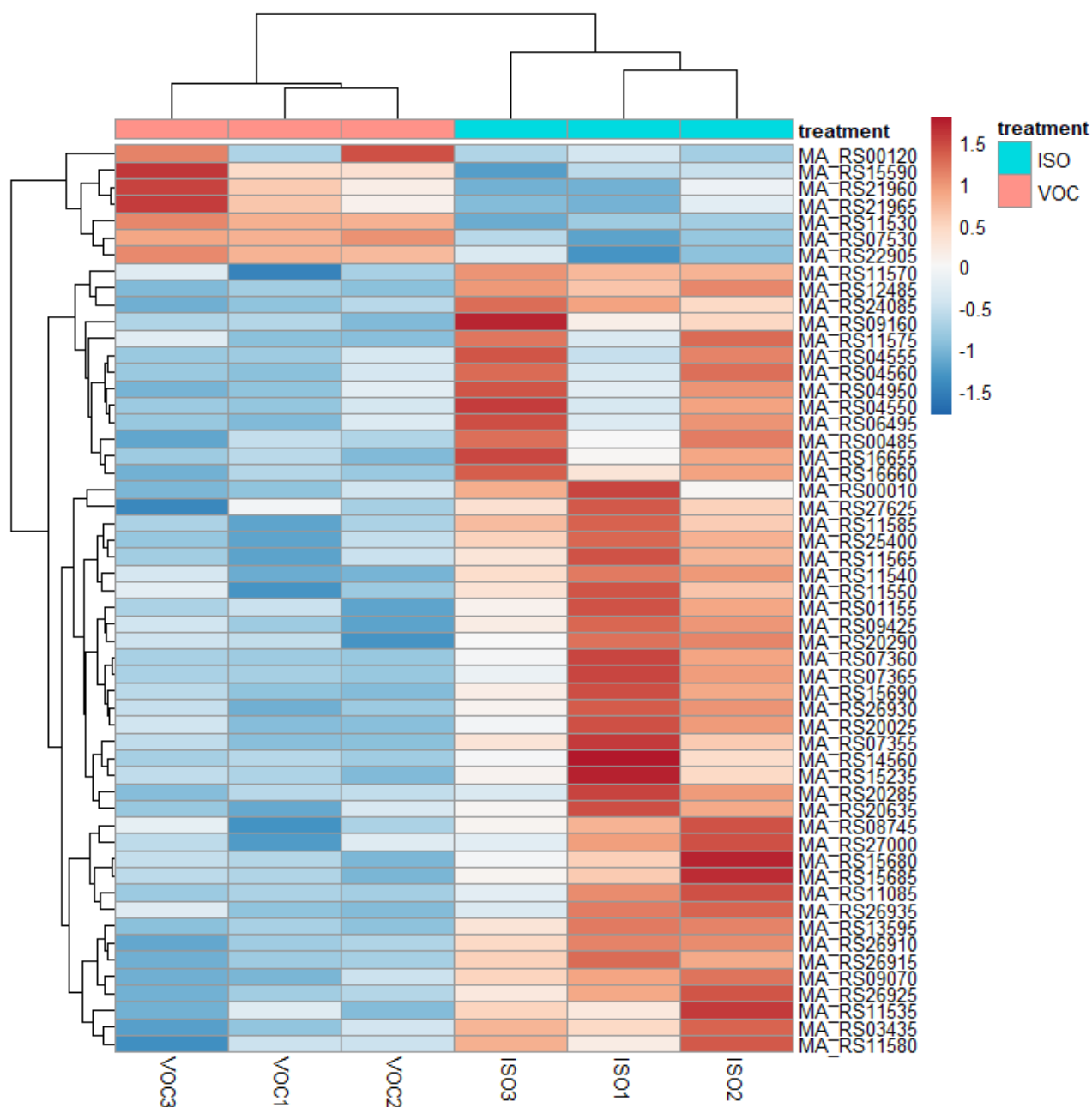
Figure 3. Heatmap of significantly expressed genes in isoprene producing methanogens compared against a vector only control. The first three columns on the left (coral) indicate *M. acetivorans* containing only the vector backbone (VOC) whereas the three columns on the right (teal) indicate isoprene producing *M. acetivorans* (ISO). Genes shaded blue represent a decrease in expression compared with the vector only control whereas genes shaded red indicate increased expression in isoprene producing *M. acetivorans*.

Table 2. Differentially expressed genes in isoprene producing methanogens.

GeneID	Gene MA_RS#	log2 Fold Change	pvalue	padj	Annotation
1474886	MA_RS15690	4.57	5.64E-14	6.92E-11	indole-3-glycerol-phosphate synthase
1473305	MA_RS07355	4.32	2.54E-06	0.000541	hypothetical protein
1474884	MA_RS15680	3.89	0.000127	0.013862	tryptophan synthase subunit alpha
1474885	MA_RS15685	3.81	1.94E-09	9.53E-07	tryptophan synthase subunit beta
1473306	MA_RS07360	3.66	1.10E-11	7.73E-09	ABC transporter ATP-binding protein
1473307	MA_RS07365	3.33	5.36E-10	2.92E-07	energy-coupling factor transporter transmembrane protein EcfT
1473574	MA_RS08745	2.18	5.44E-05	0.007026	metallophosphoesterase
1474119	MA_RS11565	2.14	5.82E-09	2.38E-06	tyrosine-type recombinase/integrase
1472842	MA_RS04950	2.12	1.34E-05	0.002271	iron ABC transporter substrate-binding protein
43446072	MA_RS26935	2.03	0.000146	0.015289	hypothetical protein
1474295	MA_RS12485	2.00	6.11E-20	1.50E-16	ISL3-like element ISMac21 family transposase
1472767	MA_RS04555	1.98	3.67E-05	0.005006	hypothetical protein
1472768	MA_RS04560	1.95	9.20E-06	0.001736	hypothetical protein
1474112	MA_RS11535	1.90	4.81E-06	0.000984	tyrosine-type recombinase/integrase
24782598	MA_RS00485	1.80	3.33E-07	0.000102	hypothetical protein
43446071	MA_RS26930	1.79	4.07E-07	0.000117	hypothetical protein
43446070	MA_RS26925	1.77	0.000196	0.019276	hypothetical protein
1474113	MA_RS11540	1.77	2.36E-09	1.05E-06	hypothetical protein
43446067	MA_RS26910	1.74	1.58E-12	1.29E-09	hypothetical protein
1473139	MA_RS06495	1.73	3.67E-05	0.005006	methyltransferase domain-containing protein
1474802	MA_RS15235	1.70	1.32E-05	0.002271	SAM-dependent methyltransferase
1474121	MA_RS11575	1.65	6.73E-05	0.00846	hypothetical protein
1474123	MA_RS11585	1.65	8.16E-11	5.01E-08	DUF927 domain-containing protein
43446068	MA_RS26915	1.64	1.16E-12	1.14E-09	hypothetical protein
1475849	MA_RS20635	1.62	8.82E-05	0.010558	sodium/proline symporter PutP
1472766	MA_RS04550	1.54	0.00012	0.013656	PQQ-binding-like beta-propeller repeat protein
1474116	MA_RS11550	1.54	9.04E-06	0.001736	hypothetical protein
1474021	MA_RS11085	1.53	1.06E-05	0.001929	Fic family protein
43446085	MA_RS27000	1.44	0.000616	0.045767	hypothetical protein
1474122	MA_RS11580	1.44	1.73E-05	0.002835	hypothetical protein
1476509	MA_RS24085	1.41	9.07E-07	0.000234	2-isopropylmalate synthase
1475732	MA_RS20025	1.34	1.98E-05	0.003138	hypothetical protein
1472545	MA_RS03435	1.30	5.27E-07	0.000144	hypothetical protein
43446210	MA_RS27625	1.25	0.000298	0.025173	hypothetical protein

1474120	MA_RS11570	1.25	2.38E-06	0.000532	AAA family ATPase
3362158	MA_RS20285	1.23	0.000266	0.024171	sodium/proline symporter PutP
3362133	MA_RS01155	1.20	0.00041	0.032439	sodium/proline symporter PutP
1474675	MA_RS14560	1.19	0.000308	0.025451	class I SAM-dependent methyltransferase
32154456	MA_RS25400	1.17	2.31E-07	7.55E-05	translation initiation factor eIF-1A
1471895	MA_RS00010	1.14	4.81E-05	0.006372	sodium/proline symporter PutP
1474498	MA_RS13595	1.13	1.21E-07	4.42E-05	tetratricopeptide repeat protein
3362159	MA_RS20290	1.11	0.000202	0.01944	sodium/proline symporter PutP
1473635	MA_RS09070	1.11	1.26E-07	4.42E-05	ABC transporter ATP-binding protein
1475083	MA_RS16660	1.09	1.91E-06	0.000447	sodium/proline symporter PutP
1473651	MA_RS09160	1.04	0.000445	0.03414	nickel-responsive transcriptional regulator NikR
3362146	MA_RS09425	1.04	2.32E-05	0.003562	sodium/proline symporter PutP
1475082	MA_RS16655	1.01	0.000244	0.022976	MarR family transcriptional regulator
1476274	MA_RS22905	-1.29	3.00E-05	0.004332	methylamine methyltransferase corrinoid protein reductive activase
1476102	MA_RS21965	-1.36	0.000158	0.016116	P-II family nitrogen regulator
24782985	MA_RS15590	-1.53	2.90E-05	0.004319	hypothetical protein
1476101	MA_RS21960	-1.65	0.000283	0.024788	ammonium transporter
24782745	MA_RS07530	-2.19	4.40E-18	7.20E-15	hypothetical protein
1471916	MA_RS00120	-2.29	0.000146	0.015289	ABC transporter ATP-binding protein
1474111	MA_RS11530	-2.71	2.99E-30	1.47E-26	sodium/proline symporter PutP
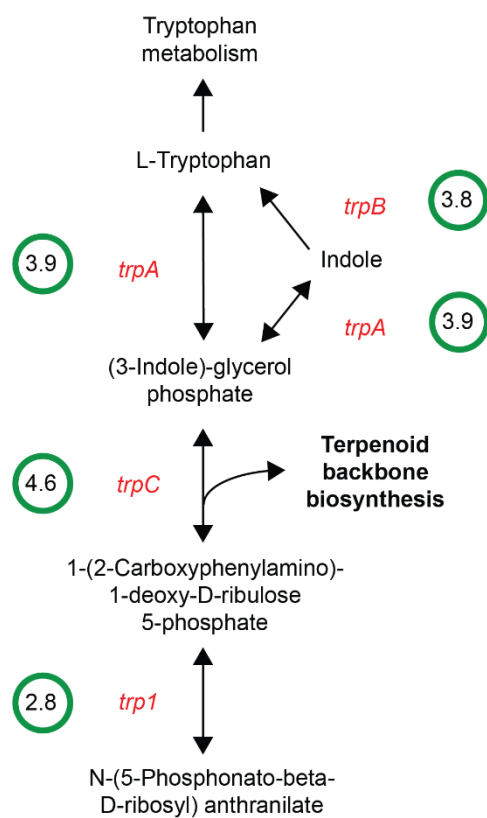
Figure 4. Upregulated genes associated with tryptophan biosynthesis in isoprene producing

Methanosarcina acetivorans. The genes involved in tryptophan biosynthesis are indicated in red,

Phosphoribosyl-anthranilate isomerase (trp1), tryptophan biosynthesis protein subunit A (trpA),

tryptophan biosynthesis protein subunit B (trpB), tryptophan biosynthesis protein subunit C

(trpC). The green circles indicate the fold change increase in expression of the genes.
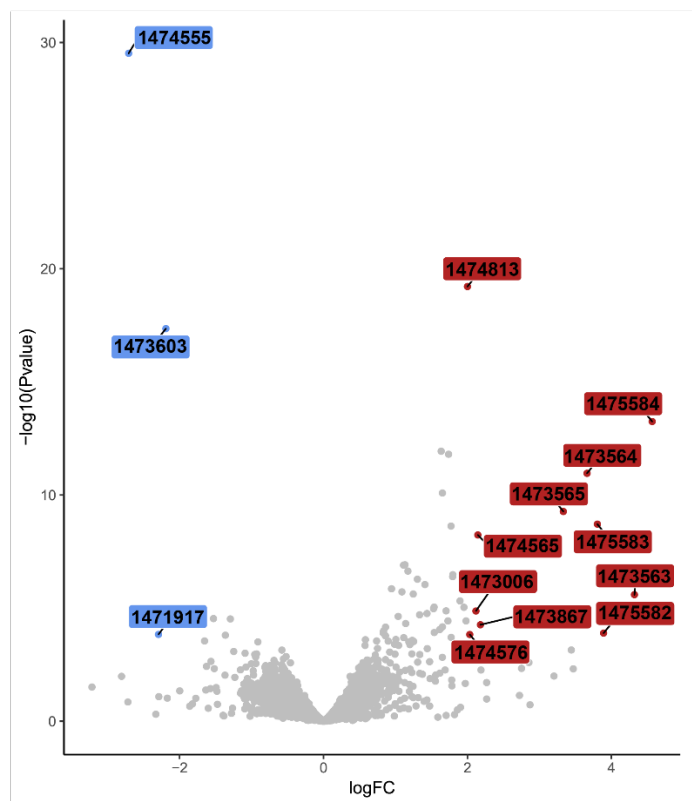
Figure 5. Most significantly differentially expressed genes in isoprene producing *M. acetivorans*. The X-axis indicates log-fold change with genes downregulated in isoprene producing *M. acetivorans* on the left and upregulated genes on the right. The Y-axis indicated the magnitude of significance of the of the differential expression. Genes significantly downregulated are colored blue whereas genes significantly upregulated are represented in red. Genes either below 2-fold change in expression or below a significance of p=0.05 are shaded grey.

Table 3. Most significantly differentially expressed genes in isoprene producing *M. acetivorans*

in figure 5. A blue dot indicates which were downregulated in isoprene producing *M. acetivorans*

whereas a red dot indicates genes which were upregulated.

Gene ID	P Value	Log Fold Change	Gene Name	Function	Genome Context
1474555●	2.99E-30	-2.71	Aldolase	Sugar metabolism, methanopterin synthesis. Methanopterin is a primary coenzyme responsible for C1 transport during methanogenesis.	Monocistronic
1473603●	4.40E-18	-2.19	Uncharacterized MA1715-like protein	Required for optimum growth with sufide as the sole sulfur source.	Monocistronic
1471917●	0.000146	-2.29	Metal ABC transporter permease	Mn2+/Zn2+ transport system	Part of a potential metal transport operon promoted by

				permease component.	a GeneID 1471914, a metal-depented transcriptional regulator.
1474813●	6.11E-20	2.00	Hypothetical	Unknown.	Monocistronic
1474576●	0.000146	2.03	SDR family oxidoreductase	Short chain NAD-/NADP-dependent oxidoreductase.	Part of an operon otherwise filled with Domains of Unknown Function. Unknown regulator.
1473006●	1.34E-05	2.12	ABC transporter permease	Contains SalY domain which in other organisms functions as an antimicrobial peptide transport system.	Part of an operon regulated by GeneID 1473010, a MarR family transcriptional regulator.
1474565●	5.82E-09	2.15	Inorganic diphosphatase	Pyrophosphatase	Monocistronic
1473867●	5.44E-05	2.18	Molybdopterin synthase	Cofactor synthesis, redox regulation	Co-transcribed with GeneID1473866, a molybdenum cofactor guanylyltransferase

1473565●	5.36E-10	3.33	APC family permease.	Permease	Co-transcribed with hypothetical protein GeneID 1473565
1473564●	1.10E-11	3.66	Hypothetical protein.	Unknown	Co-transcribed with GeneID 1473564
1475583●	1.94E-09	3.81	IF-2 subunit gamma.	Translation initiation factor. GTPase associated promoting ribosomal initiation complex to facilitate translation of mRNA to protein [39].	Part of operon containing DNA-directed RNA polymerases (GeneIDs 1475586, 1475584, and 1475585), a DNA binding proteins (GeneID 1475584), a protein containing domains of unknown function (GeneID 1475580), and the gene encoding 5-formaminoimidazole-4-carboxamide-1-(beta)-D-ribofuranosyl 5'-monophosphate

					synthetase (GeneID1475582).
1475582●	0.000127	3.89	5-formaminoimidazole-4-carboxamide-1-(beta)-D-ribofuranosyl 5'-monophosphate synthetase.	Signature archaeal gene associated with purine metabolism. Important metabolic regulator determining carbon flux between energy generation and amino acid synthesis [16].	Part of operon containing DNA-directed RNA polymerases (GeneIDs 1475586 and 1475585, 1475584), a DNA binding proteins (GeneID 1475584), a protein containing domains of unknown function (GeneID1475580), and the gene encoding for IF-2 subunit Gamma (GeneID 1475583).
1473563●	2.54E-06	4.32	TauE/SafE family protein.	Membrane-bound protein associated with the export of sulfite [40].	Monocystronic

| 1475584● | 5.64E-14 | 4.57 | DNA-binding protein. | Contains PIN-like domain potentially associated with DNA replication and repair, mRNA degradation, transcriptional regulation, and ncRNA maturation [41]. | Part of operon containing other DNA-directed RNA polymerases (GeneIDs 1475586 and 1475585), a DNA binding proteins (GeneID 1475584), a protein containing domains of unknown function (GeneID 1475580), the gene encoding for IF-2 subunit Gamma (GeneID 1475583), and the gene encoding 5-formaminoimidazole-4-carboxamide-1-(beta)-D-ribofuranosyl 5'-monophosphate synthetase (GeneID 1475582). |

Figure 6. Structure of methanopterin. Methanopterin is an essential coenzyme in methanogenesis responsible for the transfer of methyl groups during the reduction into methane or oxidation into CO_2.
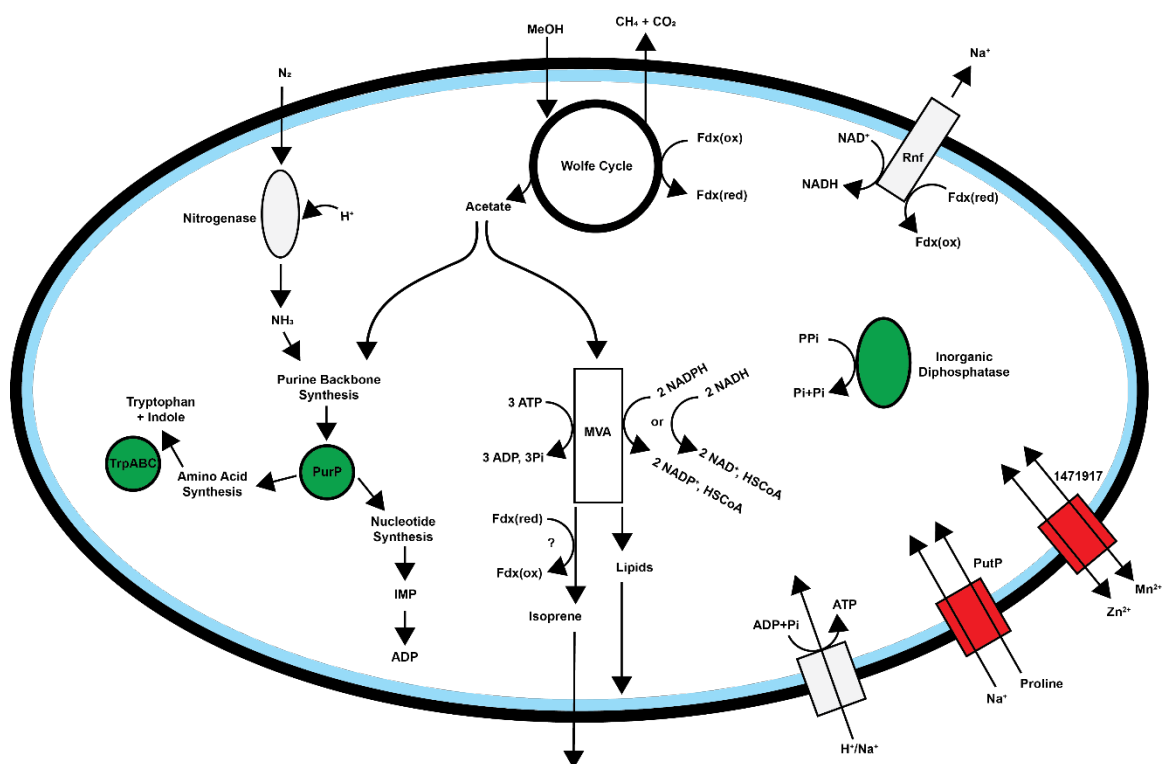
Figure 7. Effect of isoprene production on metabolite and redox flux *M. acetivorans*. The blue ring represents the methanogen cell membrane. Proteins encoded by genes which

showed decreased expression in isoprene producing *M. acetivorans* are represented in

red. Proteins encoded by genes which showed increased expression in isoprene producing

M. acetivorans are shown in green. MVA; mevaolate pathway. Fd; ferredoxin.

References

1.	Ferry, J.G., *Methanogenesis: ecology, physiology, biochemistry & genetics*. 2012: Springer Science & Business Media.

2.	Balch, W., et al., *Methanogens: reevaluation of a unique biological group.* Microbiological reviews, 1979. **43**(2): p. 260.

3.	Cavicchioli, R., et al., *Scientists' warning to humanity: microorganisms and climate change.* Nature Reviews Microbiology, 2019. **17**(9): p. 569-586.

4.	Buan, N.R., *Methanogens: pushing the boundaries of biology.* Emerging Topics in Life Sciences, 2018. **2**(4): p. 629-646.

5.	Rouviere, P.E. and R. Wolfe, *Novel biochemistry of methanogenesis.* Journal of Biological Chemistry, 1988. **263**(17): p. 7913-7916.

6.	Thauer, R.K., *The Wolfe cycle comes full circle.* Proceedings of the National Academy of Sciences, 2012. **109**(38): p. 15084-15085.

7.	Buan, N.R. and W.W. Metcalf, *Methanogenesis by Methanosarcina acetivorans involves two structurally and functionally distinct classes of heterodisulfide reductase.* Molecular microbiology, 2010. **75**(4): p. 843-853.

8.	Catlett, J.L., A.M. Ortiz, and N.R. Buan, *Rerouting cellular electron flux to increase the rate of biological methane production.* Applied and environmental microbiology, 2015. **81**(19): p. 6528-6537.

9.   Garrett, R.A. and H.-P. Klenk, *Archaea: evolution, physiology, and molecular biology*. 2008: John Wiley & Sons.

10.   Aldridge, J., et al., *Anaerobic Production of Isoprene by Engineered Methanosarcina Species Archaea.* Applied and environmental microbiology, 2021. **87**(6): p. e02417-20.

11.   Carr, S., J. Aldridge, and N.R. Buan, *Isoprene Production from Municipal Wastewater Biosolids by Engineered Archaeon Methanosarcina acetivorans.* Applied Sciences, 2021. **11**(8): p. 3342.

12.   Sowers, K.R., J.E. Boone, and R.P. Gunsalus, *Disaggregation of Methanosarcina spp. and Growth as Single Cells at Elevated Osmolarity.* Appl Environ Microbiol, 1993. **59**(11): p. 3832-9.

13.   Owens, N.D., E. De Domenico, and M.J. Gilchrist, *An RNA-Seq protocol for differential expression analysis.* Cold Spring Harbor Protocols, 2019. **2019**(6): p. pdb. prot098368.

14.   Guss, A.M., et al., *New methods for tightly regulated gene expression and highly efficient chromosomal integration of cloned genes for Methanosarcina species.* Archaea, 2008. **2**(3): p. 193-203.

15.   Love, M.I., W. Huber, and S. Anders, *Moderated estimation of fold change and dispersion for RNA-seq data with DESeq2.* Genome biology, 2014. **15**(12): p. 1-21.

16.   Ownby, K., H. Xu, and R.H. White, *A Methanocaldococcus jannaschii archaeal signature gene encodes for a 5-formaminoimidazole-4-carboxamide-1-β-D-ribofuranosyl 5'-monophosphate synthetase: a new enzyme in purine biosynthesis.* Journal of Biological Chemistry, 2005. **280**(12): p. 10881-10887.

17.   Flaks, J.G., M.J. Erwin, and J.M. Buchanan, *BIOSYNTHESIS OF THE PURINES: XVIII. 5-AMINO-1-RIBOSYL-4-LMIDAZOLECARBOXAMIDE 5'-PHOSPHATE TRANSFORMYLASE AND INOSINICASE.* Journal of Biological Chemistry, 1957. **229**(2): p. 603-612.

18.   Thauer, R.K., *Biochemistry of methanogenesis: a tribute to Marjory Stephenson:1998 Marjory Stephenson Prize Lecture.* Microbiology, 1998. **144**(9): p. 2377-2406.

19.   Macario, E.C.d. and A.J. Macario, *Molecular biology of stress genes in methanogens: potential for bioreactor technology.* Biomethanation I, 2003: p. 95-150.

20.   Macario, A.J., et al., *Stress genes and proteins in the archaea.* Microbiology and Molecular Biology Reviews, 1999. **63**(4): p. 923-967.

21.   Sivy, T.L., R. Fall, and T.N. Rosenstiel, *Evidence of isoprenoid precursor toxicity in Bacillus subtilis.* Bioscience, biotechnology, and biochemistry, 2011: p. 1111022722-1111022722.

22.   Holden, J.F. and J.A. Baross, *Enhanced thermotolerance and temperature-induced changes in protein composition in the hyperthermophilic archaeon ES4.* Journal of bacteriology, 1993. **175**(10): p. 2839-2843.

23.   Osorio, G. and C.A. Jerez, *Adaptive response of the archaeon Sulfolobus acidocaldarius BC65 to phosphate starvation.* Microbiology, 1996. **142**(6): p. 1531-1536.

24.   Prathiviraj, R. and P. Chellapandi, *Comparative genomic analysis reveals starvation survival systems in Methanothermobacter thermautotrophicus ΔH.* Anaerobe, 2020. **64**: p. 102216.

25.   Fuchs, G. and E. Stupperich, *Evidence for an incomplete reductive carboxylic acid cycle in Methanobacterium thermoautotrophicum.* Archives of microbiology, 1978. **118**(1): p. 121-125.

26.   Huynen, M.A., T. Dandekar, and P. Bork, *Variation and evolution of the citric-acid cycle: a genomic perspective.* Trends in microbiology, 1999. **7**(7): p. 281-291.

27.   Galagan, J.E., et al., *The genome of M. acetivorans reveals extensive metabolic and physiological diversity.* Genome research, 2002. **12**(4): p. 532-542.

28.   Yan, Z. and J.G. Ferry, *Electron bifurcation and confurcation in methanogenesis and reverse methanogenesis.* Frontiers in microbiology, 2018. **9**: p. 1322.

29.   Yanofsky, C., *Using studies on tryptophan metabolism to answer basic biological questions.* Journal of Biological Chemistry, 2003. **278**(13): p. 10859-10878.

30.   Akashi, H. and T. Gojobori, *Metabolic efficiency and amino acid composition in the proteomes of Escherichia coli and Bacillus subtilis.* Proceedings of the National Academy of Sciences, 2002. **99**(6): p. 3695-3700.

31.   Xie, G., et al., *Ancient origin of the tryptophan operon and the dynamics of evolutionary change.* Microbiology and Molecular Biology Reviews, 2003. **67**(3): p. 303-342.

32.   Prasse, D., et al., *Regulatory RNAs in archaea: first target identification in Methanoarchaea.* Biochem Soc Trans, 2013. **41**(1): p. 344-349.

33.   Prasse, D., et al., *sRNA154 a newly identified regulator of nitrogen fixation in Methanosarcina mazei strain Gö1.* RNA biology, 2017. **14**(11): p. 1544-1558.

34.   Koussounadis, A., et al., *Relationship between differentially expressed mRNA and mRNA-protein correlations in a xenograft model system.* Scientific reports, 2015. **5**(1): p. 1-9.

35.   Guimaraes, J.C., M. Rocha, and A.P. Arkin, *Transcript level and sequence determinants of protein abundance and noise in Escherichia coli.* Nucleic acids research, 2014. **42**(8): p. 4791-4799.

36.   Siegert, M., et al., *Accelerated methanogenesis from aliphatic and aromatic hydrocarbons under iron-and sulfate-reducing conditions.* FEMS microbiology letters, 2011. **315**(1): p. 6-16.

37.   Lemaire, O.N. and T. Wagner, *A Structural View of Alkyl-Coenzyme M Reductases, the First Step of Alkane Anaerobic Oxidation Catalyzed by Archaea.* Biochemistry, 2022.

38.   Wang, Y., et al., *Expanding anaerobic alkane metabolism in the domain of Archaea.* Nature microbiology, 2019. **4**(4): p. 595-602.

39.   Marzi, S., et al., *Ribosomal localization of translation initiation factor IF2.* Rna, 2003. **9**(8): p. 958-969.

40.   Weinitschke, S., et al., *The DUF81 protein TauE in Cupriavidus necator H16, a sulfite exporter in the metabolism of C2 sulfonates.* Microbiology, 2007. **153**(9): p. 3055-3060.

41.   Matelska, D., K. Steczkiewicz, and K. Ginalski, *Comprehensive classification of the PIN domain-like superfamily.* Nucleic acids research, 2017. **45**(12): p. 6995-7020.

Chapter 6: Metabolic Feedback Inhibition Influences Metabolite Secretion by the Human Gut Symbiont *Bacteroides thetaiotaomicron*

This chapter represents the contents of: Jennie L. Catlett, Jonathan Catazaro, Mikaela Cashman, Sean Carr, Robert Powers, Myra B. Cohen, and Nicole R. Buan. "Metabolic feedback inhibition influences metabolite secretion by the human gut symbiont *Bacteroides thetaiotaomicron*." Msystems 5, no. 5 (2020): e00252-20.

https://doi.org/10.1128/mSystems.00252-20

Author contributions: J.L.C. designed and carried out experiments, analyzed data, and edited the paper. M.C. designed and carried out experiments, analyzed data, and wrote and edited the paper. J.C. designed and carried out experiments, analyzed data, and wrote and edited the paper. S.C. analyzed data and edited the manuscript. R.P. designed metabolomics experiments and edited the paper. M.B.C. designed *in silico* experiments and edited the paper. N.R.B. designed the experiments, analyzed data, and wrote and edited the paper.

Abstract

Microbial metabolism and trophic interactions between microbes give rise to complex multispecies communities in microbe-host systems. *Bacteroides thetaiotaomicron* (*B. theta*) is a human gut symbiont thought to play an important role in maintaining host health. Untargeted nuclear magnetic resonance metabolomics revealed

B. theta secretes specific organic acids and amino acids in defined minimal medium. Physiological concentrations of acetate and formate found in the human intestinal tract were shown to cause dose-dependent changes in secretion of metabolites known to play roles in host nutrition and pathogenesis. While secretion fluxes varied, biomass yield was unchanged, suggesting feedback inhibition does not affect metabolic bioenergetics but instead redirects carbon and energy to CO_2 and H_2. Flux balance analysis modeling showed increased flux through CO_2-producing reactions under glucose-limiting growth conditions. The metabolic dynamics observed for *B. theta*, a keystone symbiont organism, underscores the need for metabolic modeling to complement genomic predictions of microbial metabolism to infer mechanisms of microbe- microbe and microbe-host interactions.

Introduction

Microbes, whether in the environment or associated with host organisms, form complex multispecies communities that cooperate and compete to metabolize nutrients. The host gut ecosystem is a constantly changing landscape where symbiont organisms manage to establish long-term colonization despite the fact that the host regularly ingests and eliminates nutrients and transient microbes. This results in a constantly fluctuating environment where diverse microbes are secreting metabolic fermentation products and other secondary metabolic chemicals that may inhibit or stimulate neighboring organisms as they compete for nutrients. While there is recognition that microbes play important roles in host nutrition, health, and disease (1), it is difficult to conceptualize how diverse microbes interact with each other and the host in such a way as to be able to develop

treatments or recommendations that preserve host-symbiont and beneficial microbe-microbe interactions while disfavoring pathogens.

Considering that bacterial virulence factors are often triggered by nutritional limitation (carbon, nitrogen, phosphorous, iron, etc.) (2–4) or physical stress (temperature, oxidative burst, etc.) (5, 6) and, at the molecular level, cause changes in intracellular metabolic flux and redox state/energy charge (7), the availability of nutrients and the physical factors that influence metabolism are at the crux of whether microbes induce virulence factors. Virulence factors such as cell invasion, chemotaxis, and siderophore and antibiotic synthesis, among others, can be recast as "nutrient searching" behaviors that are triggered by changes in the environment that result in decreased intracellular metabolic fluxes (8). Quorum sensing, in which bacteria secrete a small molecule that triggers expression of community-level behavior (sporulation, adherence, virulence, etc.) when it reaches a critical concentration (9), can also be "eavesdropped" by neighboring organisms in anticipation of intensification of competition for nutrients (10).

Symbionts have evolved to cooperate with hosts to establish long-term colonization strategies that do not result in disease and even protect the host from pathogens. It has been shown that establishing host-symbiont trophic relationships protects hosts from virulent interlopers by physically and nutritionally limiting the ability of pathogens to establish infections (11, 12), stimulating gut epithelial growth (13), and also modulating local immune response to maintain a healthy state (14, 15). It is hypothesized that perturbations of symbiont bacterial metabolism, such as through diet or antibiotic use, can disrupt this natural defensive relationship and predispose the host to

disease by allowing pathogens to gain a metabolic foothold (16). By this reasoning, the dynamic interplay of nutrition and metabolism of colonizing symbiont bacteria (17) is crucial as they form the foundation of the host microbiome community with which transient and pathogenic microbes must compete for survival.

Bacteroides species are Gram-negative bacteria that are especially adept at metabolizing complex carbohydrates (18) and are often the dominant bacterial phylum in the digestive systems of many herbivorous and omnivorous animals, including humans (19). *Bacteroides thetaiotaomicron* (*B. theta*) is a nonpathogenic human gut symbiont that colonizes infants within a day of normal birth (20, 21). While *B. theta* is classified as nonpathogenic and has been shown to protect the host from *Salmonella* infection (22), it was shown to exacerbate infection by *Citrobacter rodentium* in a mouse model of enterohemorrhagic *Escherichia coli* (EHEC) disease (23), underscoring the complicated contributions of symbiont microbes to human health and disease. *B. theta* is closely related to sister species (24) that are implicated in irritable bowel disease (25) and periodontal disease (26) and has also been shown to carry and transmit antibiotic resistance genes through profligate conjugation with other bacteria (27, 28).

It was previously shown that *B. theta* secretes acetate, formate, propionate, and succinate into culture medium (29–31). Bacteroides species have been shown to produce low-molecular-weight heat-stable compounds that impair host defense by inhibiting migration and killing polymorphonuclear leukocyte (PMN) phagocytes (32, 33). Succinate and propionate, as low-molecular-weight heat-stable metabolites, have been hypothesized to fit the description and were shown to irreversibly inhibit superoxide and hydrogen peroxide production by neutrophils by lowering cytoplasmic pH (34).

Propionate-secreting *B. theta* have also been shown to protect mice from colonization by *Salmonella*, presumably due to the same membrane-permeable pH-lowering property that is inherent to short-chain fatty acids (22). Acetate is also a membrane permeable (35) "switch" that reduces ATP synthesis in *E. coli* and regulates expression of virulence genes in many bacteria (36). Secretion of acetate, formate, propionate, and succinate by *B. theta* is therefore proposed to reduce the effectiveness of host response to pathogens and to have species-specific effects (enhancing or abrogating) bacterial colonization and virulence.

 B. theta secretes metabolites as a result of starch, extracellular matrix, or glucose metabolism (18). *B. theta* catabolizes glucose via the Embden-Meyerhof-Parnas (EMP) pathway (glycolysis) to pyruvate, which is a major intracellular metabolite used as the substrate in gluconeogenesis, the tricarboxylic acid cycle (TCA cycle), and for biosynthesis of acetyl coenzyme A (acetyl-CoA), enzyme cofactors, and amino acids. Acetate, the major secreted product, can be synthesized with ATP using two metabolic pathways: (i) by hydrolysis of the CoA thioether bond by acetyl-CoA synthase (Acs) in the acetyl-CoA pathway, or (ii) by phosphotransacetylase (Pta) and acetate kinase (Ack) enzymes in the Ack/Pta pathway (see Table S1 in the supplemental material). The high concentration of secreted acetate suggests acetate is the primary energy-conserving overflow (37) by-product of *B. theta*. The second most abundant secreted product is succinate, which is produced by hydrolysis of succinyl-CoA by succinyl-CoA synthetase with generation of ATP in the TCA cycle. In the forward TCA cycle direction, succinate is funneled to succinate dehydrogenase, which oxidizes succinate to fumarate with the generation of reduced ubiquinone for generating a transmembrane proton gradient for

ATP synthesis. These data suggest rapidly growing *B. theta* cells are limited in the turnover rate of reduced/oxidized quinone and secrete succinate as an intermediate product to maintain rates of glycolysis and glucose consumption (38). In the reverse TCA direction, succinate synthesis requires ATP and HCO_3^- (pyruvate carboxylase), NADH (malate dehydrogenase), and reduced quinone (succinate dehydrogenase), and though enzyme steps are reversible, succinate synthesis by reverse TCA can only occur when there is a surplus of ATP generated as a result of forward TCA pathway flux.

The next most abundant secreted products are formate and propionate. Formate is synthesized by pyruvate formate-lyase, which uses pyruvate and coenzyme A as the substrates to produce formate and acetyl-CoA. Formate is therefore an energy neutral overflow metabolite that nevertheless increases the enzymatic routes to acetyl-CoA. Propionate is synthesized from succinyl-CoA to propionyl-CoA by methylmalonyl-CoA mutase, methylmalonyl-CoA epimerase, and propionyl-CoA carboxylase enzymes, with subsequent thioesterase activity by the same Acs or Ack/Pta pathways used to synthesize acetate. Ultimately, propionate synthesis yields 2 ATP, but the pathway requires multiple enzyme steps and cofactors, suggesting this overflow pathway could be kinetically limited (39). A small amount of lactate is secreted. Lactate is synthesized by lactate dehydrogenase from pyruvate, NADH, and a proton and is therefore energy consuming for the cell.

These original data were obtained using liquid chromatography technology, but since then, our ability to collect high-resolution untargeted one-dimensional proton nuclear magnetic resonance (1D ^{1}H NMR) data and the statistical methods to deconvolute complicated spectra has evolved considerably, making untargeted NMR metabolomics of

B. theta cultures feasible (40–42). Our study aimed to use untargeted metabolomics, systems biology, and biological modeling techniques to revisit the metabolism of this important human symbiont to account for nutrient inputs and outputs and to gain insight into how *B. theta* responds to physiological concentrations of metabolic fermentation products that are encountered in the gut ecosystem.

Methods

Strains and culture conditions

Bacteroides thetaiotaomicron vpi-5482 (ATCC 29148, Buan lab strain collection number NB203) was grown in minimal defined medium as described but with minor modifications (64–66). Cultures were grown under strict anaerobic conditions at 37°C in 18-mm by 150-mm Balch tubes in either tryptone and yeast extract (TYG) growth medium (vitamin K omitted) or a defined medium (vitamin K omitted). Media were supplemented with glucose to 0.05% (wt/vol) (2.78 mM) under a 5% H_2, 20% CO_2, N_2 atmosphere with the following additions as appropriate: sodium acetate (10 mM), sodium formate (10 mM), or a combination of both 10 mM sodium acetate and 10 mM sodium formate. Growth was measured using optical density at 600 nm using a Spectronic D spectrophotometer (Thermo Fisher Scientific) fitted with a Balch tube (18 mm) sample chamber. Biomass and optical density were found correlate linearly with 0.54 ± 0.056 g dry weight OD-1 liter-1 in defined medium.

NMR sample preparation. Five replicates of *B. theta* cultures were grown to late exponential stage in 10 ml defined medium with 0.05% glucose and one of the following concentrations of acetate: 0.5 mM, 1 mM, 5 mM, 10 mM, or a 10 mM formate and 10

mM acetate control. Cells were separated from medium with 0.2-µm filters by vacuum. Samples of filtered medium were flash frozen in liquid nitrogen and then lyophilized overnight.

NMR data collection and analysis

One-dimensional (1D) 1H NMR data collection and analysis were completed as described previously (40–42, 67–69). Briefly, samples from each class were prepared for NMR analysis by dissolving the lyophilized culture medium into 600 µl of 50 mM phosphate buffer (pH 7.2, uncorrected) in 99.8% D_2O with 50 µM 3-(tetramethylsilane)propionic acid-2,2,3,3-d4 (TMSP). NMR spectra were recorded at 298 K on a Bruker Avance III-HD 700 MHz spectrometer equipped with a 5-mm inverse quadruple-resonance (^1H, ^{13}C, ^{15}N, and ^{31}P) cryoprobe with cooled ^1H and ^{13}C channels and a z-axis gradient. A SampleJet automated sample changer with Bruker ICON-NMR software was used to automate the NMR data collection. 1D ^1H spectra were collected using excitation sculpting to remove the solvent signal and avoid any need for baseline corrections (70). A total of 16,000 data points with a spectral width of 5482.5 Hz, 8 dummy scans, and 128 scans were used to obtain each spectrum.

The 1D ^1H NMR spectra were processed and analyzed using our MVAPACK metabolomics toolkit (http://bionmr.unl.edu/mvapack.php) (71). The 1D ^1H NMR spectra were Fourier transformed and phased prior to normalization using phase scatter correction (72). Residual solvent peaks and noise regions were removed, and the spectra were referenced to TMSP at 0.0 ppm. The spectra were then binned using an intelligent adaptive binning algorithm (73) or aligned with the icoshift algorithm (74). The data were

scaled using the Pareto method prior to principal-component analysis (PCA) or orthogonal projections to latent structures (OPLS) analysis (69).

Binned data were used for the PCA model, whereas the full spectral data were utilized for the OPLS models. OPLS model results were validated using analysis of variance of the cross-validated residuals (CV-ANOVA) significance testing (75). Fractions of explained variation ($R^2{}_x$ and $R^2{}_y$) were computed during the OPLS model training. The OPLS models were also internally cross-validated using 7-fold Monte Carlo cross-validation to compute Q^2 values (76, 77).

The validated OPLS models enabled the generation of back-scaled loading plots to identify the spectral features (NMR peaks) that primarily contributed to the observed group separation. The relative peak intensities in these "pseudospectra" highlight the magnitude of the metabolite's contribution to the group separation in the OPLS scores plot. Similarly, the relative sign of the peak indicates if the metabolite's concentration increases or decreases due to the effects of the growth medium. All nonoverlapping ^{1}H NMR peaks identified by the back-scaled loading plots as a major contributor to group separation in the OPLS scores plot were assigned to a metabolite using the Chenomx NMR suite

7.0 (Chenomx Inc., Edmonton, AB, Canada). 1H NMR peaks with significant overlap and multiple metabolite assignments were excluded from further analysis.

Empirical modeling of metabolomics data

Secretion flux maps were generated using the following equation:

$$F(x) = 100 * \frac{xmolC_x}{\sum_{n=1}^{i} x_n molC_{x_n}} \qquad (1)$$

where the secretion flux (F) of any metabolite (x [mM]) is expressed as a % C mol fraction ($molC_x$) of the total carbon secreted.

Feedback inhibition was estimated using the following equation:

$$x_{sec} = x_{obs} - x_{init}$$

(2)

where metabolite secretion (x_{sec}) is determined by subtracting the amount of each metabolite in the 0 mM control treatment (x_{init}) from the amount of the metabolite observed (x_{obs}) following the addition of acetate.

The fold variance in metabolite secretion was estimated by:

$$x_{var} = \left(\frac{x_{obs} - A_{sup}}{x_{init}} \right) - 1$$

(3)

where x_{obs} in the observed concentration of each metabolite, A_{sup} indicated the concentration of acetate supplemented, and x_{var} is the magnitude of each "missing" metabolite.

In silico modeling and software

In silico experimentation is conducted using the Department of Energy's Systems Biology Knowledgebase (KBase) (78). A public narrative with all experiments recreated can be found in KBase (https://narrative.kbase.us/narrative/ws.53087.obj.1). Applications used are part of the fba_tools module version 1.7.6 (78). Model creation begins with the genome *Bacteroides thetaiotaomicron* VPI-5482 uploaded through KBase's public NCBI RefSeq genome database. Using the "build metabolic model" application, the draft metabolic models were created from an annotated genome. The fba_tools default parameters were used. The *in silico* experimentation process with KBase consists of four steps: (i) creating a draft metabolic model from the *B. theta* genome, (ii) defining the

medium composition, (iii) gap filling the draft model to add in missing reactions, and (iv)

running a flux balance analysis (FBA). FBA provides a measurement of growth resulting

from flux through the biomass reaction (grams of dry weight of biomass)

(https://kbase.us/metabolic-modeling-faq/).

It is critical to note that the draft *B. theta* model we employed may have missing

reactions (gaps) due to incorrect or incomplete functional genome annotations. We used

the "gapfill metabolic model" application on the draft model to identify a minimal set of

biochemical reactions that, when added to the draft model, allow it to achieve biomass on

the specified media (https://kbase.us/metabolic-modeling-faq/) (79). Gap filling uses

linear programming to find the optimized metabolic model that uses the fewest added

reactions to satisfy the biomass reaction and to balance the flux balance equation. We gap

filled once for each of the eight media in our experimentation, creating eight metabolic

models. Then, starting with a base medium file containing 25 substrate compounds (full

medium compositions can be found in supplemental material), we added glucose,

formate, and acetate at their desired maximum uptake concentrations.

The "run flux balance analysis" (FBA) application was used to run the simulation.

The FBA algorithm is a constraint-based approach that estimates growth-optimal fluxes

through all the reactions specified by the metabolic network constructed in the previous

step (https://kbase.us/metabolic-modeling-faq/). This resulted in a rate of biomass

production as a measure of growth. For each FBA, we used the gap-filled model on the

medium of interest and used each medium as input to the FBA algorithm to maximize

biomass (bio1). From the output of the FBA application, the objective value was used as

a measurement of growth and to capture the reaction and exchange fluxes, which were

used to find flux values of interest. All data and results are presented in our public KBase narrative (https://narrative.kbase.us/narrative/ws.53087.obj.1).

The FBA models were created with either high or low levels of glucose, which were combined with either the absence or presence of acetate and/or formate. This resulted in eight experiments: high glucose, high glucose with acetate, high glucose with formate, high glucose with acetate and formate, low glucose, low glucose with acetate, low glucose with formate, and low glucose with acetate and formate. The amount of each compound used in the model is specified in the medium file, which defines maximum uptake as measured in millimoles per gram cell dry weight per hour. Low glucose was defined as 0.1 maximum uptake, high glucose was defined as 2.78 maximum uptake, and the presence of formate or acetate was set to 10 maximum uptake. The absence of formate or acetate was set to 0 maximum uptake.

Results

Untargeted metabolomics reveals *B. theta* secretes a subset of amino acids in addition to organic acid fermentation products

B. theta was grown in minimal defined medium on glucose as sole carbon and energy sources, and spent culture medium was analyzed using 1D ^{1}H NMR to detect the secreted metabolome and to identify any new secreted metabolites (see Fig. S1 in the supplemental material). We confirmed previous observations that the major secreted metabolic products were acetate, succinate, formate, and propionate, with small amounts of lactate. In addition, we were able to detect histidine, cysteine, cystine (Cys-Cys disulfide), glutathione, asparagine, and alanine (Fig. 1). These endpoint metabolic

products were then used to build a secretion flux map (Fig. 2). Notably, relatively few metabolites of similar size, chemical composition, reactivity, or metabolic importance to the cell were detected. Accordingly, these results suggest the secreted metabolites were products of specific cellular processes rather than through nonspecific leaky transporters.

The secretion of amino acids is significantly lower than the major organic acid fermentation products (excluding lactate) but also suggests these metabolites are overflows for purine metabolism (histidine), the TCA cycle (alanine, asparagine, and glutathione), and the serine cycle (cysteine/cystine and glutathione) (Fig. 2). Notably, the amino acid secretions were generally lower than those of lactate, suggesting amino acid secretion is less favorable, likely reflecting the fact that amino acid synthesis is energetically costly and requires multiple enzymatic steps in contrast to a single enzyme for lactate synthesis. The network map illustrates that in minimal defined medium, secreted products can be easily derived from pyruvate, acetyl-CoA, and succinate after minor biochemical transformation. This suggests the secreted metabolites are "overflow" from the EMP pathway.

B. theta growth is inhibited by acetate and formate

Acetate and formate are major metabolic products of many organisms (43), and it is thought that both acetate and formate may inhibit cell growth by feedback inhibition and/or by transporting protons across the cell membrane and collapsing the transmembrane ion gradient necessary for ATP synthesis (44, 45). This suggests that the acetate and formate produced by competing organisms in the gut may also have a strong inhibitory effect on *B. theta* metabolism. We tested these hypotheses by growing *B. theta*

with increasing acetate, formate, or a combination of both in a culture medium at physiological concentrations (46).

When *B. theta* is grown in minimal defined medium with increasing concentrations of acetate or formate, population doubling time increased by approximately 25% (Fig. 3a and b; Table 1). Conversely, the final optical density of the culture was not affected by supplementation with acetate and/or formate (Fig. 3c), and because optical density (OD) and biomass are correlated, it suggests that biomass yield is also not affected (47). These data suggest ATP synthesis and metabolic efficiency have not been altered. Instead, a direct or indirect kinetic biochemical feedback inhibition is the primary factor in acetate- and formate-dependent inhibition of *B. theta* growth. The stationary-phase cultures were observed to exhibit a modest statistically significant decrease in pH from 7.14 ± 0.064 to 7.03 ± 0.051 ($P = 0.03$) with the addition of acetate despite the medium being buffered at pH 7.2 with 1 M potassium phosphate (Table 2). The total amount of secreted organic acids and supplemental acetate cannot account for the observed pH change. Thus, the drop in pH may be attributed to an increase in CO_2 concentration, which is converted to carbonic acid (H_2CO_3) with a pK_a of 3.6 in water. An increase in the CO_2 partial pressure produced by cells in sealed anaerobic culture tubes is known to decrease the pH of culture medium (48).

Feedback inhibition by acetate causes suppression of metabolite secretion

The concentration for each of the metabolites in the culture medium changed independently as a function of the amount of supplemental acetate (Fig. 3d). The effect of supplemental acetate on metabolite secretion (xsec) was unmasked (Fig. 4a) by

subtracting the amount of each metabolite in the 0 mM control treatment (xinit) from the amount of the metabolite observed (xobs) after acetate supplementation.

The observed concentration for each metabolite should be the same as in the initial 0 mM treatment condition if the supplemental acetate had no effect on metabolite secretion. The xsec should also be equal to zero if the metabolite is neither a substrate nor product of acetate metabolism (null hypothesis). Instead, the concentration for each secreted metabolite changed as a result of the additional acetate in the culture medium. For instance, acetate only increased by 4.21 ($\pm$ 0.55) mM in the culture medium after the 10 mM acetate treatment (Fig. 4a). This is significantly less than expected if no feedback inhibition occurred and the acetate concentrations were simply additive. The acetate concentration detected in the culture medium should have been the sum of the total amount of acetate derived from glucose (6.6 $\pm$ 0.5 mM) (Fig. 3d) plus the 10 mM acetate supplemented for a final concentration of 16.60 mM.

Similar decreases in secretion were observed for formate (0.18 $\pm$ 0.02), propionate (0.47 $\pm$ 0.02), and amino acids, while succinate (0.83 $\pm$ 0.13 mM) secretion increased. These results suggest supplemented acetate was taken up by cells and altered metabolic fluxes such that secretion of acetate, formate, propionate, and amino acids are suppressed, while a portion of the acetate is secreted as succinate.

Next, the fold variance (x_{var}) between the observed and the null model was calculated assuming the secretions of acetate and the other metabolites are correlated (Fig. 4b). The observed concentration of each metabolite indicated a negative variance from the null model. As acetate supplementation increased, the magnitude of the variance also increased, indicating "missing" metabolites. The increasing negative correlation as a

function of supplemental acetate suggests these missing metabolites are a result of an unknown inhibitory mechanism or process.

The slope of the linear regression Δx_{var} is the relative molar acetate suppression coefficient (Table 3). Accordingly, alanine and the amino acids have the highest molar acetate suppression coefficient despite acetate secretion having a higher magnitude of inhibition. Relative molar flux suppression was mapped onto a metabolic network as shown in Fig. 4c. The flux analysis shows that acetate supplementation has the highest inhibitory effect on alanine secretion, an intermediate effect on amino acid secretion, and the smallest inhibitory effect on the major fermentation products: acetate, succinate, formate, and propionate.

Feedback inhibition is the primary driver of acetate inhibition effects

In addition to a direct competitive feedback inhibition (e.g., carbonic anhydrase) (49), supplemental acetate and formate may also induce a noncompetitive inhibition through posttranslational modification (formylation) (50). A direct or indirect effect on gene expression may occur as growing cells adapt to the stress. To determine the relative contribution of feedback inhibition and gene expression changes to secretion fluxes, the following hypotheses were modeled with the assumption that secreted metabolites mirror intracellular metabolic fluxes: (a) secretion is additive with no destruction and no regulation (see Fig. S2a); (b) secretion fluxes are constant with balanced secretion and absorption (Fig. S2b); (c) there is feedback inhibition with no regulation (Fig. S2c); (d) there is synergistic negative feedback inhibition with compensatory gene regulation (Fig. S2d); and (e) there is positive upregulation in response to increasing acetate (Fig. S2e). The modeling results (Fig. 4b versus Fig. S2d) indicate that the experimental data most

closely match a feedback inhibition model with no gene regulation. The only exception is for acetate and succinate, which were discussed previously. *B. theta* appears to respond to low concentrations of exogenous acetate (<0.5 mM) by adjusting gene expression to decrease metabolic flux, but at acetate levels up to 10 mM, no further changes in gene expression or other metabolic rerouting occur.

Formate causes synergistic feedback inhibition of acetate, propionate, succinate, histidine, cysteine, and glutathione

Formate is a major fermentation by- product encountered in anaerobic environments. Like acetate, formate is produced from the Embden-Meyerhof-Parnas fermentation pathway; however, formate can be used as either an energy sink or an energy source depending on the levels of CO_2 and H_2 or the redox state of ferredoxin. Thus, high formate concentrations may be synergistic, additive, or have independent effects on secretion fluxes compared to those for acetate alone. To differentiate between these possibilities, cultures were supplemented with 10 mM both acetate and formate. NMR metabolomics was then used to characterize the secreted metabolome. Growth experiments demonstrated that formate had a synergistic effect on population doubling time (Table 1). Supplemented acetate and formate appeared to be taken up from the culture medium, but the additional acetate and/or formate did not affect biomass yield or pH. No new secreted metabolites were observed in the culture medium, but a subset of organic acids (Fig. 5a) and amino acids (Fig. 5b) did exhibit concentration changes relative to those in treatments with only 10 mM acetate. Notably, lactate, alanine, and asparagine secretion levels were unchanged. These data suggest those biosynthetic

reactions are unaffected by acetate or formate, while other reactions are either directly affected by enzyme inhibition or indirectly affected by changes in metabolic flux.

Visualization of dynamic metabolite secretion and effects of feedback inhibition. Animations of the dynamics of metabolic secretion (Movie S1), acetate inhibition (Movie S2), and the modulation of acetate inhibition by formate supplementation (Movie S3) are presented in the supplemental material. The animated models assume linear secretion fluxes and illustrate the accumulation of secreted products in the culture medium as a function of time and acetate and/or formate supplementation.

High-glucose models do not predict feedback inhibition by acetate or formate

Empirical modeling suggested that the bioenergetics of glucose metabolism does not change when acetate and/or formate accumulates in the culture medium. Therefore, the observed changes in secreted metabolites must be due to increased CO_2 and/or H_2 secretion fluxes. To determine if in silico *B. theta* metabolic models can reproduce the observed growth phenotypes, we conducted a series of in silico experiments to obtain flux values for all reactions in the metabolic model and exchange fluxes for all substrate compounds and product metabolites.

A limited effect on the key reaction fluxes (defined in millimoles per gram cell dry weight per hour) was observed under high-glucose (0.02% [wt/vol]) conditions. In the high-glucose flux balance analysis (FBA) models, there were no changes in predicted biomass, which remained constant at 0.39 in all four experiments (Fig. 6a), or in exchange fluxes with either acetate and/or formate supplementation (Fig. 6b). There was only one discrepancy in a predicted reaction flux. The model shifts from using asparagine synthetase (aspartate + glutamine + ATP + H_2O ↔ asparagine + glutamate + AMP + PPi)

to using aspartate ammonium ligase (aspartate + NH$_3$ + ATP ¡ asparagine + AMP + PPi)

when either acetate and/or formate is included in the culture medium (see Data Set S1).

However, the glutamate, glutamine, asparagine, and aspartate exchange fluxes were not

altered in the model despite the changes in reaction flux. We confirmed that either

pathway can be deleted in the model and results in the same exchange fluxes regardless

of whether acetate or formate is supplemented. Thus, the simulations show either

metabolic pathway for asparagine synthesis can occur interchangeably in *B. theta* under

the culture conditions we modeled.

Modeling suggests acetate and formate affect metabolism when glucose

concentrations are low

The presence of acetate under low-glucose conditions (0.002% [wt/vol]) results in

an abundance of metabolic changes. When acetate was added, whether in the presence or

absence of formate, biomass decreased to 0.14 (Fig. 6a). Exchange flux values for several

metabolites were also affected (Fig. 6c and Data Set S1). Some pathways, such as malate

dehydrogenase, serine ammonia-lyase, and formate-tetrahydrofuran (THF) ligase show a

net flux of zero. Other reaction fluxes, such as those corresponding to enzymes lactate

dehydrogenase, succinyl-CoA synthetase, and aspartate aminotransferase, incurred a

change in directionality. The reaction for aspartate oxidase had a zero-net flux under

glucose-only or glucose and formate conditions; however, the reaction had a flux of

0.0009 when acetate was present. Other reactions retained their directionality, but the net

flux exhibited a change in magnitude. In the forward direction, examples of reactions that

increased exchange flux in the presence of added acetate included pyruvate kinase and

aspartate aminotransferase, while pyruvate carboxylase, pyruvate synthase, pyruvate

dehydrogenase, and acetate kinase had decreased flux. In the reverse reaction direction, pyruvate phosphate dikinase had increased exchange flux and phosphotransacetylase had decreased flux. No additional effect was observed when formate was combined with acetate.

The interchangeability of asparagine synthetase and aspartate ammonia ligase pathways for asparagine synthesis was also observed under low-glucose conditions, similar to what was seen under high glucose conditions (Fig. 6d). In addition, when formate was added under low glucose conditions, the net flux of the pyruvate formate-lyase reaction (formate + acetyl-CoA $\leftrightarrow$ CoA + pyruvate) decreased from -3.74 to -0.122, where a negative flux value indicates the reaction was being executed from right to left. Under this condition, biomass decreased to a value of 0.27 (Fig. 6a).

The low-glucose model also predicts increased uptake of acetate and decreased uptake of CO_2 and cysteine when acetate is supplemented into the culture medium, which is consistent with metabolomics data and the observed pH decrease. None of the simulations resulted in changes in the secretion of organic acids or amino acids to the culture medium. Modeling instead showed decreased production of a small amount of molecular oxygen, lack of nitrite secretion, and increased secretion of xanthine under low-glucose conditions with addition of acetate.

Discussion

Feedback inhibition reveals metabolic plasticity and resiliency of *B. theta*

B. theta is a ubiquitous and abundant member of the human gut microbiome. Accordingly, *B. theta* is an attractive organism for investigating the interaction between

genes, environment, and system-level behaviors. *B. theta* is a strict anaerobe grown in sealed culture tubes. Thus, by the law of conservation of mass, all mass inputs (culture medium ingredients) and outputs (biomass and secreted metabolites) are accounted for in the cell culture. Secreted metabolites, especially organic acids and amino acids, are important mediators in microbial food webs and may play simultaneous roles as nutrients, stimulators, and inhibitors. In this manner, secreted metabolites may affect overall system behavior.

Metabolomics and cell growth data suggest fermentation products, acetate and formate, cause large metabolic changes even when biomass yield is unaffected. *B. theta* has two bidirectional acetate enzyme systems, Ack/Pta and acetyl-CoA pathways, and the metabolomics and modeling data are consistent with *B. theta* using both of these pathways to secrete acetate as an "overflow" of acetyl-CoA biosynthesis. Overflow metabolism has been studied extensively in *E. coli* (37), where it is thought that excess carbon from glucose is secreted as acetate due to metabolic bottleneck at pyruvate and acetyl-CoA as a result of redox imbalance (38). In *E. coli* and Salmonella, secreted acetate is recouped by the Ack and Pta enzymes during late stationary phase (51), where the glyoxylate shunt is used to incorporate acetyl-CoA into biomass (52). While the enzymes involved in acetate secretion and uptake are conserved between *E. coli* and *B. theta*, *B. theta* lacks the glyoxylate shunt and is an anaerobe that cannot carry out oxidative respiration. The addition of acetate to the culture medium caused the inhibition of acetate, formate, and propionate secretion by *B. theta*, but increased succinate secretion as the next available "overflow valve." This result may be explained by feedback inhibition of acetyl-CoA hydrolysis and increased succinyl-CoA hydrolysis

later in the TCA cycle. Consequently, there was a decrease in the secretion of other metabolic products (cysteine and other amino acids) downstream of succinate biosynthesis. *B. theta* biomass yield was unaffected by supplemented acetate, as expected by the lack of a glyoxylate shunt. The biomass yield did not increase despite a decrease in the secretion of amino acids, indicating intracellular amino acid biosynthesis was sufficient for maximum growth.

The addition of formate to the culture medium caused an inhibition in the secretion of acetate and a subset of amino acids, while metabolites derived from oxaloacetate and aspartate (lactate, asparagine, and alanine) were not affected. Formate and acetate are both synthesized from pyruvate but have different effects on downstream "over- flow" metabolites. One possible explanation for this difference is the fact that formate is a substrate for C_1 metabolism (ultimately for glycine, serine, cysteine, and methyl transfer reactions). Thus, the addition of formate increases the synthesis of amino acids, lactate, and pyruvate (through serine ammonia-lyase), which may compensate for the inhibition of acetate, succinate, and propionate.

Unexpectedly, not all metabolites were secreted and no new metabolites were detected in culture medium as a result of acetate and/or formate inhibition. Several central metabolites are simply too large to be nonspecifically secreted (phosphosugars and CoA-oxoacids), but many nonsecreted TCA and amino acid biosynthetic intermediates are chemically similar to secreted metabolites. This suggests that metabolite secretion is highly discriminated by transporters. *B. theta* also seems unable to relax transporter specificity or to produce new transporters through changes in gene

expression. In effect, *B. theta* did not relieve acetate or formate inhibition by secreting other biosynthetic intermediates.

Another surprise was the observation that biomass yield was unaffected by the physiological concentrations of acetate and/or formate. Accordingly, net bioenergetics (ATP moles synthesized per mole substrate consumed) were also likely unaffected, even though the rate of growth was significantly lower and there were large changes in secretion profiles. The FBA model was able to accurately predict that acetate and formate supplementation does not affect biomass (Fig. 3c versus Fig. 6a) under high-glucose conditions. This leads to the question of where the unaccounted carbon could have gone. A likely explanation is that the missing carbon mass was released as CO_2. Increased CO_2 synthesis would manifest as a decrease in pH but would not necessarily affect CO_2-yielding decarboxylation reactions. At the partial pressures tested here, decarboxylation reactions are virtually irreversible unidirectional reactions. Malate dehydrogenase reversibly catalyzes the decarboxylation of oxaloacetate to produce pyruvate and CO_2. Malate dehydrogenase also reversibly oxidizes malate to produce pyruvate, CO_2, and NADPH. Our results can be explained if the forward malate dehydrogenase reaction is favored, with increased pyruvate being secreted as acetate and formate. The low-glucose FBA models support this hypothesis and show that addition of acetate results in nearly a 50% decrease in CO_2 uptake from the culture medium (see Data Set S1 in the supplemental material).

The FBA models for *B. theta* were unable to model secretion of organic acids and amino acids (Fig. 2 versus Data Set S1), and though lowering the glucose concentration in the growth medium caused some metabolic network changes, they did not completely

predict the effect of acetate and formate on exchange fluxes (compare Fig. 4c versus Fig. 6c and Fig. 5c versus Fig. 6d). One possibility is that the carbon predicted to be secreted as xanthine (which was not detected experimentally) is instead used to synthesize organic acids and amino acids. Under both the high-glucose and low- glucose conditions, there were also unexpected results with respect to nitrite and ammonia fluxes, suggesting unexplored C/N metabolic or regulatory relationships in *B. theta*. Another possibility is that transporters (either specifically or nonspecifically) secrete accumulated metabolite pools as part of "overflow metabolism." These discrepancies likely reflect technological limitations of in silico modeling, such as an inability to predict allosteric or competitive inhibition, gene expression changes that might result in specific or nonspecific activity of transmembrane transporters, or perhaps the activity of poorly characterized enzymes or nonspecific aminotransferases and decarboxylases (or other enzymes) that may affect exchange fluxes in unknown ways. By using untargeted NMR metabolomics, we were able to detect and quantify metabolites in culture medium with minimal sample processing in a relatively "agnostic" approach. NMR data sets can be used to produce secretion flux maps that describe metabolic behaviors without requiring genomic, biochemical, or transcriptomic information or, in the reverse direction, may be used to infer the existence of unknown biochemical pathways. We suggest that untargeted NMR metabolomics may be a useful tool to inexpensively curate genome-scale metabolic models and could be essential for developing accurate dynamic FBA models.

Are *B. theta* secretion signals of relevance to a host-microbiome system?

It has been hypothesized that amino acids can function as a "shared good" in microbe-host ecosystems in which secreted "overflow" amino acids can be taken up by

the host or neighboring community members (commensalism). In this regard, a cell can dispose of its excess amino acids while also benefitting near neighbors (mutualism). It is also possible that these secreted amino acids are used in mutually beneficial metabolite exchange (syntrophy) (53–55), for example, when metabolite secretion causes metabolic feedback inhibition that can be relieved by a consumer partner. Detection of amino acid products in *B. theta* culture supernatants supports the postulation that *B. theta* is primed to participate in such cross-feeding interactions in the gut (56). Humans are known to require branched-chain amino acids (leucine, isoleucine, and valine) and conditionally essential amino acids (arginine, proline, cysteine, and glycine) as well as lysine, threonine, methionine, tryptophan, phenylalanine, and histidine (57). The essential amino acid histidine and the conditionally essential amino acids cysteine and glycine (as glutathione) were observed to be secreted by *B. theta*.

Besides nutrition, amino acids also have a wide range of roles in gut epithelial metabolism and gut immune/neurological function. In fact, several amino acids are secreted at high concentrations by *B. theta*. In gut epithelial cells, glutamate, aspartate, and glutamine are substrates for ATP synthesis, glutamine, glycine, and aspartate are used for nucleic acid synthesis, and threonine, cysteine, and proline are used for mucin synthesis. Thus, a symbiotic relationship may exist between *B. theta* and gut epithelium, where *B. theta* may provide essential amino acids critical for gut epithelial metabolism.

Glutathione is a tripeptide of cysteine, glutamate, and glycine, which also has an important role in epithelial cell viability. It can provide a source of amino acids, it can protect against toxic xenobiotics, and it is important for cell signaling. Glutathione also serves as a redox buffer and can protect cells from reactive oxygen species (ROS) or

oxidative stress (58). Thus, it is notable that *B. theta* was observed to secrete 121 ± 16 µM glutathione into the culture medium. Since lactic acid bacteria produce H_2O_2 in the gut to compete with anaerobes such as *B. theta* for glycan nutrients (59, 60), the secretion of glutathione by *B. theta* may protect *B. theta* from these competing microbes. Secreted glutathione may also protect *B. theta* from oxidative stress generated by host epithelia at the microbe-host interface (61–63). The amino acid components of glutathione, glutamine, and glycine may act as neurotransmitters between gut epithelia and the nerve cells that innervate the intestinal tract.

Cysteine (242 ± 22 µM) and cystine (209 ± 47 µM) were also secreted by *B. theta*. Cysteine and cystine, like glutathione, can abiotically react with ROS or xenobiotic compounds to protect cells from oxidative damage. Histidine was also secreted at high levels (101 ± 12 µM), which was nearly equivalent to that of lactate (120 ± 25 µM). Histidine is an essential amino acid and is a precursor to the immunological effector histamine. Secretion of amino acids and glutathione by *B. theta* could potentially play an important role in host nutrition, oxidative stress, neurological function, and immunology.

Our metabolomics, theoretical modeling, and cell viability results support the hypothesis that microbes in complex communities modulate *B. theta*'s metabolic efficiency, which leads to changes in secreted metabolites that, in turn, are sensed as chemical messages by the microbial community and host (54). Metabolic feedback inhibition by fermentation products such as acetate and formate would be expected to function through generalized cellular processes rather than through specific quorum sensing. However, because acetate and formate are highly conserved major metabolic end products synthesized by anaerobic microbes in the millimolar and high micromolar

concentration ranges, the local concentration achieved in gut microenvironments could be sufficiently high to profoundly affect metabolism of neighboring microbes and thus metabolism of the gut community as a whole.

Acknowledgements

References

1.   Cho I, Blaser MJ. 2012. The human microbiome: at the interface of health and disease. Nat Rev Genet 13:260 –270. https://doi.org/10.1038/ nrg3182.

2.   Mekalanos JJ. 1992. Environmental signals controlling expression of virulence determinants in bacteria. J Bacteriol 174:1–7. https://doi.org/ 10.1128/jb.174.1.1-7.1992.

3.   Litwin CM, Calderwood SB. 1993. Role of iron in regulation of virulence genes. Clin Microbiol Rev 6:137–149. https://doi.org/10.1128/cmr.6.2.137.

4.   Lamarche MG, Wanner BL, Crepin S, Harel J. 2008. The phosphate regulon and bacterial virulence: a regulatory network connecting phosphate homeostasis and pathogenesis. FEMS Microbiol Rev 32:461– 473. https://doi.org/10.1111/j.1574-6976.2008.00101.x.

5.   Konkel ME, Tilly K. 2000. Temperature-regulated expression of bacterial virulence genes. Microbes Infect 2:157–166. https://doi.org/10.1016/ S1286-4579(00)00272-0.

6.   Hebrard M, Viala JP, Meresse S, Barras F, Aussel L. 2009. Redundant hydrogen peroxide scavengers contribute to *Salmonella* virulence and oxidative stress resistance. J Bacteriol 191:4605– 4614. https://doi.org/10.1128/JB.00144-09.

7.   Frawley ER, Crouch ML, Bingham-Ramos LK, Robbins HF, Wang W, Wright GD, Fang FC. 2013. Iron and citrate export by a major facilitator superfamily pump regulates metabolism and stress resistance in *Salmonella typhimurium*. Proc Natl Acad Sci U S A 110:12054 –12059. https://doi.org/10.1073/pnas.1218274110.

8.   Rohmer L, Hocquet D, Miller SI. 2011. Are pathogenic bacteria just looking for food? Metabolism and microbial pathogenesis. Trends Microbiol 19:341–348. https://doi.org/10.1016/j.tim.2011.04.003.

9.   Rutherford ST, Bassler BL. 2012. Bacterial quorum sensing: its role in virulence and possibilities for its control. Cold Spring Harb Perspect Med 2:a012427. https://doi.org/10.1101/cshperspect.a012427.

10.   Williams P. 2007. Quorum sensing, communication and cross-kingdom signalling in the bacterial world. Microbiology 153:3923–3938. https:// doi.org/10.1099/mic.0.2007/012856-0.

11.   Nakatsuji T, Chen TH, Narala S, Chun KA, Two AM, Yun T, Shafiq F, Kotol PF, Bouslimani A, Melnik AV, Latif H, Kim JN, Lockhart A, Artis K, David G, Taylor P, Streib J, Dorrestein PC, Grier A, Gill SR, Zengler K, Hata TR, Leung DY, Gallo RL. 2017. Antimicrobials from human skin commensal bacteria protect against *Staphylococcus aureus* and are deficient in atopic dermatitis. Sci Transl Med 9:eaah4680. https://doi.org/10.1126/ scitranslmed.aah4680.

12.   Buffie CG, Pamer EG. 2013. Microbiota-mediated colonization resistance against intestinal pathogens. Nat Rev Immunol 13:790 – 801. https://doi.org/10.1038/nri3535.

13.   Hamer HM, Jonkers D, Venema K, Vanhoutvin S, Troost FJ, Brummer RJ. 2008. Review article: the role of butyrate on colonic function. Aliment Pharmacol Ther 27:104 –119. https://doi.org/10.1111/j.1365-2036.2007.03562.x.

14.   Raqib R, Sarker P, Bergman P, Ara G, Lindh M, Sack DA, Nasirul Islam KM, Gudmundsson GH, Andersson J, Agerberth B. 2006. Improved outcome in shigellosis associated with butyrate induction of an endogenous peptide antibiotic. Proc Natl Acad Sci U S A 103:9178 –9183. https://doi.org/10.1073/pnas.0602888103.

15.   Chang PV, Hao LM, Offermanns S, Medzhitov R. 2014. The microbial metabolite butyrate regulates intestinal macrophage function via histone deacetylase inhibition. Proc Natl Acad Sci U S A 111:2247–2252. https://doi.org/10.1073/pnas.1322269111.

16.   Pham NT, Lawley TD. 2014. Pathogens' exploitation of the intestinal food web. Cell Host Microbe 16:703–705. https://doi.org/10.1016/j.chom.2014.11.012.

17.   Moens F, Verce M, De Vuyst L. 2017. Lactate- and acetate-based cross- feeding interactions between selected strains of *Lactobacilli*, *Bifidobacteria* and colon bacteria in

the presence of inulin-type fructans. Int J Food Microbiol 241:225–236.

https://doi.org/10.1016/j.ijfoodmicro.2016.10.019.

18.   Porter NT, Luis AS, Martens EC. 2018. *Bacteroides thetaiotaomicron*. Trends

Microbiol 26:966 –967. https://doi.org/10.1016/j.tim.2018.08.005.

19.   Comstock LE, Coyne MJ. 2003. *Bacteroides thetaiotaomicron*: a dynamic, niche-

adapted human symbiont. Bioessays 25:926 –929. https://doi.org/ 10.1002/bies.10350.

20.   Gronlund MM, Lehtonen OP, Eerola E, Kero P. 1999. Fecal microflora in healthy

infants born by different methods of delivery: permanent changes in intestinal flora after

cesarean delivery. J Pediatr Gastroenterol Nutr 28:19 –25.

https://doi.org/10.1097/00005176-199901000-00007.

21.   Fanaro S, Chierici R, Guerrini P, Vigi V. 2003. Intestinal microflora in early

infancy: composition and development. Acta Paediatr Suppl 91:48 –55.

https://doi.org/10.1111/j.1651-2227.2003.tb00646.x.

22.   Jacobson A, Lam L, Rajendram M, Tamburini F, Honeycutt J, Pham T, Van

Treuren W, Pruss K, Stabler SR, Lugo K, Bouley DM, Vilches-Moure JG, Smith M,

Sonnenburg JL, Bhatt AS, Huang KC, Monack D. 2018. A gut commensal-produced

metabolite mediates colonization resistance to *Salmonella* infection. Cell Host Microbe

24:296.e7–307.e7. https://doi.org/10.1016/j.chom.2018.07.002.

23.   Curtis MM, Hu Z, Klimko C, Narayanan S, Deberardinis R, Sperandio V. 2014.

The gut commensal *Bacteroides thetaiotaomicron* exacerbates enteric infection through

modification of the metabolic landscape. Cell Host Microbe 16:759 –769.

https://doi.org/10.1016/j.chom.2014.11.005.

24.   Love DN, Jones RF, Bailey M. 1981. Characterization of *Bacteroides* species isolated from soft tissue infections in cats. J Appl Bacteriol 50:567–575. https://doi.org/10.1111/j.1365-2672.1981.tb04259.x.

25.   Prindiville TP, Sheikh RA, Cohen SH, Tang YJ, Cantrell MC, Silva J, Jr. 2000. *Bacteroides fragilis* enterotoxin gene sequences in patients with inflammatory bowel disease. Emerg Infect Dis 6:171–174. https://doi.org/10.3201/eid0602.000210.

26.   Grenier D, Mayrand D. 1987. Selected characteristics of pathogenic and nonpathogenic strains of *Bacteroides gingivalis*. J Clin Microbiol 25: 738 –740. https://doi.org/10.1128/JCM.25.4.738-740.1987.

27.   Rashtchian A, Dubes GR, Booth SJ. 1982. Transferable resistance to cefoxitin in *Bacteroides thetaiotaomicron*. Antimicrob Agents Chemother 22:701–703. https://doi.org/10.1128/aac.22.4.701.

28.   Wang Y, Rotman ER, Shoemaker NB, Salyers AA. 2005. Translational control of tetracycline resistance and conjugation in the *Bacteroides* conjugative transposon CTnDOT. J Bacteriol 187:2673–2680. https://doi.org/10.1128/JB.187.8.2673-2680.2005.

29.   Salyers AA, Vercellotti JR, West SE, Wilkins TD. 1977. Fermentation of mucin and plant polysaccharides by strains of *Bacteroides* from the human colon. Appl Environ Microbiol 33:319 –322. https://doi.org/10 .1128/AEM.33.2.319-322.1977.

30.   Salyers AA, O'Brien M, Kotarski SF. 1982. Utilization of chondroitin sulfate by *Bacteroides thetaiotaomicron* growing in carbohydrate-limited continuous culture. J Bacteriol 150:1008 –1015. https://doi.org/10.1128/JB.150.3.1008-1015.1982.

31. Kotarski SF, Salyers AA. 1981. Effect of long generation times on growth of *Bacteroides thetaiotaomicron* in carbohydrate-induced continuous culture. J Bacteriol 146:853– 860. https://doi.org/10.1128/JB.146.3.853-860.1981.

32. Namavar F, Verweij AM, Bal M, van Steenbergen TJ, de Graaff J, MacLaren DM. 1983. Effect of anaerobic bacteria on killing of *Proteus mirabilis* by human polymorphonuclear leukocytes. Infect Immun 40: 930 –935. https://doi.org/10.1128/IAI.40.3.930-935.1983.

33. Rotstein OD, Pruett TL, Sorenson JJ, Fiegel VD, Nelson RD, Simmons RL. 1986. A *Bacteroides* by-product inhibits human polymorphonuclear leukocyte function. Arch Surg 121:82– 88. https://doi.org/10.1001/archsurg.1986.01400010096012.

34. Rotstein OD, Nasmith PE, Grinstein S. 1987. The *Bacteroides* by-product succinic acid inhibits neutrophil respiratory burst by reducing intracellular pH. Infect Immun 55:864 – 870. https://doi.org/10.1128/IAI.55.4.864-870.1987.

35. Axe DD, Bailey JE. 1995. Transport of lactate and acetate through the energized cytoplasmic membrane of *Escherichia coli*. Biotechnol Bioeng 47:8 –19. https://doi.org/10.1002/bit.260470103.

36. Wolfe AJ. 2005. The acetate switch. Microbiol Mol Biol Rev 69:12–50. https://doi.org/10.1128/MMBR.69.1.12-50.2005.

37. Bernal V, Castano-Cerezo S, Canovas M. 2016. Acetate metabolism regulation in *Escherichia coli*: carbon overflow, pathogenicity, and beyond. Appl Microbiol Biotechnol 100:8985–9001. https://doi.org/10.1007/s00253-016-7832-x.

38. Varma A, Palsson BO. 1994. Stoichiometric flux balance models quantitatively predict growth and metabolic by-product secretion in wild-type *Escherichia coli* W3110.

Appl Environ Microbiol 60:3724 –3731. https:// doi.org/10.1128/AEM.60.10.3724-3731.1994.

39.   Basan M, Hui S, Okano H, Zhang Z, Shen Y, Williamson JR, Hwa T. 2015. Overflow metabolism in *Escherichia coli* results from efficient proteome allocation. Nature 528:99 –104. https://doi.org/10.1038/nature15765.

40.   Bhinderwala F, Lei S, Woods J, Rose J, Marshall DD, Riekeberg E, Leite ADL, Morton M, Dodds ED, Franco R, Powers R. 2019. Metabolomics analyses from tissues in Parkinson's disease. Methods Mol Biol 1996: 217–257. https://doi.org/10.1007/978-1-4939-9488-5_19.

41.   Bhinderwala F, Powers R. 2019. NMR metabolomics protocols for drug discovery. Methods Mol Biol 2037:265–311. https://doi.org/10.1007/978-1-4939-9690-2_16.

42.   Somerville GA, Powers R. 2014. Growth and preparation of *Staphylococcus epidermidis* for NMR metabolomic analysis. Methods Mol Biol 1106: 71–91. https://doi.org/10.1007/978-1-62703-736-5_6.

43.   Sawers RG, Clark DP. 2004. Fermentative pyruvate and acetyl-coenzyme A metabolism. EcoSal Plus 1:3.5.3. https://doi.org/10.1128/ecosalplus.3.5.3.

44.   Wong HC, Chen YL. 1988. Effects of lactic acid bacteria and organic acids on growth and germination of *Bacillus cereus*. Appl Environ Microbiol 54:2179 –2184. https://doi.org/10.1128/AEM.54.9.2179-2184.1988.

45.   Pinhal S, Ropers D, Geiselmann J, de Jong H. 2019. Acetate metabolism and the inhibition of bacterial growth by acetate. J Bacteriol 201:e00147-19. https://doi.org/10.1128/JB.00147-19.

46.   Cummings JH, Macfarlane GT. 1991. The control and consequences of bacterial fermentation in the human colon. J Appl Bacteriol 70:443– 459. https://doi.org/10.1111/j.1365-2672.1991.tb02739.x.

47.   Kim DJ, Chung SG, Lee SH, Choi JW. 2012. Relation of microbial biomass to counting units for *Pseudomonas aeruginosa*. Afr J Microbiol Res 6:4620 – 4622.

48.   Pines D, Ditkovich J, Mukra T, Miller Y, Kiefer PM, Daschakraborty S, Hynes JT, Pines E. 2016. How acidic is carbonic acid? J Phys Chem B 120:2440 –2451. https://doi.org/10.1021/acs.jpcb.5b12428.

49.   Innocenti A, Vullo D, Scozzafava A, Casey JR, Supuran C. 2005. Carbonic anhydrase inhibitors. Interaction of isozymes I, II, IV, V, and IX with carboxylates. Bioorg Med Chem Lett 15:573–578. https://doi.org/10.1016/j.bmcl.2004.11.057.

50.   Laursen BS, Sorensen HP, Mortensen KK, Sperling-Petersen HU. 2005. Initiation of protein synthesis in bacteria. Microbiol Mol Biol Rev 69: 101–123. https://doi.org/10.1128/MMBR.69.1.101-123.2005.

51.   Starai VJ, Garrity J, Escalante-Semerena JC. 2005. Acetate excretion during growth of *Salmonella enterica* on ethanolamine requires phosphotransacetylase (EutD) activity, and acetate recapture requires acetyl- CoA synthetase (Acs) and phosphotransacetylase (Pta) activities. Microbiology 151:3793–3801. https://doi.org/10.1099/mic.0.28156-0.

52.   Chung T, Klumpp DJ, LaPorte DC. 1988. Glyoxylate bypass operon of *Escherichia coli*: cloning and determination of the functional map. J Bacteriol 170:386 – 392. https://doi.org/10.1128/jb.170.1.386-392.1988.

53. Sieber JR, McInerney MJ, Gunsalus RP. 2012. Genomic insights into syntrophy: the paradigm for anaerobic metabolic cooperation. Annu Rev Microbiol 66:429 – 452. https://doi.org/10.1146/annurev-micro-090110-102844.

54. Pacheco AR, Moel M, Segre D. 2019. Costless metabolic secretions as drivers of interspecies interactions in microbial ecosystems. Nat Commun 10:103. https://doi.org/10.1038/s41467-018-07946-9.

55. Pacheco AR, Segre D. 2019. A multidimensional perspective on microbial interactions. FEMS Microbiol Lett 366:fnz125. https://doi.org/10.1093/ femsle/fnz125.

56. Rakoff-Nahoum S, Foster KR, Comstock LE. 2016. The evolution of cooperation within the gut microbiota. Nature 533:255–259. https://doi.org/10.1038/nature17626.

57. Reeds PJ. 2000. Dispensable and indispensable amino acids for humans. J Nutr 130:1835S–1840S. https://doi.org/10.1093/jn/130.7.1835S.

58. Owens RA, Hartman PE. 1986. Glutathione: a protective agent in *Salmonella tiphimurium* and *Escherichia coli* as measured by mutagenicity and by growth delay assays. Environ Mutagen 8:659 – 673. https://doi.org/10.1002/em.2860080503.

59. Whittenbury R. 1964. Hydrogen peroxide formation and catalase activity in the lactic acid bacteria. J Gen Microbiol 35:13–26. https://doi.org/10.1099/00221287-35-1-13.

60. Vandenbergh PA. 1993. Lactic acid bacteria, their metabolic products and interference with microbial growth. FEMS Microbiology Rev 12: 221–238. https://doi.org/10.1111/j.1574-6976.1993.tb00020.x.

61.   Reniere ML, Whiteley AT, Hamilton KL, John SM, Lauer P, Brennan RG, Portnoy DA. 2015. Glutathione activates virulence gene expression of an intracellular pathogen. Nature 517:170 –173. https://doi.org/10.1038/ nature14029.

62.   Masip L, Veeravalli K, Georgiou G. 2006. The many faces of glutathione in bacteria. Antioxid Redox Signal 8:753–762. https://doi.org/10.1089/ars.2006.8.753.

63.   Dahl TA, Midden WR, Hartman PE. 1989. Comparison of killing of Gram-negative and Gram-positive bacteria by pure singlet oxygen. J Bacteriol 171:2188 –2194. https://doi.org/10.1128/jb.171.4.2188-2194.1989.

64.   Wexler HM. 2007. Bacteroides: the good, the bad, and the nitty-gritty. Clin Microbiol Rev 20:593– 621. https://doi.org/10.1128/CMR.00008-07.

65.   Samuel BS, Gordon JI. 2006. A humanized gnotobiotic mouse model of host-archaeal-bacterial mutualism. Proc Natl Acad Sci U S A 103: 10011–10016. https://doi.org/10.1073/pnas.0602187103.

66.   Bacic MK, Smith CJ. 2008. Laboratory maintenance and cultivation of bacteroides species. Curr Protoc Microbiol Chapter 13:Unit 13C 11. https://doi.org/10.1002/9780471729259.mc13c01s9.

67.   Halouska S, Zhang B, Gaupp R, Lei S, Snell E, Fenton RJ, Barletta RG, Somerville GA, Powers R. 2013. Revisiting protocols for the NMR analysis of bacterial metabolomes. J Integr OMICS 3:120 –137. https://doi.org/10.5584/jiomics.v3i2.139.

68.   Zhang B, Halouska S, Schiaffo CE, Sadykov MR, Somerville GA, Powers R. 2011. NMR analysis of a stress response metabolic signaling network. J Proteome Res 10:3743–3754. https://doi.org/10.1021/pr200360w.

69.   Worley B, Powers R. 2013. Multivariate analysis in metabolomics. Curr Metabolomics 1:92–107. https://doi.org/10.2174/2213235X11301010092.

70.   Nguyen BD, Meng X, Donovan KJ, Shaka AJ. 2007. SOGGY: solvent- optimized double gradient spectroscopy for water suppression. A comparison with some existing techniques. J Magn Reson 184:263–274. https://doi.org/10.1016/j.jmr.2006.10.014.

71.   Worley B, Powers R. 2014. MVAPACK: a complete data handling package for NMR metabolomics. ACS Chem Biol 9:1138 –1144. https://doi.org/10.1021/cb4008937.

72.   Worley B, Powers R. 2014. Simultaneous phase and scatter correction for NMR datasets. Chemometr Intell Lab Syst 131:1– 6. https://doi.org/10.1016/j.chemolab.2013.11.005.

73.   De Meyer T, Sinnaeve D, Van Gasse B, Tsiporkova E, Rietzschel ER, De Buyzere ML, Gillebert TC, Bekaert S, Martins JC, Van Criekinge W. 2008. NMR-based characterization of metabolic alterations in hypertension using an adaptive, intelligent binning algorithm. Anal Chem 80: 3783–3790. https://doi.org/10.1021/ac7025964.

74.   Savorani F, Tomasi G, Engelsen SB. 2010. icoshift: a versatile tool for the rapid alignment of 1D NMR spectra. J Magn Reson 202:190 –202. https:// doi.org/10.1016/j.jmr.2009.11.012.

75.   Eriksson L, Trygg J, Wold S. 2008. CV-ANOVA for significance testing of PLS and OPLS models. J Chemometrics 22:594 – 600. https://doi.org/10.1002/cem.1187.

76.   Shao J. 1993. Linear-model selection by cross-validation. J Am Stat Assoc 88:486 – 494. https://doi.org/10.1080/01621459.1993.10476299.

77. Xu QS, Liang YZ, Du YP. 2004. Monte Carlo cross-validation for selecting a model and estimating the prediction error in multivariate calibration. J Chemom 18:112–120. https://doi.org/10.1002/cem.858.

78. Arkin AP, Cottingham RW, Henry CS, Harris NL, Stevens RL, Maslov S, Dehal P, Ware D, Perez F, Canon S, Sneddon MW, Henderson ML, Riehl WJ, Murphy-Olson D, Chan SY, Kamimura RT, Kumari S, Drake MM, Brettin TS, Glass EM, Chivian D, Gunter D, Weston DJ, Allen BH, Baumohl J, Best AA, Bowen B, Brenner SE, Bun CC, Chandonia JM, Chia JM, Colasanti R, Conrad N, Davis JJ, Davison BH, DeJongh M, Devoid S, Dietrich E, Dubchak I, Edirisinghe JN, Fang G, Faria JP, Frybarger PM, Gerlach W, Gerstein M, Greiner A, Gurtowski J, Haun HL, He F, Jain R, et al. 2018. KBase: the United States Department of Energy systems biology knowledgebase. Nat Biotechnol 36:566 –569. https://doi.org/10.1038/nbt.4163.

79. Henry CS, DeJongh M, Best AA, Frybarger PM, Linsay B, Stevens RL. 2010. High-throughput generation, optimization and analysis of genome-scale metabolic models. Nat Biotechnol 28:977–982. https://doi.org/10.1038/nbt.1672.
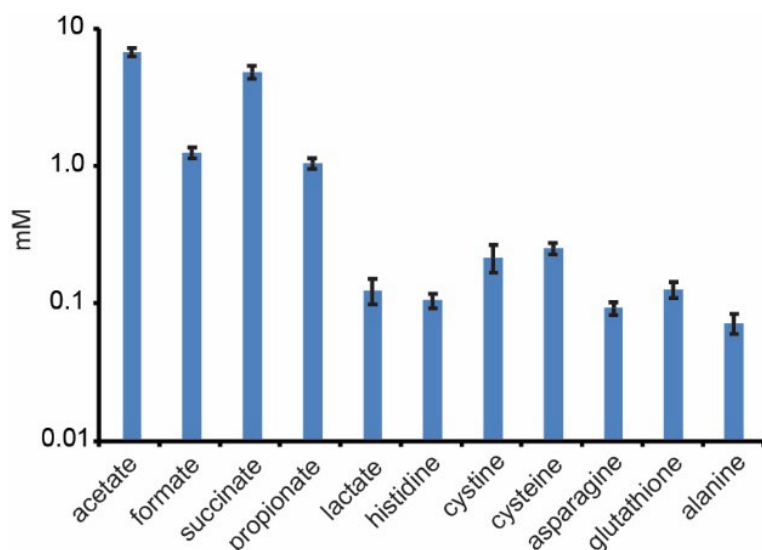
Figure 1: Metabolites secreted by *B. theta*. Concentrations of secreted metabolites detected after batch growth in defined minimal glucose medium (mean of 5 biological and 5 technical replicates, *n* = 25).
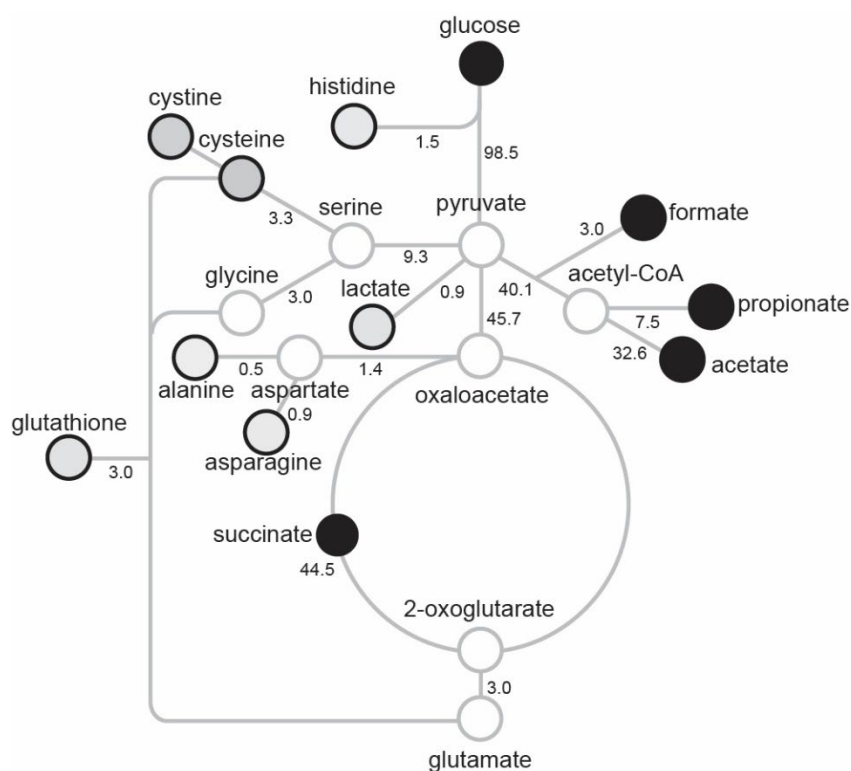

Figure 2: Secretion fluxes of organic acids and amino acids in defined minimal medium. Numbers represent percent mole carbon fluxes (not shown, CO_2 inferred, 4.6%). Gray outlined circles represent undetected intracellular metabolic nodes. Black outlined circles indicate secreted metabolites. Shading is proportional to concentration in culture medium.
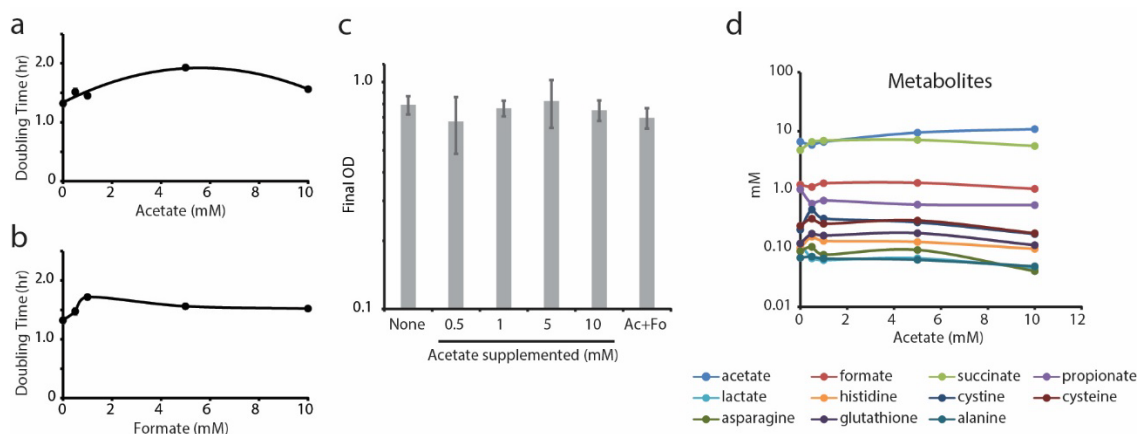
Figure 3: Effect of metabolic feedback inhibition on growth. (a) Population doubling time of cultures on defined minimal medium supplemented with acetate ($n = 8$ biological replicates, $P < 0.01$ versus 0 mM, $r^2 = 0.94$). (b) Population doubling time of cultures on defined minimal medium supplemented with formate ($n = 5$ biological replicates, $P < 0.01$ versus 0 mM). (c) Final optical densities of cultures with and without supplementation of 10 mM acetate (Ac) and 10 mM formate (Fo) ($n = 5$ biological replicates, $P > 0.05$ versus 0 mM). (d) Concentrations of secreted metabolites with increasing acetate supplementation (means from 5 biological and 5 technical replicates, $n = 25$). P values are shown in Table S1 in the supplemental material. Curves were fit according to parabolic functions (a) or least-squares regression (b and d). Error bars may be obscured by symbols.
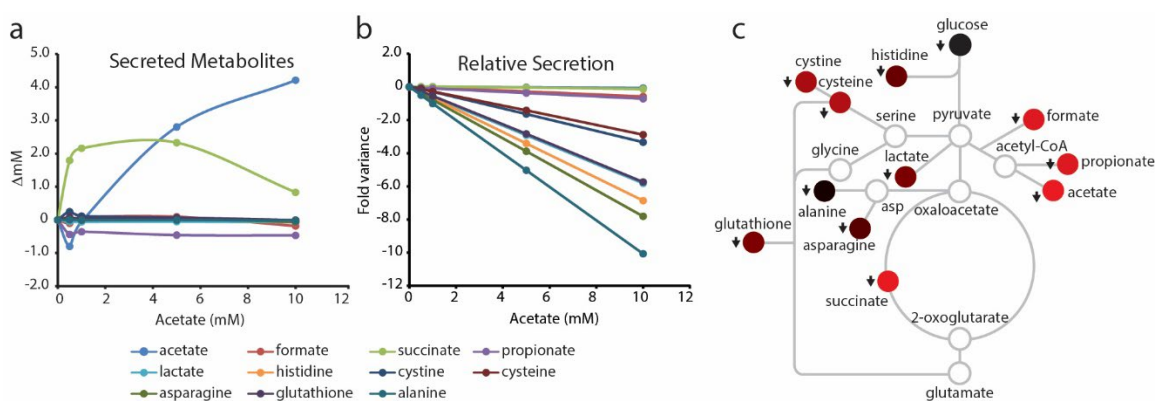
Figure 4: Effect of acetate feedback inhibition on secretion fluxes. (a) Concentrations of secreted metabolites with increasing acetate supplementation (means from 5 biological and 5 technical replicates, $n = 25$). P values are shown in Table S2. Error bars may be obscured by symbols. (b) Change in secretion fluxes with increasing acetate supplementation (means from 5 biological and 5 technical replicates, $n = 25$). P values are shown in Table S3. (c) Effect of acetate feedback inhibition (10 mM) mapped onto a metabolic network. Red, decreased secretion. Shading is

proportional to flux magnitude. Gray outlined circles represent undetected intracellular metabolic nodes. asp, aspartate.
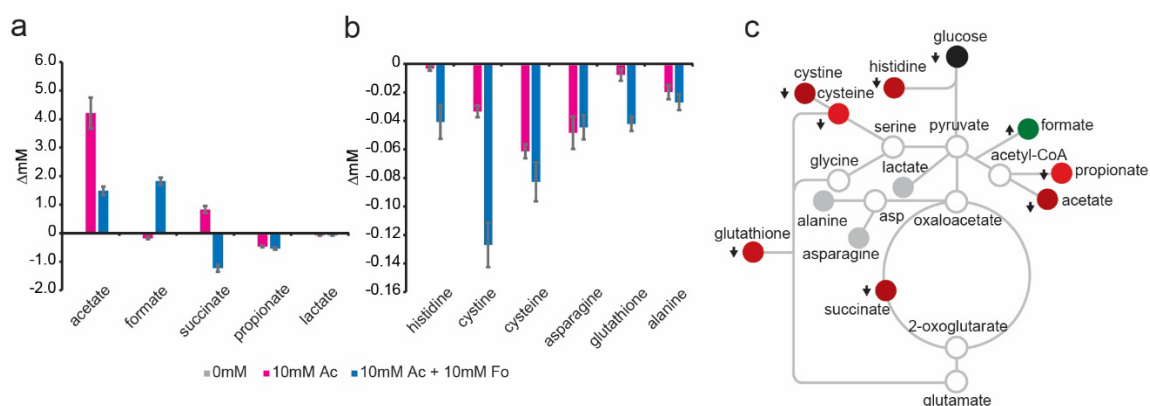

Figure 5: Effect of formate supplementation on acetate feedback inhibition. (a) Change in organic acid secretion with and without supplementation of 10 mM acetate or a combination of 10 mM acetate (Ac) and 10 mM formate (Fo). (b) Change in secreted amino acids with and without supplementation. (c) Effect of 10 mM formate supplementation on 10 mM acetate feedback inhibition mapped to the metabolic network. Green, increased secretion; red, decreased secretion; gray, no significant difference between 10 mM acetate versus 10 mM acetate and 10 mM formate conditions. Shading is proportional to flux magnitude. Gray outlined circles represent undetected intracellular metabolic nodes. asp, aspartate. *P*-values for data in panels a and b are shown in Table S4. Error bars may be too small to see.
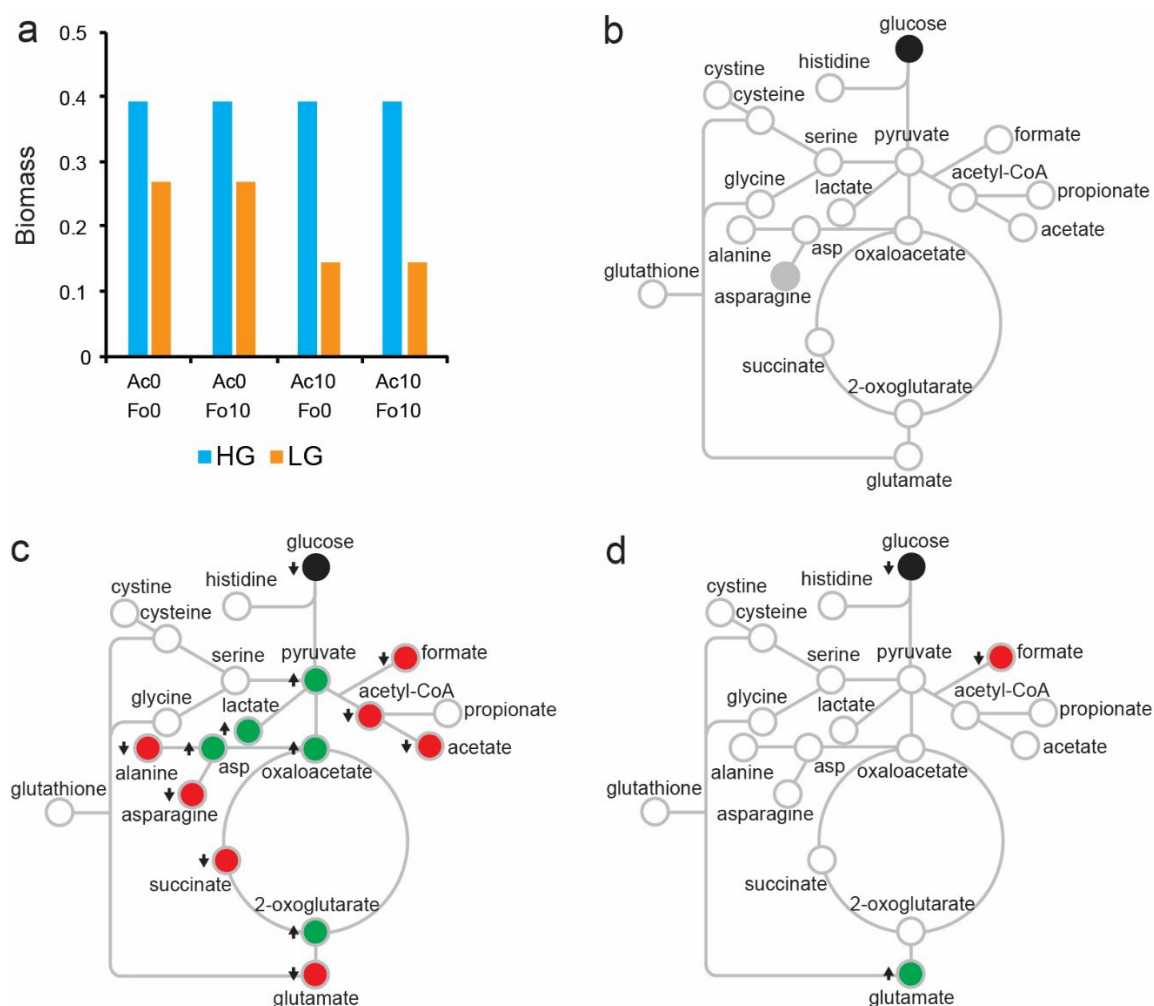
Figure 6: Simulation of the effect of feedback inhibition on metabolism. (a) Predicted biomass in high-glucose (HG) and low-glucose (LG) medium as acetate (Ac) and formate (Fo) concentrations were varied from 0 mM to 10 mM. (b) Predicted effect of acetate and/or formate on exchange fluxes in HG medium. (c) Predicted effect of acetate on exchange fluxes in LG medium. (d) Predicted effect of formate on exchange fluxes in LG medium. Green, increased exchange flux; red, decreased exchange flux; gray, no net change in exchange flux due to metabolic rerouting; white, no change predicted.

Table 1: Effect of formate and acetate on *B. theta* growth rate in defined medium

Treatment[a]	Doubling Time (h)	SD	P-value vs 0mM Fo	vs 10 mM Ac + 10 mM Fo
0 mM	1.322	0.047	1	
0.5 mM Ac	1.516	0.052	0.000	0.000
1 mM Ac	1.452	0.034	0.000	0.000
5 mM Ac	1.929	0.037	0.000	0.000
10 mM Ac	1.562	0.028	0.000	0.000
0.5 mM Fo	1.474	0.042	0.000	0.000
1 mM Fo	1.718	0.078	0.000	0.704[b]
5 mM Fo	1.561	0.034	0.000	0.000
10 mM Fo	1.521	0.034	0.000	0.000
10 mM Ac+10 mM Fo	1.734	0.05	0.000	1

a Ac, acetate; Fo, formate. Data were obtained from six biological replicates ($n = 6$).

b Not statistically significant ($P > 0.05$).

Table 2: pH of stationary-phase cultures in buffered medium

Treatment[a]	pH	SD	P value vs 0 mM
0 mM control	7.14	0.064	1
0.5 mM Ac	7.07	0.079	0.196[b]
1 mM Ac	7.03	0.077	0.059[b]
5 mM Ac	7.06	0.034	0.064[b]
10 mM Ac	7.03	0.051	0.030
10 mM Ac+10 mM Fo	7.06	0.046	0.083[b]

a Ac, acetate; Fo, formate. Data were obtained from six biological replicates ($n = 6$).

b Not statistically significant ($P > 0.05$).

Table 3: Acetate suppression coefficients of secreted metabolites

Metabolite	Fold suppression coefficient ($\therefore ix_{var}$)	Pearson correlation (R^2)
Acetate	-0.00535	0.93736
Formate	-0.05783	0.99941
Succinate	-0.01478	0.94946
Propionate	-0.07022	0.99859
Cysteine	-0.28908	0.99990
Cystine	-0.33741	0.99955
Glutathione	-0.57522	0.99995
Lactate	-0.57985	0.99998
Histidine	-0.68781	0.99997
Asparagine	-0.78083	0.99999
Alanine	-1.00662	1.00000

Chapter 7: Metabolic synergy between human symbionts *Bacteroides* and *Methanobrevibacter*

This chapter represents the contents of: Jennie L. Cattlet, Sean Carr, Mikaela Cashman, Megan D. Smith, Mary Walter, Zahmeeth Sakkaff, Christine Kelley, Massimiliano Pierobon, Myra B. Cohen, and Nicole R. Buan. "Metabolic Synergy between Human Symbionts *Bacteroides* and *Methanobrevibacter*." *Microbiology Spectrum* (2022): e01067-22. https://doi.org/10.1128/spectrum.01067-22

Author contributions: J.L.C. designed and carried out experiments, analyzed data, and edited the paper. S.C. designed and carried out experiments, analyzed data, wrote, and edited the paper. M.C. designed and carried out experiments, analyzed data, and wrote and edited the paper. M.D.S. carried out experiments and analyzed data. M.P. designed experiments, analyzed data, and edited the paper. M.B.C. designed *in silico* experiments and edited the paper. N.R.B. designed the experiments, analyzed data, and wrote and edited the paper.

Abstract

Trophic interactions between microbes are postulated to determine whether a host microbiome is healthy or causes predisposition to disease. Two abundant taxa, the Gram negative heterotrophic bacterium *Bacteroides thetaiotaomicron (B. theta)* and the methanogenic archaean *Methanobrevibacter smithii,* are proposed to have a synergistic metabolic relationship. Both organisms play vital roles in human gut

health; *B. theta* assists the host by fermenting dietary polysaccharides whereas *M. smithii* consumes end-stage fermentation products and is hypothesized to relieve feedback inhibition of upstream microbes such as *B. theta*. To study their metabolic interactions, we defined and optimized a co-culture system and used software testing techniques to analyze growth under a range of conditions representing the nutrient environment of the host. We verify that *B. theta* fermentation products are sufficient for *M. smithii* growth, and accumulation of fermentation products alters secretion of metabolites by *B. theta* to benefit *M. smithii.* Studies suggest *B. theta* metabolic efficiency is greater in the absence of fermentation products or in the presence of *M. smithii*. Under certain conditions *B. theta* and *M. smithii* form interspecies granules consistent with behavior observed for syntrophic partnerships between microbes in soil or sediment enrichments and anaerobic digesters. Furthermore, when vitamin B$_{12}$, hematin, and hydrogen gas are abundant, coculture growth is greater than the sum of growth observed for monocultures, suggesting both organisms benefit from a synergistic mutual metabolic relationship.

Importance

The human gut functions through a complex system of interactions between the host human tissue and the microbes which inhabit it. These diverse interactions are difficult to model or examine under controlled laboratory conditions and is necessary to simplify the system in order to test mechanistic hypotheses. We studied the interactions between two dominant human gut microbes *B. theta* and *M. smithii* using a seven-component culturing approach that allows the systematic examination of the metabolic

complexity of this binary microbial system. We then use decision trees to identify cooperative, neutral, and competitive interactions between nutrients, metabolites, and organisms that are otherwise missed in community-level microbiome studies. By combining high throughput methods with machine learning techniques, we were able to investigate the interactions between two dominant genera of the gut microbiome in a wide variety of environmental conditions. Our approach can be broadly applied to studying microbial interactions and may be extended to evaluate and curate computational metabolic models. The software tools developed for this study are available as user-friendly tutorials in the Department of Energy KBase.

Introduction

From birth, the human microbiome plays an important role in maintaining human health.[1-4] Newborns are colonized in their first days of life[5-7] and the microbiome grows and develops with the child into adulthood.[5,8] Depending on the age, geographic location, diet, and health of its host, 10-100 trillion microbial cells reside in the intestines alone.[1,9] These organisms are part of a dynamic, closely interconnected ecosystem made up of Bacteria, Archaea, and Eukarya.[7,8,10] Interactions between host-associated microbes affect many aspects of human health. A well-balanced, healthy microbiota offers protection against infection,[11,12] metabolizes nutritional compounds,[13] provides essential vitamins and nutrients, adds 15 - 30% of human caloric intake,[14,15] manages weight gain,[16] and influences the human immune system and its development.[17-19] However, an unbalanced microbiome is linked to obesity, infections, asthma, allergies, Crohn's disease, irritable bowel disease, neurodegenerative disease, and cancer.[1-4,12,17,19-34]

It has been proposed that mutualistic relationships within the gut microbiome maintain a balance that is necessary for a healthy host digestive system.[8,29,35] The dynamic interactions between microbes in a multispecies gut community are difficult to study both in the laboratory and using computational modeling and analysis due to the sheer complexity of the system. This complexity is due to many factors including the combinatorial genetic space, sampling heterogeneity, unknown environmental conditions (e.g. local microvariation in temperature and pH, and nutrient availability), and unknown relationships between interacting genetic and environmental variables that make it difficult to confidently ascribe major (or minor) organism functions in a mixed microbiome community. Fortunately, cutting-edge software systems research approaches such as statistical sampling and decision trees can be used to develop tools for management and analysis of complex microbial systems.[36] To benchmark new computational tools we constrain the gut microbiome system to studying the relationship between two key human gut inhabitants: the fermenter *Bacteroides thetaiotaomicron* (*B. theta*) and the methanogenic archaeon, *Methanobrevibacter smithii* (*M. smithii*).

B. theta is one of the most prominent fermenters in the human gut, making up between 5 and 50% of the overall gut community.[15] *B. theta* a generalist fermenter: it consumes dietary plant polysaccharides such as starch as well as mucosal glycans such as heparin and produces fermentation products such as hydrogen, carbon dioxide, formate, acetate and succinate.[15] It plays a crucial digestive role by partially breaking down polysaccharides human cells are unable to degrade and produces short-chain fatty acids for human and microbial consumption (acetate, succinate, propionate, lactate). In the

process, it protects intestines against infection by activating host immune defenses, through direct interactions, and by competition with other bacteria.[12,37]

M. smithii is the dominant methanogen in the human gut and makes up between 1% and 10% of the human gut community.[38,39] It colonizes the human gut in infancy and remains present in the majority of the population through adulthood[6,38] and has been detected in up to 95.7% of individuals.[39-42] Imbalance in M. smithii gut communities has been associated with obesity and malnutrition-related digestive diseases.[30,41,43,44] M. smithii is a hydrogenotrophic methanogen and can conserve energy through methanogenesis using carbon dioxide and hydrogen gas or formate as substrates.[39,45, 46] M. smithii has an incomplete reductive tricarboxylic acid (TCA) cycle and must assimilate acetate as a carbon substrate. It is hypothesized that growth of M. smithii in the gut could benefit B. theta and other fermenters by metabolizing fermentation products that would inhibit further fermentation by feedback inhibition as they accumulate. Moreover, the removal of hydrogen could allow B. theta to increase metabolic efficiency and contribute to effective metabolism of dietary substrates, since high hydrogen partial pressure inhibits bacterial NADH dehydrogenases, reducing the yield of ATP and causing fermentation overall to become endergonic (unfavorable).[35,47] The proposed nature of the complementary metabolism between B. theta and M. smithii suggests a mutualistic relationship in which M. smithii relies on the metabolic products of B. theta fermentation to survive, while B. theta relies on M. smithii to remove products that would inhibit fermentation, which would be an example of metabolic syntrophy.[47]

Syntrophy is a form of mutualism in which two organisms form a tightly coupled, mutually beneficial metabolic relationship.[47-50] Syntrophic relationships allow bacteria to

overcome energy barriers and to break down substrates more efficiently.[35,48,50,51] Methanogens have often been observed in syntrophic relationships with soil bacteria, removing hydrogen gas and other fermentation inhibitors to benefit the bacteria.[47,50,52] *B. theta* and *M. smithii* have been previously proposed to form a syntrophic relationship based on genomic evidence.[46] Gnotobiotic mouse studies suggest that the presence of *M. smithii* assists *B. theta* in the breakdown of polysaccharides and increases host digestive efficiency,[35] and our previous study showed that *B. theta* is feedback inhibited by acetate and formate,[53] suggesting that a partner organism that consumes these metabolic byproducts, such as *M. smithii*, may benefit *B. theta*. However the relationship between *B. theta* and *M. smithii* is not fully characterized. One of the greatest obstacles is the difficulty in systematically identifying what conditions could lead to a synergistic metabolic relationship, such as syntrophy, that benefits both organisms.

To examine the metabolic relationship between *B. theta* and *M. smithii*, we established laboratory conditions in which both monocultures and co-cultures of *B. theta* and *M. smithii* can be studied and characterized. We leverage an approach to test complex software; partitioning the input space and systematically manipulating program inputs and inferring interactions and relationships between the inputs. In the system we studied here, we observed organism and coculture growth behaviors as outputs dependent on culture nutrient inputs. We then devised an assay to compare monocultures and cocultures in 128 different nutrient conditions and evaluated growth using decision trees from machine learning to identify neutral, favorable, and unfavorable conditions for *M. smithii* and *B. theta* growing in co-culture.

Materials and Methods:

Strains and culturing conditions

  B. thetaiotaomicron vpi-5482 (ATCC29148, NB203)[54,55] and *M. smithii*

DSM0861 (ATCC35061, NB215)[45] were used for the described studies. Strains were

grown at 37˚C in 18 mm x 150 mm Balch culture tubes under strict anaerobic conditions,

in either a rich tryptone and yeast extract growth medium (TYG) or a defined medium.

Previous work with *B. theta* utilized tryptone, yeast extract and glucose medium (TYG)

as a rich growth medium.[15,35,56] Rich medium for *M. smithii* was also dependent on yeast

extract.[57,58] Using TYG as a base, the recipes were combined to ensure growth for both

organisms. *M. smithii* was initially grown in DSMZ *Methanobacterium* Medium 119[58]

then passaged into the modified rich medium supplemented with 10 mM formate and

10mM acetate with 138 kPa 20% CO_2 80% H_2 headspace atmosphere. The defined

medium was designed through a comparison of recipes.[45,46,59-62] Rich medium contained

tryptone peptone (10 g), Bacto yeast extract (5 g), 100 mM KPO_4 pH 7.2, 40 ml TYG

salts (0.5 g $MgSO_4 \bullet 7H_2O$, 10 g $NAHCO_3$, 2 g NaCl per liter), 54.4 μM $CaCl_2$, 1.4 μM

$FeSO_4$, 4 μM resazurin, 2.8 mM cysteine•HCl, 25 μM Na_2S, per liter. Defined medium

contained 7.5 mM NH_4SO_4, 11.9 mM Na_2CO_3, 100 mM KPO_4 pH 7.2, 14 μM $FeSO_4$, 50

mL mineral salts (18 g NaCl, 0.53 g $CaCl_2 \bullet 2H_2O$, 0.40 g $MgCl_2 \bullet 6H_2O$, 0.20 g

$MnCl_2 \bullet 4H_2O$, 0.20 g $CoCl_2 \bullet 6H_2O$ per liter), 4 μM resazurin, 2.8 mM cysteine•HCl, 25

μM Na_2S, per liter. When indicated, cultures were supplemented with 10 mM sodium

acetate, 10 mM formate, 20 μM histidine and 2 μM hematin, 3.7 nM vitamin B_{12}

(cyanocobalamin), or 5.8 mM vitamin K_3 (menadione). *B. theta* was supplemented with

glucose to 0.05% (2.78 mM). Culture headspace was either 20% CO_2, 80% N_2 or 5% H_2,

20% CO_2, 75% N_2 atmosphere at 138 kPa. *M. smithii* was grown on a rotary shaker operating at 45 rpm. *M. smithii* culture tubes were pressurized to 138 kPa with a 20% CO_2 80% H_2 gas mixture twice daily during growth curves or every three days for culture maintenance. Preliminary data suggested that vitamin K_3 may hinder *M. smithii* growth. *B. theta* / *M. smithii* co-cultures were grown on or off the shaker under a 5% H_2, 20% CO_2, 75% N_2 atmosphere in rich or defined medium supplemented with glucose to 0.05% (2.78 mM).

Growth Curves

B. theta and *M. smithii* were grown in 10ml TYG, then transferred to media containing appropriate carbon sources and compounds. Growth in 18 mm x 150 mm anaerobic culture tubes was assessed by measuring changes in optical density at 600 nm using a Spec20D spectrophotometer modified with an 18mm tube adapter. Growth in 96 well plates was assessed by measuring change in optical density at 600 nm using a Tecan Sunrise plate reader under a 5% H_2 20% CO_2, 75% N_2 atmosphere.

Microscopy

Microscopy was performed using an EVOS FL Auto Cell Imaging System with DAPI, Texas Red, and Green Florescent Protein LED light cubes in the University of Nebraska Morrison Microscopy Core Facility. *B. theta* and *M. smithii* were grown in medium containing an appropriate carbon source as above. Co-cultures were grown in defined medium with only glucose as a carbon source. 500 μl samples were taken in an anaerobic atmosphere and stained with a combination of 5 μl propidium iodide and 1 μl

SYTO 9 Green per 500 µl cells while remaining in anaerobic conditions. *M. smithii* coenzyme F_{420} auto-fluorescence was viewed using a DAPI light cube,[6,38,45,63] propidium iodide with a Texas Red light cube, and Syto 9 Green with a Green Florescent Protein light cube.

Flow cytometry

Flow cytometry was performed using a BD Biosciences FACS Aria II Flow Cytometer (BD Biosciences) in the Nebraska Center for Biotechnology Flow Cytometry Core Facility. *B. theta* and *M. smithii* were grown anaerobically in rich medium supplemented with variable concentrations of glucose and sodium acetate over 4 and 9 days. Cell concentrations were recorded via OD_{600} and cultures were concentrated anaerobically via centrifugation at a 500 x g for 10 minutes in a ThermoScientific Sorvall Legend Micro21 rotor, washed with phosphate-buffered saline (PBS; 137mM NaCl, 2.7mM KCl, 10mM Na_2HPO_4, 1.8mM KH_2PO_4) and resuspended to a concentration of ~$1.0x10^6$ cells per mL. Cells were dyed using LIVE/DEAD™ Fixable Yellow Dead Cell Stain Kit (Invitrogen) according to the protocol provided. Flow Cytometry was performed exciting with a 405nm laser until 10,000 events were recorded. Flow cytometry size standards were obtained from Fisher (1.0-15 µm diameter; catalog number F13838). The gating control is shown in Supplementay Data **Figure S1**.

qPCR quantification

B. theta and *M. smithii* were grown in rich media supplemented with glucose. Cultures were incubated at 37°C and 1ml samples were collected anaerobically on day 4 and 9 of growth. DNA was isolated from the cells using a phenol-chloroform extraction[64] and qPCR was performed on a Mastercycler® RealPlex^2 instrument (Eppendorf)

detecting SYBR Green using probes for 16s regions of the *B. theta* (B theta 16S fwd: 5'GGGATGCGTTCCATTAGGC; B theta 16S rev: 5'GGGACCTTCCTCTCAGAACC) and *M. smithii* (M smithii 16S fwd: 5'CGGCCGATTAGGTAGTTGGT; M smithii 16S rev: 5'GTTCCATCTCCGGGCTCTT) genomes. Ct values were normalized to input DNA, amplification efficiency, and the apparent number of genomes per cell. To account for variability in chromosome copy number between the two organisms an apparent genome count was calculated by counting cells using a hemocytometer and carefully extracting the DNA from 1 ml of cells. The DNA quantity was measured via NanoDrop Spectrophotometer (Thermo Scientific) and was divided by the genome size to calculate average number of genomes per cell which would then be divided by the number of cells harvested in 1mL.

Dropout media preparation and growth assays

For each biological replicate of the 7-component growth assay, dropout media were prepared that contained all combinations of vitamin K_3, vitamin B_{12}, formate, acetate, histidine-hematin, and glucose. Media were dispensed into 16 sterile 96-well culture plates, with two plates for each layout. One plate of each layout was kept under a 5% H_2, 0.1% H_2S, 20% CO_2, 74.9% N_2 atmosphere, the other under 0.1% H_2S, 20% CO_2, 79.9% N_2, resulting in 128 media combinations total.

B. theta and *M. smithii* were grown in 10ml rich medium and used to inoculate prepared 96 well culture plates. For monocultures, 1:20 inocula (5 μl) of *B. theta*, 1:10 inocula (10 μl) of *M. smithii*, or a co-culture of both were added to sample wells. The inoculum volumes for each strain were empirically determined to yield measurable culture turbidity within the two-week experiment. One plate of each layout was placed in

a 35˚C anaerobic incubator with either 5% H_2, 0.1% H_2S, 20%CO_2, 74.9% N_2 or 0.1%

H_2S, 20% CO_2, 79.9% N_2 atmosphere. A Tecan Sunrise plate reader measured optical

density at 600nm after 7 days or 14 days under strict anaerobic conditions. The process

was repeated for a total of three biological replicates.

Growth data analysis

The plate reader data was expected to contain errors due to splashing during

handling, evaporation and the formation of bubbles or cell clumps. Because each set of 8

samples or blanks contained similar contents, cells, and medium components, a normal

distribution was assumed and Chauvenet's criterion was applied to eliminate statistical

outliers in preparation for statistical and algorithmic analysis.[65] Chauvenet's criterion

specifies a probability band around the mean with a probability of $1 - \frac{1}{2n}$. Data within the

band is retained, while data outside the band are considered outliers. For 8 samples,

Chauvenet's criterion specifies a probability band that encompasses 93.8 % of the

population (**Equation 1**):

$$P = 1 - \frac{1}{2 \cdot 8} = 0.937$$

This corresponds to 1.863 standard deviations from the mean. Samples or blanks

outside the band with a standard deviation greater than 1.863 were eliminated as outliers.

After applying Chauvenet's criterion, differences in medium color were minimized by the

subtraction of the mean value of the medium blanks from each sample. To allow data

comparison across experiments, all samples were divided by the mean of a universal

positive control grown in a H_2 atmosphere and containing glucose, vitamin B_{12}, hematin,

formate, and acetate. These samples were joined. To compare error across biological

replicates, we assumed that the standard deviations should be approximately equal across datasets and calculated pooled variance s_p^2 according to (**Equation 2**):

$$s_p^2 = \frac{\sum_{i=1}^{k}(n_i - 1)s_i^2}{\sum_{i=1}^{k}(n_i - 1)}$$

Where n; is the sample size of population i and s_i^2, is the sample variance for population i, or square of the standard deviation. Pooled standard error can then be calculated with (**Equation 3**):

$$SE_p = \sqrt{\sum_{i=1}^{k} \frac{s_p^2}{n_i}}$$

Trees. Decision trees are a divide-and-conquer machine learning technique that sorts data according to the data attributes that best divide the data. C4.5 decision trees were generated by running the data sets into a J28 classifier as previously described and drawn using Adobe Illustrator.[36] BioSIMP software and tutorials can be found on the U.S. Department of Energy's Knowledge Base (KBase).[66] For analysis of monoculture data and co-culture time course, sample averages were sorted into 4 buckets relative to a positive control containing glucose, hematin, vitamin B_{12}, acetate, formate and grown under a 5% H_2 atmosphere. Buckets related the growth to the positive control as follows: no growth (NONE < 0.25); low growth: (LOW ≥ 0.25, < 0.75); similar growth: (SIMILAR ≥ 0.75, < 1.25); and high growth: (HIGH ≥ 1.25).

Synergistic Interaction Index Calculations

If all the cells in a co-culture or consortium grow entirely independently of each other, with no interactions, the number of cells in the coculture ($n_{co-culture}$) would be

equivalent to the sum of the number of monoculture cells grown under the same

conditions, or in our case (**Equation 4**):

$$n_{co-culture} = n_{B.theta} + n_{M.smithii}$$

Because the optical density of the culture is directly proportional to the number of

cells, we can compare the relative growth $R_{s,i}$ of each culture of taxon s under culture

condition i (**Equation 5**):

$$R_{s,i} = \frac{OD_i}{OD_{ctrl}}$$

As long as each organism can grow independently in a positive control ($ctrl$)

condition, an x -component coculture of *B. theta* and *M. smithii* should have an overall

growth that is an average of the monocultures (**Equation 6**):

$$R_{co-culture,i} = \frac{OD_{co-culture,i}}{OD_{co-culture,ctrl}} = \frac{1}{x} \cdot \sum_{s=1}^{x} R_{s,i}$$

Therefore, assuming independent growth within a co-culture of *B. theta* and *M.*

smithii, the relative growth R of a co-culture will equal (**Equation 7**):

$$R_{co-culture,i} = \frac{R_{B.theta,i} + R_{M.smithii,i}}{2}$$

This relationship will only be true if the growth of *B. theta* and *M. smithii* are

independent of each other (null hypothesis). If the cells are interacting in a positive,

syntrophic way, the co-culture will contain more cells than the sum of the monocultures.

If the cells are competitive, total growth will be inhibited and there will be fewer cells in

the co-cultures than expected. To express co-culture interactions as a numerical value, we

divide the observed co-culture growth by the sum of the independent cultures, creating a

Synergistic Interaction index for each culture condition, I_i (**Equation 8**):

$$I_i = \frac{R_{B.theta,i} + R_{M.smithii,i}}{2R_{co-culture,i}}$$

A few caveats to this method should be considered depending on the organisms being studied. Under very high culture densities the linear relationship between optical density and cell number is no longer valid as the culture becomes increasingly opaque. In these situations, the index would be an underestimate of the coculture productivity. Another issue to keep in mind is that flocculation or aggregate formation would complicate experimental reproducibility. In spectrophotometric microplate readers, aggregates may be indicated when biological replicates produce signal variability depending on whether the beam hits an aggregate by chance. The result is high biological and technical variability that confounds statistical analysis. In either case, the Index may be adapted by substituting biomass or another proxy growth measurement in place of *OD* variables in the above equations.

Results

***B. theta* and *M. smithii* grow independently in both rich and defined medium when supplemented with appropriate carbon sources**

Before we can examine the interactions between *B. theta* and *M. smithii* we needed to understand how they grow separately in monocultures. The rich medium is based on a standard tryptone yeast-extract recipe with high nutrient availability. In sealed anaerobic culture tubes supplemented with 0.05% glucose (**Figure 1a**), *B. theta* doubled every 1.48 hours (**Table 1**). Supplemented with 10mM acetate and 10mM formate under an atmosphere of 80% H_2, *M. smithii* grew at a much slower rate (**Figure 1b**) with a doubling time of 8.8 hours (**Table 1**). The difference in growth rates means that if two

cultures are started at the same time, *B. theta* has already reached the stationary stage of growth when *M. smithii* is entering early log growth (**Figure 1ab**). In defined medium the difference *B. theta* and *M. smithii* monoculture growth is more pronounced. *B. theta* doubled every 1.4 hours while *M. smithii* doubled every 15.4 hours (**Figure 1ab, Table 1**).

The presence of *B. theta* is sufficient for *M. smithii* growth in co-cultures

In defined medium optical density of cocultures was very similar to *B. theta* monocultures (**Table 1**) except culture density did not decrease after 50 hours during stationary phase. A decrease in culture optical density may indicate a number of causes; among these are cell lysis or a change in cell shape or volume. The observation that cocultures did not show this decrease in optical density suggested that either *M. smithii* protects *B. theta* from lysis, that it prevents a change in cell shape or volume, or that the optical density reflected growth of *M. smithii* even though *M. smithii* monocultures do not grow in medium lacking H_2+CO_2 or formate and acetate (**Figure 1c**). When cocultures were grown in rich medium in anaerobic culture tubes supplemented with 0.05% glucose we observed aggregation of cells after one week of incubation (**Figure 2a**). We did not observe aggregation in *B. theta* monocultures of the same age (**Figure 2b**). Microscopy indicated aggregates were comprised of intact *B. theta* with associated *M. smithii* (**Figure 2cd**) in addition to intact planktonic and extracellular matrix or dead cells (**Figure 2ef**). The accumulation of *M. smithii* cells in coculture lacking methanogenic substrates indicates that *B. theta* fermentation products are sufficient to support *M. smithii* growth. It should be noted that while lysed *B. theta* may provide metabolite precursors, *M. smithii* has an absolute requirement for acetate for acetyl-CoA

biosynthesis and it is restricted to using H_2+CO_2 and possibly formate as carbon and energy sources.

Quantification of *B. theta* and *M. smithii* in coculture

To determine if the interaction is solely a cross-feeding interaction or if *B. theta* also benefits from coculture with *M. smithii* during long-term cultivation with glucose as the sole carbon and energy source , the ratio of each organism in coculture populations was quantified using qPCR and flow cytometry. We calculated cell ratios by qPCR by probing for the 16S rRNA coding region of the genome. Between 4 and 9 days of coculture there was no change in the coculture optical density and the ratio of *B. theta* to *M. smithii* remained steady at 11.56 (+/- 3.03) on Day 4 to 14.25(+/- 4.72) on Day 9 (p=0.313). To confirm the qPCR results, we also developed a flow cytometry assay to quantify changes in the population ratio according to cell wall staining and to measure cell aggregation. We found that when grown in the presence *M. smithii, B. theta* (**Figure 3 panels b-d and f-h**) forms larger cells or aggregates which mimics the phenotype observed when *B. theta* is grown in rich medium with 0.5x glucose (**Figure 3 panels a and e**). When 0.5x glucose is provided, cultures deplete glucose carbon source and enter stationary phase more rapidly. Consistent with the qPCR data, after 4 days the ratio of planktonic *B. theta* to *M. smithii* cells was 10.97 (+/- 3.81). These results suggest that *B. theta* and *M. smithii* reach balanced growth, in contrast to a purely crossfeeding interaction in which we would expect the ratios to transition from *B. theta*-dominated to *M. smithii*-dominated cultures over time. ENREF_53Culturing, microscopy, and quantification experiments suggest that *B. theta* forms irregular aggregates under limiting nutrient conditions that either passively "trap" or actively recruit *M. smithii*.

Evidence for metabolic crossfeeding between *B. theta* and *M. smithii*

M. smithii growth may be supported by *B. theta* fermentation products acetate, formate, and H_2+CO_2. We next assessed the effect of acetate on cocultures, as acetate is required for *M. smithii* growth. Under these conditions, growth of *M. smithii* still requires H_2 and CO_2 provided by *B. theta*, as *M. smithii* cannot grow on acetate as an energy source. When cocultures were supplemented with 20 mM acetate, *B. theta* cells were larger, formed aggregates, and the relative proportion of *B. theta* to *M. smithii* decreased to 4.52 (+/- 1.56) (**Figure 3 panels d and h**). The decrease in the relative proportion of *B. theta* to *M. smithii* with acetate supplementation is interpreted to suggest acetate is growth-limiting for *M. smithii* in cocultures.

We hypothesized that if *B. theta* and *M. smithii* have a metabolic relationship, whether it be crossfeeding or syntrophy, then one or both of them may secrete unknown small molecules such as amino acids, bacteriocins, toxins, or quorum-sensing factors to promote growth of the other organism. We tested whether preconditioned medium may have a positive effect on growth of monocultures. In these experiments, media were preconditioned by inoculating with either *B. theta* or *M. smithii* monocultures and allowing the monoculture to grow to stationary phase before filter sterilizing with a 0.2 μm filter to remove intact cells. When *B. theta* was grown on rich medium that had been preconditioned by *B. theta* monocultures, growth was slower and maximum optical density was decreased (**Figure 4a**). When *B. theta* was grown on medium that had been sequentially preconditioned first by *B. theta*, then by *M. smithii*, cultures grew faster to a higher maximum optical density, however the growth enhancement was not significant versus growth of *B. theta* on rich medium preconditioned by *B. theta* (**Figure 4a**). *B.*

theta + *M. smithii* cocultures grown on defined medium that had been preconditioned by

M. smithii or *B. theta* monocultures grew similarly to *B. theta* cultures using medium that

had been preconditioned by sequential culturing of *B. theta* then *M. smithii* monocultures.

,. These results suggest that when grown sequentially *B. theta* depletes rich medium of

one or more nutrients that are provided at a low level by *M. smithii*. In an attempt to

identify nutrients that might improve growth of *B. theta* we supplemented rich and

defined medium with hematin, vitamin B_{12}, vitamin K_3, formate, and acetate. Growth

experiments indicate that the lysis observed in rich medium was reduced by addition of

hematin with vitamin K (**Figure 4b**). In defined medium, vitamin B_{12}, hematin, formate

and acetate had no effect, but vitamin K improved growth (**Figure 4b**). We also tested

whether *M. smithii* growth is enhanced by rich medium preconditioned by *B. theta*. *M.*

smithii was able to grow solely on rich medium preconditioned by *B. theta* suggesting

molecules secreted by *B. theta* were responsible for stimulating *M. smithii* growth

(**Figure 4c**). *M. smithii* growth was further enhanced by adding hematin, acetate, and

formate. However, the growth stimulation observed using preconditioned media were not

as dramatic as the growth observed in cocultures (**Figure 1c and Figure 2**). Crossfeeding

data indicated a comprehensive systematic approach was needed to characterize the

complex metabolic relationship between *B. theta* and *M. smithii* in coculture.

B. *theta* growth is inhibited by the presence of hydrogen gas, formate, and acetate

To tease apart the metabolic interactions between *B. theta*, *M. smithii*, and the

culture environment we used a machine learning technique to analyze large-scale growth

culture phenotype data. We assessed the growth of each organism alone and in coculture

in 128 different combinations of culture media (2^7). The combinatorial media recipes

included or omitted the following nutrient components: 0.05% glucose, 10 mM acetate, 10mM formate, 5.8 mM vitamin K_3, 0.0037 μM vitamin B_{12}, and a mixture of 0.2 mM histidine and 0.02mM hematin in the presence or absence of 5% H_2 headspace gas. The optical densities of *B. theta* (**Figure 5**), *M. smithii* (**Figure 6**), and cocultures (**Figure 8**) were measured after 1 day to capture maximal *B. theta* optical density, 7 days to capture slow-growing *B. theta* and maximal *M. smithii* optical density, and 14 days to measure culture stability after prolonged incubation. The same time points were observed to allow comparisons between monocultures and cocultures for every growth condition. To analyze and visualize these data we utilized C4.5 decision trees to identify the relationships between nutrient factors in the culture medium.[36] Decision trees draw branch nodes depending on whether the presence or absence of the factors (in this case, the provided nutrients) affects growth of the culture.

In defined medium glucose was the only carbon source available to *B. theta* and was the primary determinant of growth (**Figure 5a**). The structure of the decision tree suggests that the presence of hydrogen gas alone inhibits growth (**Figure 5b**). Hydrogen gas inhibited *B. theta* growth up to 37.6% (**Figure 7a**). When combined with acetate and formate supplementation growth is decreased by 55% (**Supplementary Data**). Acetate and formate alone do not have a significant effect on growth of *B. theta* (**Figure 7a**), although the tree suggests the presence of acetate and formate in combination may increase growth under certain conditions. Interestingly, the tree indicates the inhibition caused by H_2 is mitigated by the presence of vitamin K or a combination of vitamin B_{12} and hematin/histidine, (**Figure 5b**). Additional experiments are needed to understand how this could be occurring, as inhibition of growth by hydrogen gas is not well

understood in *B. theta*. *M. smithii* is unable to grow under conditions that favor *B. theta*

unless hydrogen, formate, and acetate are present (**Figure 7c**).

M. smithii grows best on a combination of glucose, vitamin B$_{12}$, hematin, acetate,

formate, and H$_2$ gas but depends on acetate for biomass

As expected, *B. theta* is incapable of growth (**Figure 7b**) under conditions that *M.*

smithii prefers (**Figure 7d**). *M. smithii* grew well in defined medium containing formate,

acetate, and hydrogen, even with the addition of glucose, vitamin B$_{12}$, and hematin

(**Figure 7c**). Overall *M. smithii* was able to grow under a wider variety of conditions than

B. theta, albeit to a lower maximum optical density (**Figure 6a**). The decision tree for *M.*

smithii suggests that acetate is the primary determinant for the growth of *M. smithii*

(**Figure 6b**). The presence of hydrogen or formate are necessary, but not sufficient for

growth (**Figure 7d**). Both vitamin K$_3$ (menadione) and vitamin B$_{12}$ can inhibit *M. smithii*

growth, but under certain circumstances vitamin B$_{12}$ rescues vitamin K inhibition and

hematin can rescue vitamin B$_{12}$ inhibition (**Figure 6b**).

Dynamics of coculture phenotypes

To compare the growth of the co-cultures to the monocultures, growth was

normalized to the control treatment that contains the necessary additive requirements for

both organisms: glucose, hematin, vitamin B$_{12}$, formate, acetate, and H$_2$. Relative to the

control, co-culture growth closely resembles the *B. theta* monoculture tree after one day,

(**Figure 8a**) but increasingly resembles *M. smithii* by day 7 through day 14 (**Figure 8bc**).

On day one, glucose is the primary growth factor (**Figure 8a**). By day 7, biomass is

primarily linked to glucose catabolism, but acetate and hydrogen gas also influence

coculture growth (**Figure 8b**). By day 14, growth is less dependent on glucose and more on acetate, indicating increased importance of *M. smithii* in the coculture. However, the decision trees for the coculture do not directly mimic the monoculture trees. These data indicate that the metabolic relationship between *B. theta* and *M. smithii* is dynamic over a two-week period and that coculture growth is not a simple additive relationship that can be easily predicted from monoculture data. This is consistent with observations made by others in which metabolism of diverse microbes are shaped by other members in a consortium.[67,68]

The Synergistic Interaction index uncovers nutrient-dependent trophic interactions

The complex growth patterns we observed suggested that under some conditions *B. theta* and *M. smithii* could be growing independently, while in other culture medium they may crossfeed each other and/or may compete for nutrients. We developed a Synergistic Interaction index to analyze the growth time course data (**Figure 10**). Because *B. theta* will not grow without glucose, only the cases where glucose was supplemented were examined, and the synergistic interaction index (SI) was determined at 7 and 14 days (**Figure 9, Supplementary Data**). The SI for the control condition was 1 on both days, indicating an additive mutualistic relationship between *B. theta* and *M. smithii* growth as expected (**Table 2**). After 7 days, two co-cultures (glucose + vitamin B_{12} + heme + H_2 and glucose + vitamin B_{12} + H_2) had a SI $\geq$ 1.5, indicating the relative growth of the co-culture was at least 1.5x that of the two monocultures together (**Supplementary Data**). One of these conditions (glucose + vitamin B_{12} + H_2) had SI = 2.307, indicating co-culture growth 2 times that of the monocultures together (**Table 2**). By 14 days 7 cocultures had SI $\geq$ 1.5 with a maximum value of 2.36 for the glucose +

vitamin B_{12} + H_2 condition (**Table 2**). Cultures showing the highest indexes on day 14

were supplemented with vitamin B_{12}, which is surprising because B_{12} inhibited *M. smithii*

growth in monoculture (**Figure 6b**). One of the seven conditions with SI $\geq$ 1.5 included

two fermentation products, acetate and hydrogen, and four cultures supplemented with

acetate showed an increase of at least 0.5 SI units between days 7 and 14. Of the 11

cultures with day 14 SI > 1.25, 10 showed an increase from day 7 to day 14, likely

indicating the differences in growth rates between *B. theta* and *M. smithii*, and suggesting

that depletion of glucose (and starvation of *B. theta*) is required for synergistic growth

under these culture conditions. Measurement of SI after 7 days correlated very well with

SI measured at 14 days with r^2 = 0.7922 (**Figure 10a**). 24 cultures had SI < 0.75,

suggesting the possibility of antagonistic inhibition or competition between *B. theta* and

M. smithii. Of those 24 cultures, 20 saw a decrease in index from day 7 to day 14.

Overall, synergistic growth was dependent on the availability of heme, vitamin B_{12},

acetate, and hydrogen (**Figure 9**).

Synergistic growth is correlated with nutrient limitation and feedback inhibition

      We noted that conditions indicating coculture synergy occurred when *B. theta*

monocultures grew poorly. When the Day 7 SI is compared to the growth of *B. theta* in

monocultures under the same conditions, we observed a strong inverse correlation with r^2

= 0.6118 (**Figure 10b**). In contrast, the Day 7 SI was only very weakly correlated with *M.*

smithii growth with r^2 = 0.0657 (**Figure 10c**). The decision tree analysis (**Figure 8**)

shows that highest growth occurs when the coculture is supplemented with acetate,

formate, and hematin. When cocultured, the data suggests both organisms compete for

hematin (**Figure 9, panels c and d**), especially when *M. smithii* growth is stimulated by added formate, acetate, and/or hydrogen (**Supplementary Data**).

Discussion

Our study highlights the benefit of using an interdisciplinary approach to discern patterns of microbial growth as environmental conditions are varied. We have been able to adapt the use of decision trees from machine learning to parse through large-scale phenotype data to identify critical nutrient factors that contribute to growth. Machine learning decision trees are an unbiased tool to search for patterns in large-scale data to uncover hierarchy and interactions between variables. Here, we used optical density to measure culture growth as an output dependent variable due to the ease of obtaining high-throughput data. However, decision trees can be adapted to use for any combination of dependent and independent variables in biological systems. This approach allowed us to ascertain patterns in growth phenotypes as well as emergent behaviors: in this case competition and synergistic growth, when two species are cocultured. We then developed a method to quantify these emergent behaviors in the form of a Synergistic Interaction index. Our approaches apply well to studying the interactions between microbes as diverse as the Gram negative bacterium *B. theta* and the archaeal methanogen *M. smithii*. While we used end-point optical density as an output parameter, which may mask phenotypes such as changes in cell size, shape, lysis and aggregation, other complementary signals such as 16S sequence or metatranscriptomic abundance, biomass, metabolites produced or consumed, or the rates of change of these signals could theoretically be used instead with minimal adaptation. Likewise, while we constrained

our study here to two organisms, with minor adjustment to account for number of species in Equations 6-8 the approach could be retooled for more complex microbial communities. A major consideration when studying complex microbial communities would be to use statistical sampling techniques such as BioSIMP[69] to develop technically and logistically feasible experiments that still retain a suitable confidence interval for observed responses. BioSIMP involves using statistical sampling techniques to reduce the number of experiments required to uncover unexpected behavior/interactions in a biological system. For instance, instead of testing a full-factorial array of environmental conditions, statistical subsampling can be used to reduce the experiments by 50% or more to find which culture conditions can be expected to produce a growth effect of a certain magnitude. Precious resources in time, money, materials, and personnel can be devoted to more detailed mechanistic experiments that require full-factorial experimentation once "interesting" or "unexpected" results are identified for follow-up study.

The results of this study show that fermentation products secreted by *B. theta* are sufficient to support growth of *M. smithii* (**Figure 1c**) and that *M. smithii* enhances growth of *B. theta* (as determined by growth curve data (Figure 1c), microscopy (Figure 2e), and qPCR experiments). One explanation for this result could be that *B. theta* becomes feedback inhibited by secreted metabolic byproducts but in the presence of *M. smithii* the products are consumed thus reducing growth inhibition**.** We showed in a previous study that the major fermentation products secreted by *B. theta* during growth on glucose suppresses *B. theta* growth rates and alters metabolism resulting in increased production of carbon dioxide and amino acids.[53] *M. smithii* is capable of growing solely on the metabolites secreted by *B. theta* (**Figure 1c**), and medium that has been

sequentially conditioned first by *B. theta* and then by *M. smithii* supports higher *B. theta* biomass than medium that was preconditioned by *B. theta* alone (**Figure 4a**). It is unknown what *M. smithii* might secrete besides methane, biomass, or intracellular metabolites such as heme or corrinoids released by lysed cells. Heme iron is a well-studied nutrient requirement and bacteria have many heme acquisition mechanisms such as siderophores and pathogenesis factors that they synthesize to acquire iron for enzyme cofactor synthesis from the environment, from neighboring microbes, or from the host.[70,71] Corrinoids have also been shown to play a key role in several interspecies systems and competition for B12 is thought to be a significant factor that shapes human gut microbial community ecology.[72] Our results show that *B. theta* is capable of growth in medium without supplemented heme or B12 when grown in coculture with *M. smithii* presumably because *B. theta* can scavenge heme and corrinoids synthesized by *M. smithii*.

It is formally possible that *B. theta* and *M. smithii* secrete one or more unknown small molecules that are sensed as interspecies signals in addition to the central metabolic interactions we tested in our treatments. Synergistic growth could be mediated by soluble and insoluble signals that may be expressed when *B. theta* is undergoing the starvation response. It is tempting to speculate that *B. theta* forms multicellular aggregates under starvation conditions to attract *M. smithii*, which would benefit from physical association with *B. theta* by allowing rapid mass transfer of hydrogen and acetate (**Figure 2**). Intriguingly, these aggregates and the association of *M. smithii* with them statistically decreased when acetate was supplemented into the culture medium (**Figure 3**), suggesting that either acetate induces signaling molecules by *B. theta*, or that *M. smithii*,

which requires exogenous acetate for growth, secretes molecule(s) that promote aggregate formation with *B. theta*. Whether the increase in *B. theta* growth is a result of secreted product from *M. smithii* or by the protective effect of removing inhibitory compounds is still to be decided. Additional experiments are needed to identify any attractants secreted by *B. theta* and/or *M. smithii* under conditions that favor and disfavor aggregate formation.

Finally, we developed a Synergistic Interaction index to score the likelihood that two or more organisms are growing synergistically, independently, or are inhibiting each other. The index scores suggest that in some situations, the coculture is metabolically more efficient than expected from the biomass observed from independent monocultures. While the index does not identify the molecular mechanism of synergy or inhibition, by using a multi-component culturing strategy and decision trees, we are able to discern patterns of coculture behavior that can lead to testable hypotheses. Our observations suggest that *B. theta* and *M. smithii* have a mutually beneficial syntrophic relationship when vitamin B_{12} and hydrogen gas are provided, and that they compete for hematin when sufficient acetate, formate and/or hydrogen gas are available for *M. smithii* to grow. Future experiments are needed to determine how *B. theta* and *M. smithii* compete for heme. We speculate competition could proceed via passive mechanisms (autolysis, diffusion, and ATP-dependent transport) or by active processes using small molecules such as bacteriocins, toxins, quorum-sensing factors, or other mechanisms to obtain iron that have been discovered in other microbes.[73-75]

Acknowledgements

References

1.   Flint, H. J., Scott, K. P., Louis, P. & Duncan, S. H. The role of the gut microbiota in nutrition and health. *Nat Rev Gastroenterol Hepatol* **9**, 577-589, 10.1038/nrgastro.2012.156 (2012).

2.   Kim, G., Deepinder, F., Morales, W., Hwang, L., Weitsman, S., Chang, C., Gunsalus, R. & Pimentel, M. *Methanobrevibacter smithii* is the predominant methanogen in patients with constipation-predominant IBS and methane on breath. *Digest Dis Sci* **57**, 3213-3218 (2012).

3.   Chaudhary, P. P., Conway, P. L. & Schlundt, J. Methanogens in humans: potentially beneficial or harmful for health. *Appl Microbiol Biotechnol* **102**, 3095-3104, 10.1007/s00253-018-8871-2 (2018).

4.   Brown, E. G., Tanner, C. M. & Goldman, S. M. The Microbiome in Neurodegenerative Disease. *Curr Geriatr Rep* **7**, 81-91, 10.1007/s13670-018-0240-6 (2018).

5.   Palmer, C., Bik, E. M., DiGiulio, D. B., Relman, D. A. & Brown, P. O. Development of the human infant intestinal microbiota. *PLoS Biol* **5**, e177, 10.1371/journal.pbio.0050177 (2007).

6.   Grine, G., Boualam, M. A. & Drancourt, M. *Methanobrevibacter smithii,* a methanogen consistently colonising the newborn stomach. *Eur J Clin Microbiol Infect Dis* **36**, 2449-2455, 10.1007/s10096-017-3084-7 (2017).

7.   Bjursell, M. K., Martens, E. C. & Gordon, J. I. Functional genomic and metabolic studies of the adaptations of a prominent adult human gut symbiont, *Bacteroides*

thetaiotaomicron, to the suckling period. *J Biol Chem* **281**, 36269-36279, 10.1074/jbc.M606509200 (2006).

8.   Backhed, F., Ley, R. E., Sonnenburg, J. L., Peterson, D. A. & Gordon, J. I. Host-bacterial mutualism in the human intestine. *Science* **307**, 1915-1920, 10.1126/science.1104816 (2005).

9.   Savage, D. C. Microbial ecology of the gastrointestinal tract. *Annu Rev Microbiol* **31**, 107-133, 10.1146/annurev.mi.31.100177.000543 (1977).

10.   Yatsunenko, T., Rey, F. E., Manary, M. J., Trehan, I., Dominguez-Bello, M. G., Contreras, M., Magris, M., Hidalgo, G., Baldassano, R. N., Anokhin, A. P., Heath, A. C., Warner, B., Reeder, J., Kuczynski, J., Caporaso, J. G., Lozupone, C. A., Lauber, C., Clemente, J. C., Knights, D., Knight, R. & Gordon, J. I. Human gut microbiome viewed across age and geography. *Nature* **486**, 222-227, 10.1038/nature11053 (2012).

11.   Stecher, B. & Hardt, W. D. Mechanisms controlling pathogen colonization of the gut. *Curr Opin Microbiol* **14**, 82-91, 10.1016/j.mib.2010.10.003 (2011).

12.   Buffie, C. G. & Pamer, E. G. Microbiota-mediated colonization resistance against intestinal pathogens. *Nat Rev Immunol* **13**, 790-801, 10.1038/nri3535 (2013).

13.   Koropatkin, N. M., Cameron, E. A. & Martens, E. C. How glycan metabolism shapes the human gut microbiota. *Nat Rev Microbiol* **10**, 323-335, 10.1038/nrmicro2746 (2012).

14.   Krajmalnik-Brown, R., Ilhan, Z. E., Kang, D. W. & DiBaise, J. K. Effects of gut microbes on nutrient absorption and energy regulation. *Nutr Clin Pract* **27**, 201-214, 10.1177/0884533611436116 (2012).

15.   Wexler, H. M. Bacteroides: the good, the bad, and the nitty-gritty. *Clin Microbiol Rev* **20**, 593-621, 10.1128/CMR.00008-07 (2007).

16.   Menni, C., Jackson, M. A., Pallister, T., Steves, C. J., Spector, T. D. & Valdes, A. M. Gut microbiome diversity and high-fibre intake are related to lower long-term weight gain. *Int J Obes (Lond)* **41**, 1099-1105, 10.1038/ijo.2017.66 (2017).

17.   Round, J. L. & Mazmanian, S. K. The gut microbiota shapes intestinal immune responses during health and disease. *Nat Rev Immunol* **9**, 313-323, 10.1038/nri2515 (2009).

18.   Hooper, L. V. & Gordon, J. I. Commensal host-bacterial relationships in the gut. *Science* **292**, 1115-1118, 10.1126/science.1058709 (2001).

19.   Nicholson, J. K., Holmes, E., Kinross, J., Burcelin, R., Gibson, G., Jia, W. & Pettersson, S. Host-gut microbiota metabolic interactions. *Science* **336**, 1262-1267, 10.1126/science.1223813 (2012).

20.   Louis, P., Hold, G. L. & Flint, H. J. The gut microbiota, bacterial metabolites and colorectal cancer. *Nature reviews Microbiology* **12**, 661-672 (2014).

21.   Carbonero, F., Benefiel, A. C. & Gaskins, H. R. Contributions of the microbial hydrogen economy to colonic homeostasis. *Nat Rev Gastroenterol Hepatol* **9**, 504-518, 10.1038/nrgastro.2012.85 (2012).

22.   Parekh, P. J., Balart, L. A. & Johnson, D. A. The Influence of the Gut Microbiome on Obesity, Metabolic Syndrome and Gastrointestinal Disease. *Clin Transl Gastroenterol* **6**, e91, 10.1038/ctg.2015.16 (2015).

23. Fernandes, J., Su, W., Rahat-Rozenbloom, S., Wolever, T. M. & Comelli, E. M. Adiposity, gut microbiota and faecal short chain fatty acids are linked in adult humans. *Nutr Diabetes* **4**, e121, 10.1038/nutd.2014.23 (2014).

24. Wilder-Smith, C. H., Olesen, S. S., Materna, A. & Drewes, A. M. Breath methane concentrations and markers of obesity in patients with functional gastrointestinal disorders. *United European Gastroenterol J* **6**, 595-603, 10.1177/2050640617744457 (2018).

25. Zhao, L. The gut microbiota and obesity: from correlation to causality. *Nat Rev Microbiol* **11**, 639-647, 10.1038/nrmicro3089 (2013).

26. Sartor, R. B. Microbial influences in inflammatory bowel diseases. *Gastroenterology* **134**, 577-594, 10.1053/j.gastro.2007.11.059 (2008).

27. Halfvarson, J., Brislawn, C. J., Lamendella, R., Vazquez-Baeza, Y., Walters, W. A., Bramer, L. M., D'Amato, M., Bonfiglio, F., McDonald, D., Gonzalez, A., McClure, E. E., Dunklebarger, M. F., Knight, R. & Jansson, J. K. Dynamics of the human gut microbiome in inflammatory bowel disease. *Nat Microbiol* **2**, 17004, 10.1038/nmicrobiol.2017.4 (2017).

28. Russell, S. L., Gold, M. J., Hartmann, M., Willing, B. P., Thorson, L., Wlodarska, M., Gill, N., Blanchet, M. R., Mohn, W. W., McNagny, K. M. & Finlay, B. B. Early life antibiotic-driven changes in microbiota enhance susceptibility to allergic asthma. *Embo Rep* **13**, 440-447, 10.1038/embor.2012.32 (2012).

29. Hooper, L. V., Littman, D. R. & Macpherson, A. J. Interactions between the microbiota and the immune system. *Science* **336**, 1268-1273, 10.1126/science.1223490 (2012).

30.   Ghavami, S. B., Rostami, E., Sephay, A. A., Shahrokh, S., Balaii, H., Aghdaei, H. A. & Zali, M. R. Alterations of the human gut *Methanobrevibacter smithii* as a biomarker for inflammatory bowel diseases. *Microb Pathog* **117**, 285-289, 10.1016/j.micpath.2018.01.029 (2018).

31.   Milani, C., Ferrario, C., Turroni, F., Duranti, S., Mangifesta, M., van Sinderen, D. & Ventura, M. The human gut microbiota and its interactive connections to diet. *J Hum Nutr Diet* **29**, 539-546, 10.1111/jhn.12371 (2016).

32.   Sommer, F. & Backhed, F. The gut microbiota--masters of host development and physiology. *Nat Rev Microbiol* **11**, 227-238, 10.1038/nrmicro2974 (2013).

33.   Huitema, M. J. D. & Schenk, G. J. Insights into the Mechanisms That May Clarify Obesity as a Risk Factor for Multiple Sclerosis. *Curr Neurol Neurosci Rep* **18**, 18, 10.1007/s11910-018-0827-5 (2018).

34.   Basseri, R. J., Basseri, B., Pimentel, M., Chong, K., Youdim, A., Low, K., Hwang, L., Soffer, E., Chang, C. & Mathur, R. Intestinal methane production in obese individuals is associated with a higher body mass index. *Gastroenterol Hepatol (N Y)* **8**, 22-28 (2012).

35.   Samuel, B. S. & Gordon, J. I. A humanized gnotobiotic mouse model of host-archaeal-bacterial mutualism. *Proc Natl Acad Sci U S A* **103**, 10011-10016, 10.1073/pnas.0602187103 (2006).

36.   Cashman, M., Catlett, J. L., Cohen, M. B., Buan, N. R., Sakkaff, Z., Pierobon, M. & Kelley, C. A. BioSIMP: Using Software Testing Techniques for Sampling and Inference in Biological Organisms. *2017 Ieee/Acm 12th International Workshop on Software Engineering for Science (Se4science)*, 2-8, 10.1109/Se4science.2017..9 (2017).

37.   Sonnenburg, J. L., Chen, C. T. & Gordon, J. I. Genomic and metabolic studies of the impact of probiotics on a model gut symbiont and host. *PLoS Biol* **4**, e413, 10.1371/journal.pbio.0040413 (2006).

38.   Demonfort Nkamga, V., Henrissat, B. & Drancourt, M. Archaea: Essential inhabitants of the human digestive microbiota. *Human Microbiome Journal* **3**, 1-8, https://doi.org/10.1016/j.humic.2016.11.005 (2017).

39.   Miller, T. L. & Wolin, M. J. Enumeration of *Methanobrevibacter smithii* in human feces. *Arch Microbiol* **131**, 14-18 (1982).

40.   Gill, S. R., Pop, M., Deboy, R. T., Eckburg, P. B., Turnbaugh, P. J., Samuel, B. S., Gordon, J. I., Relman, D. A., Fraser-Liggett, C. M. & Nelson, K. E. Metagenomic analysis of the human distal gut microbiome. *Science* **312**, 1355-1359, 10.1126/science.1124234 (2006).

41.   Dridi, B., Henry, M., El Khechine, A., Raoult, D. & Drancourt, M. High prevalence of Methanobrevibacter smithii and Methanosphaera stadtmanae detected in the human gut using an improved DNA detection protocol. *PLoS One* **4**, e7063, 10.1371/journal.pone.0007063 (2009).

42.   Hansen, E. E., Lozupone, C. A., Rey, F. E., Wu, M., Guruge, J. L., Narra, A., Goodfellow, J., Zaneveld, J. R., McDonald, D. T., Goodrich, J. A., Heath, A. C., Knight, R. & Gordon, J. I. Pan-genome of the dominant human gut-associated archaeon, *Methanobrevibacter smithii,* studied in twins. *Proc Natl Acad Sci U S A* **108 Suppl 1**, 4599-4606, 10.1073/pnas.1000071108 (2011).

43.   Million, M., Maraninchi, M., Henry, M., Armougom, F., Richet, H., Carrieri, P., Valero, R., Raccah, D., Vialettes, B. & Raoult, D. Obesity-associated gut microbiota is

enriched in *Lactobacillus reuteri* and depleted in *Bifidobacterium* animalis and *Methanobrevibacter smithii*. *Int J Obes (Lond)* **36**, 817-825, 10.1038/ijo.2011.153 (2012).

44.   Kim, G., Deepinder, F., Morales, W., Hwang, L., Weitsman, S., Chang, C., Gunsalus, R. & Pimentel, M. *Methanobrevibacter smithii* is the predominant methanogen in patients with constipation-predominant IBS and methane on breath. *Dig Dis Sci* **57**, 3213-3218, 10.1007/s10620-012-2197-1 (2012).

45.   Miller, T. L., Wolin, M. J., Conway de Macario, E. & Macario, A. J. Isolation of *Methanobrevibacter smithii* from human feces. *Appl Environ Microbiol* **43**, 227-232 (1982).

46.   Samuel, B. S., Hansen, E. E., Manchester, J. K., Coutinho, P. M., Henrissat, B., Fulton, R., Latreille, P., Kim, K., Wilson, R. K. & Gordon, J. I. Genomic and metabolic adaptations of *Methanobrevibacter smithii* to the human gut. *Proc Natl Acad Sci U S A* **104**, 10643-10648, 0704189104 (2007).

47.   Morris, B. E., Henneberger, R., Huber, H. & Moissl-Eichinger, C. Microbial syntrophy: interaction for the common good. *FEMS Microbiol Rev* **37**, 384-406, 10.1111/1574-6976.12019 (2013).

48.   Sieber, J. R., McInerney, M. J. & Gunsalus, R. P. Genomic insights into syntrophy: the paradigm for anaerobic metabolic cooperation. *Annu Rev Microbiol* **66**, 429-452, 10.1146/annurev-micro-090110-102844 (2012).

49.   McInerney, M. J., Sieber, J. R. & Gunsalus, R. P. Syntrophy in anaerobic global carbon cycles. *Curr Opin Biotechnol* **20**, 623-632, 10.1016/j.copbio.2009.10.001 (2009).

50. Kouzuma, A., Kato, S. & Watanabe, K. Microbial interspecies interactions: recent findings in syntrophic consortia. *Front Microbiol* **6**, 477, 10.3389/fmicb.2015.00477 (2015).

51. Stams, A. J. & Plugge, C. M. Electron transfer in syntrophic communities of anaerobic bacteria and archaea. *Nat Rev Microbiol* **7**, 568-577, 10.1038/nrmicro2166 (2009).

52. Stolyar, S., Van Dien, S., Hillesland, K. L., Pinel, N., Lie, T. J., Leigh, J. A. & Stahl, D. A. Metabolic modeling of a mutualistic microbial community. *Mol Syst Biol* **3**, 92, 10.1038/msb4100131 (2007).

53. Catlett, J. L., Catazaro, J., Cashman, M., Carr, S., Powers, R., Cohen, M. B. & Buan, N. R. Metabolic Feedback Inhibition Influences Metabolite Secretion by the Human Gut Symbiont *Bacteroides thetaiotaomicron*. *mSystems* **5**, 10.1128/mSystems.00252-20 (2020).

54. Cato, E. P. & Johnson, J. L. Reinstatement of Species Rank for Bacteroides-Fragilis, Bacteroides-Ovatus, Bacteroides-Distasonis, Bacteroides-Thetaiotaomicron, and Bacteroides-Vulgatus - Designation of Neotype Strains for Bacteroides-Fragilis (Veillon and Zuber) Castellani and Chalmers and Bacteroides-Thetaiotaomicron (Distaso) Castellani and Chalmers. *Int J Syst Bacteriol* **26**, 230-237, Doi 10.1099/00207713-26-2-230 (1976).

55. Kotarski, S. F. & Salyers, A. A. Isolation and characterization of outer membranes of *Bacteroides thetaiotaomicron* grown on different carbohydrates. *J Bacteriol* **158**, 102-109 (1984).

56. Bacic, M. K. & Smith, C. J. Laboratory maintenance and cultivation of bacteroides species. *Curr Protoc Microbiol* **Chapter 13**, Unit 13C 11, 10.1002/9780471729259.mc13c01s9 (2008).

57. Khelaifia, S., Raoult, D. & Drancourt, M. A versatile medium for cultivating methanogenic archaea. *PLoS One* **8**, e61563, 10.1371/journal.pone.0061563 (2013).

58. DSMZ. 119. Methanobacterium medium. (2017).

<https://www.dsmz.de/collection/catalogue/microorganisms/culture-technology/list-of-media-for-microorganisms>.

59. Varel, V. H. & Bryant, M. P. Nutritional features of Bacteroides fragilis subsp. fragilis. *Appl Microbiol* **28**, 251-257 (1974).

60. Balch, W. E., Fox, G. E., Magrum, L. J., Woese, C. R. & Wolfe, R. S. Methanogens: reevaluation of a unique biological group. *Microbiol Rev* **43**, 260-296 (1979).

61. Balch, W. E. & Wolfe, R. S. Specificity and biological distribution of coenzyme M (2-mercaptoethanesulfonic acid). *J Bacteriol* **137**, 256-263 (1979).

62. Sowers, K. R., Boone, J. E. & Gunsalus, R. P. Disaggregation of *Methanosarcina* spp. and Growth as Single Cells at Elevated Osmolarity. *Appl Environ Microbiol* **59**, 3832-3839 (1993).

63. Peck, M. W. Changes in concentrations of coenzyme F420 analogs during batch growth of *Methanosarcina barkeri* and *Methanosarcina mazei. Appl Environ Microbiol* **55**, 940-945 (1989).

64. Sambrook, J. & Russell, D. W. Purification of nucleic acids by extraction with phenol:chloroform. *CSH Protoc* **2006**, 10.1101/pdb.prot4455 (2006).

65.   Taylor, J. R.   0-1 (University Science Books, Sausalito, Calif. :, 1997).

66.   Arkin, A. P., Cottingham, R. W., Henry, C. S., Harris, N. L., Stevens, R. L., Maslov, S., Dehal, P., Ware, D., Perez, F., Canon, S., Sneddon, M. W., Henderson, M. L., Riehl, W. J., Murphy-Olson, D., Chan, S. Y., Kamimura, R. T., Kumari, S., Drake, M. M., Brettin, T. S., Glass, E. M., Chivian, D., Gunter, D., Weston, D. J., Allen, B. H., Baumohl, J., Best, A. A., Bowen, B., Brenner, S. E., Bun, C. C., Chandonia, J. M., Chia, J. M., Colasanti, R., Conrad, N., Davis, J. J., Davison, B. H., DeJongh, M., Devoid, S., Dietrich, E., Dubchak, I., Edirisinghe, J. N., Fang, G., Faria, J. P., Frybarger, P. M., Gerlach, W., Gerstein, M., Greiner, A., Gurtowski, J., Haun, H. L., He, F., Jain, R., Joachimiak, M. P., Keegan, K. P., Kondo, S., Kumar, V., Land, M. L., Meyer, F., Mills, M., Novichkov, P. S., Oh, T., Olsen, G. J., Olson, R., Parrello, B., Pasternak, S., Pearson, E., Poon, S. S., Price, G. A., Ramakrishnan, S., Ranjan, P., Ronald, P. C., Schatz, M. C., Seaver, S. M. D., Shukla, M., Sutormin, R. A., Syed, M. H., Thomason, J., Tintle, N. L., Wang, D., Xia, F., Yoo, H., Yoo, S. & Yu, D. KBase: The United States Department of Energy Systems Biology Knowledgebase. *Nat Biotechnol* **36**, 566-569, 10.1038/nbt.4163 (2018).

67.   Heyse, J., Buysschaert, B., Props, R., Rubbens, P., Skirtach, A. G., Waegeman, W. & Boon, N. Coculturing Bacteria Leads to Reduced Phenotypic Heterogeneities. *Appl Environ Microbiol* **85**, 10.1128/AEM.02814-18 (2019).

68.   Grant, M. A., Kazamia, E., Cicuta, P. & Smith, A. G. Direct exchange of vitamin B12 is demonstrated by modelling the growth dynamics of algal-bacterial cocultures. *ISME J* **8**, 1418-1427, 10.1038/ismej.2014.9 (2014).

69.	Cashman, M., Catlett, J. L., Cohen, M. B., Buan, N. R., Sakkaff, Z., Pierobon, M. & Kelley, C. A. in *Proceedings of the 12th International Workshop on Software Engineering for Science.* 2-8 (IEEE Press).

70.	Wooldridge, K. G. & Williams, P. H. Iron uptake mechanisms of pathogenic bacteria. *FEMS Microbiol Rev* **12**, 325-348, 10.1111/j.1574-6976.1993.tb00026.x (1993).

71.	Richard, K. L., Kelley, B. R. & Johnson, J. G. Heme Uptake and Utilization by Gram-Negative Bacterial Pathogens. *Front Cell Infect Microbiol* **9**, 81, 10.3389/fcimb.2019.00081 (2019).

72.	Degnan, P. H., Taga, M. E. & Goodman, A. L. Vitamin B12 as a modulator of gut microbial ecology. *Cell Metab* **20**, 769-778, 10.1016/j.cmet.2014.10.002 (2014).

73.	Zhu, W., Winter, M. G., Spiga, L., Hughes, E. R., Chanin, R., Mulgaonkar, A., Pennington, J., Maas, M., Behrendt, C. L., Kim, J., Sun, X., Beiting, D. P., Hooper, L. V. & Winter, S. E. Xenosiderophore Utilization Promotes *Bacteroides thetaiotaomicron* Resilience during Colitis. *Cell Host Microbe* **27**, 376-388 e378, 10.1016/j.chom.2020.01.010 (2020).

74.	Zafar, H. & Saier, M. H., Jr. Comparative genomics of transport proteins in seven *Bacteroides* species. *PLoS One* **13**, e0208151, 10.1371/journal.pone.0208151 (2018).

75.	Lurie-Weinberger, M. N., Peeri, M. & Gophna, U. Contribution of lateral gene transfer to the gene repertoire of a gut-adapted methanogen. *Genomics* **99**, 52-58, 10.1016/j.ygeno.2011.10.005 (2012).

| Table 1. Culture doubling times (hours).									
	B. theta 0.05% glucose			**M. smithii** 10mM acetate + 10mM formate			**Co-Culture** 0.05% glucose		
Treatment	Maximum OD	Doubling time (std dev)	p vs Rich	Maximum OD	Doubling time (std dev)	p vs Rich	Maximum OD	Doubling time (std dev)	p vs Bth	p vs Msm
Anaerobic culture tube Rich[†]	1.11 ± 0.013	1.48 ± 0.140	1	0.55 ± 0.051	8.84 ± 0.332	1	0.54 ± 0.020	1.46 ± 0.137	0.890	0.000
Anaerobic culture tube Defined[†]	0.55 ± 0.017	1.40 ± 0.092	0.699	0.15 ± 0.007	15.46 ± 1.803	0.000	0.52 ± 0.016	1.44 ± 0.05	0.872	0.000
96-well plates Rich[‡]	0.64 ± 0.033	1.62 ± 0.097	1	0.17 ± 0.024	7.93 ± 0.825	1	0.745 ± 0.016	2.02 ± 0.073	0.001	0.000
96-well plates Defined[‡]	0.69 ± 0.015	2.04 ± 0.100	0.000	0.14 ± 0.007	318 ± 23.13	0.000	0.61 ± 0.018	2.18 ± 0.067	0.030	0.000
OD: culture optical density at 600 nm. NG: no growth. Data were collected from † n= 5 or ‡ n= 8 biological replicates. Significance p values determined by unpaired Student's t-test. *Bth: B. theta. Msm: M. smithii*.									
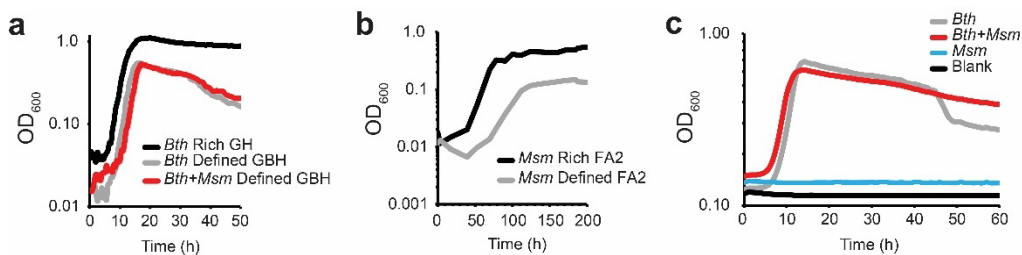
Figure 1. Growth phenotypes on rich and defined culture media. Panel a, Growth of *B. theta* monocultures in anaerobic culture tubes in rich (black) or defined medium (gray) compared to *B. theta* + *M. smithii* cocultures (red) grown on defined medium on 0.5% glucose (n=5). **Panel b**, Growth of *M. smithii* monocultures in anaerobic culture tubes in rich (black) or defined medium (gray) supplemented with 10mM acetate and 10mM formate under an atmosphere of 80% H_2 (n=5). **Panel c,** Growth of *B. theta* (gray), *M. smithii* (blue) and *B. theta* + *M. smithii* cocultures (red) on defined medium with 0.5% glucose as sole carbon and energy source in 96-well plates (n=8). Error bars have been omitted for clarity. OD_{600}, optical density at 600nm. G, 0.5% glucose; B, vitamin B_{12} (cyanocobalamin); H, hematin; F, 10mM formate; A, 10mM acetate; 2, 80% H_2 atmosphere.
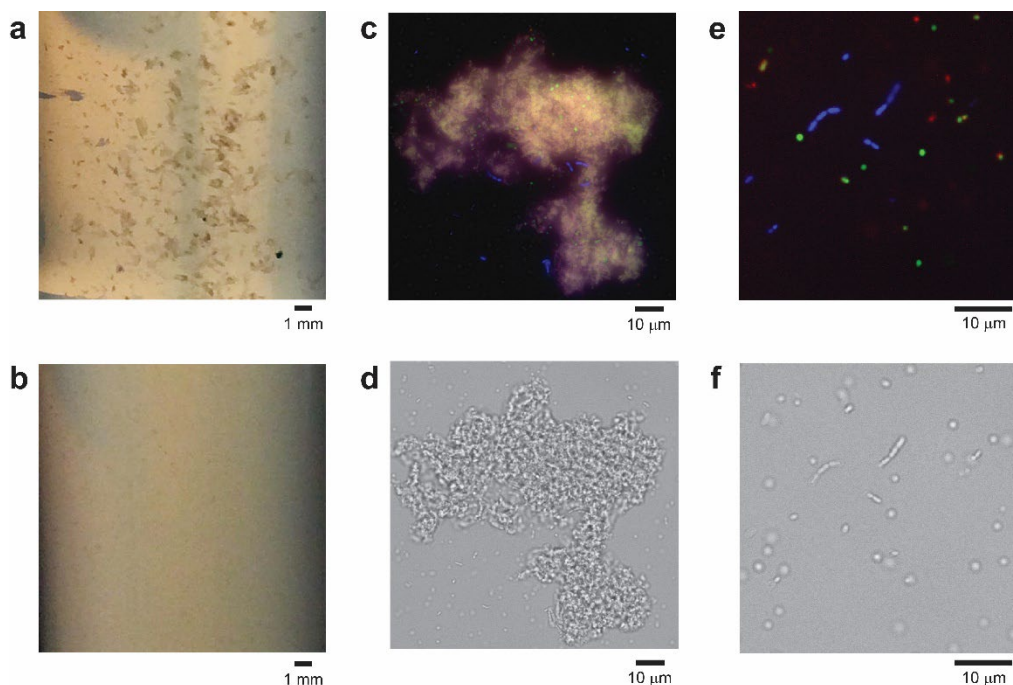
Figure 2. Microscopy of *B. theta* and *M. smithii* in cocultures grown in rich medium for 8 days. Panel a, coculture of *B. theta* and *M. smithii* grown on rich medium for one week showing visible aggregates. **Panel b,** monoculture of *B. theta* grown on rich medium for one week. **Panel c,** Live/dead staining of a coculture aggregate appears to show aggregates are comprised of live *B. theta* and *M. smithii* cells as well as what appears to be extracellular matrix and/or lysed cell debris. In live/dead micrographs intact *B. theta* cells are green, intact *M. smithii* cells are blue, and dead cells are stained red. Yellow color results from colocalization of red and green channels. Methanogens auto-fluorescence due to oxidized co-enzyme F_{420} and appear blue when viewed under a DAPI LED light filter. **Panel d**, transmission micrographs of Panel c. **Panel e**, Live/dead staining of planktonic cells in coculture showing live *B. theta* (green), live *M. smithii* (blue) and dead cells (red). **Panel f,** transmission micrograph of Panel d. Black bars indicate scale.
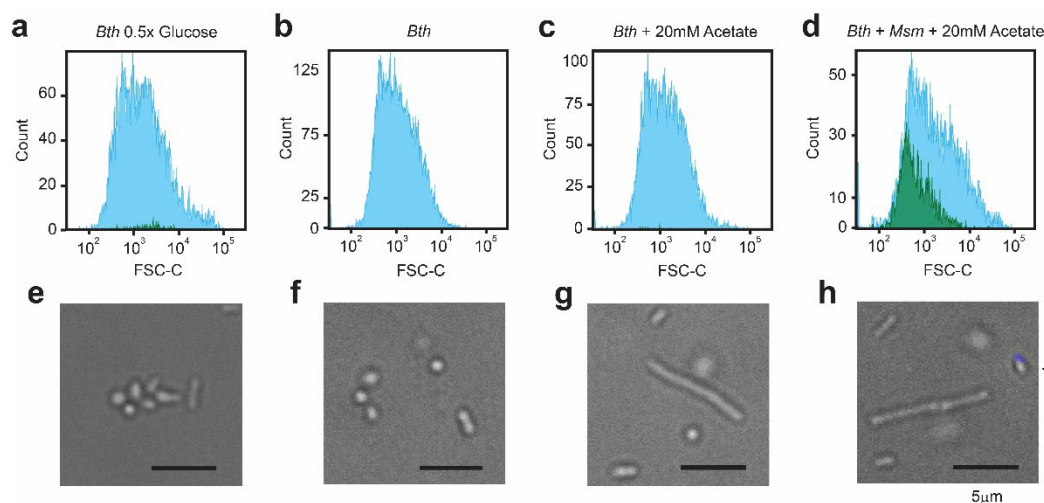
Figure 3. Quantification of *B. theta* and *M. smithii* in cocultures using flow cytometry. Panels a-d, Cells were grown in defined medium for 9 days and counted by flow cytometry. The X-axis reports forward scattering to quantify the size of the cell populations. Blue histogram indicates *B. theta* staining. Green histogram indicates *M. smithii* signal. **Panels e-h,** cells from the same experiments as in Panels a-d were visualized by transmission electron microscopy and UV fluorescence with a DAPI filter to detect *M. smithii* (arrow). Black bars indicate 5µm scale. **Panel a and e,** *B. theta* grown alone in 0.5x glucose medium. **Panels b and f,** *B. theta* grown alone on glucose defined medium. **Panels c and g,** *B. theta* grown in defined medium supplemented with 20mM acetate. **Panels d and h,** *B. theta* and *M. smithii* grown in coculture supplemented with 20mM acetate.
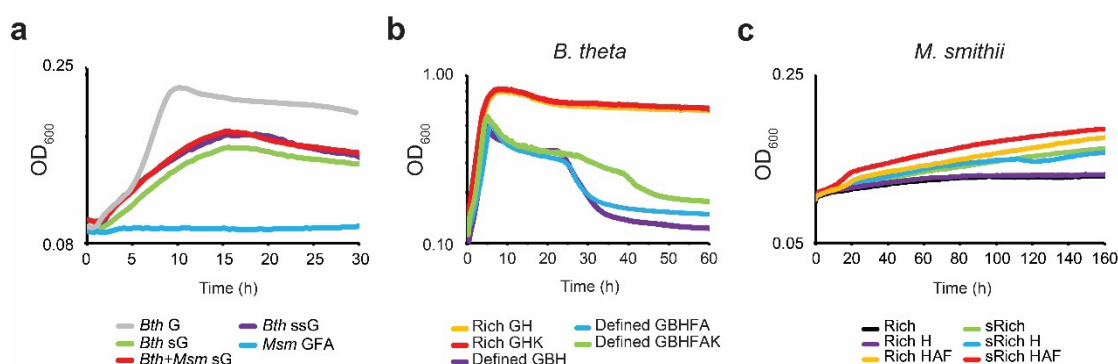

Figure 4. Stimulation of *B. theta and M. smithii* growth by preconditioning or nutrient supplementation. **Panel a,** Growth of *B. theta* monocultures (*Bth*) in rich medium is enhanced by preconditioning with *M. smithii, Msm* (n=8). *Bth* G, *B. theta* monocultures grown on control glucose medium; *Bth* sG, growth of *B. theta* monocultures on glucose medium conditioned by *B. theta*; *Bth+Msm* sG, *B. theta* + *M. smithii* cocultures grown on glucose medium conditioned by *B. theta* monoculture; *Bth* ssG, growth of *B. theta* monocultures on glucose medium preconditioned first by *B. theta* monoculture, then by *M. smithii* monoculture; *Msm* GFA, growth of *M. smithii* on rich medium control with glucose, formate, and acetate supplementation. **Panel b,** Lysis of *B. theta* monocultures

in defined medium is delayed by the addition of vitamin K_3. **Panel c**, Growth of *M. smithii* monocultures on rich medium with glucose (Rich) is enhanced when medium is preconditioned by *B. theta* (sRich, n=8). Error bars have been omitted for clarity. OD_{600}, optical density at 600nm. G, 0.5% glucose; B, vitamin B_{12}; H, hematin; K, vitamin K_3; F, 10mM formate; A, 10mM acetate.
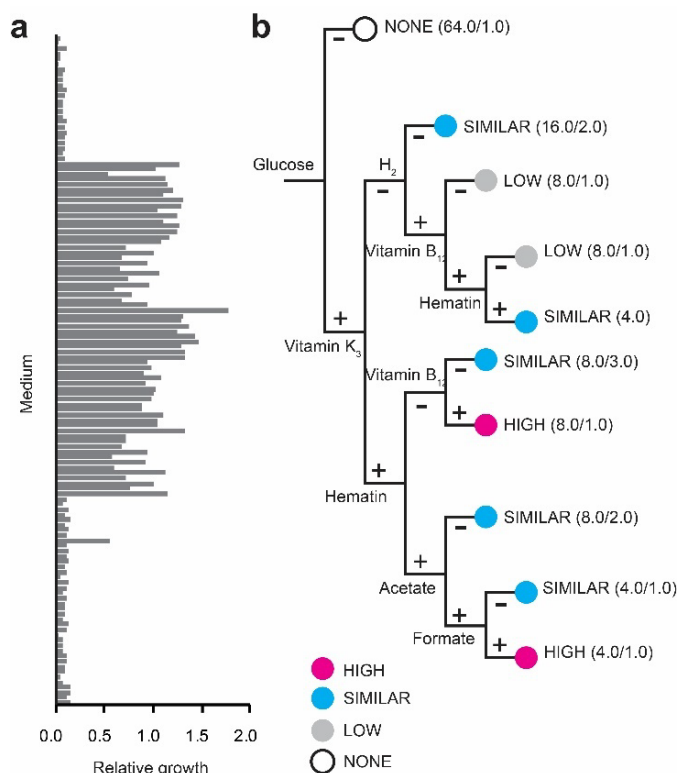

Figure 5. Effect of medium composition on *B. theta* growth. Triplicate *B. theta* monocultures were grown in replicates of 8 on defined medium supplemented with 128 different combinations of glucose, vitamin B_{12}, hematin, vitamin K_3, acetate, formate, and a 5% H_2 atmosphere. Data across 3 experiments were compared to a positive control (glucose, hematin, vitamin B_{12}, acetate, formate and 5% H_2) and combined. **Panel a**, *B. theta* growth relative to a positive control. **Panel b**, Decision tree representation of growth data relative to glucose, hematin, and vitamin B_{12} control condition. The decision tree representation is read from left to right where each node represents one of the 7 nutrient conditions. The "-" path means the nutrient was not included, the "+" path means it was included. As the path is traversed, the nutrients are additive. The values in parentheses represent how many total conditions are covered by that leaf, followed by how many are incorrectly classified by the model. Growth relative to the positive control is indicated as follows; open circles: no growth (NONE < 0.25), gray circles: low growth (LOW ≥ 0.25, < 0.75); blue circles: similar growth (SIMILAR ≥ 0.75, < 1.25); and pink circles: high growth (HIGH ≥ 1.25).
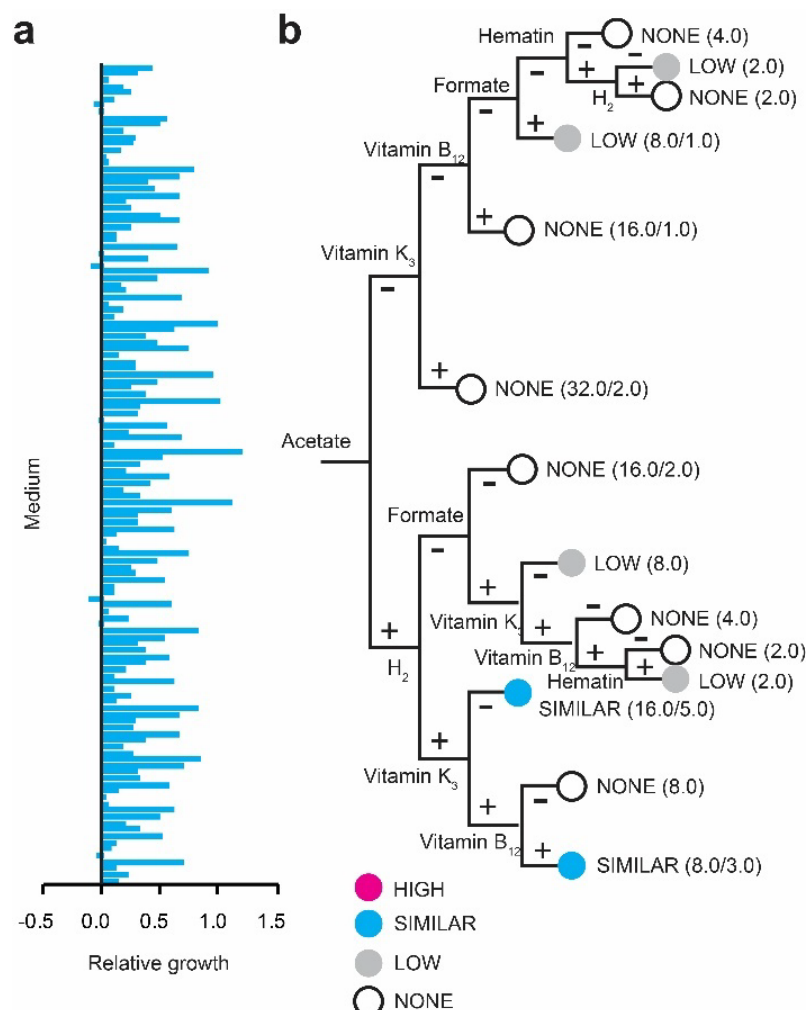
Figure 6. Effect of medium composition on *M. smithii* growth. Triplicate *M. smithii* monocultures were grown in replicates of 8 on defined medium supplemented with 128 different combinations of glucose, vitamin B12, hematin, vitamin K3, acetate, formate, and a 5% H2 atmosphere. Data across 3 experiments were compared to a positive control of acetate, formate and 5% H2 and combined. **Panel a,** *M. smithii* growth relative to a positive control. **Panel b,** Decision tree representation of growth data relative to H2, acetate control condition. Growth relative to the positive control is indicated as follows; open circles: no growth (NONE < 0.25), gray circles: low growth (LOW ≥ 0.25, < 0.75); blue circles: similar growth (SIMILAR ≥ 0.75, < 1.25); and pink circles: high growth (HIGH ≥ 1.25).
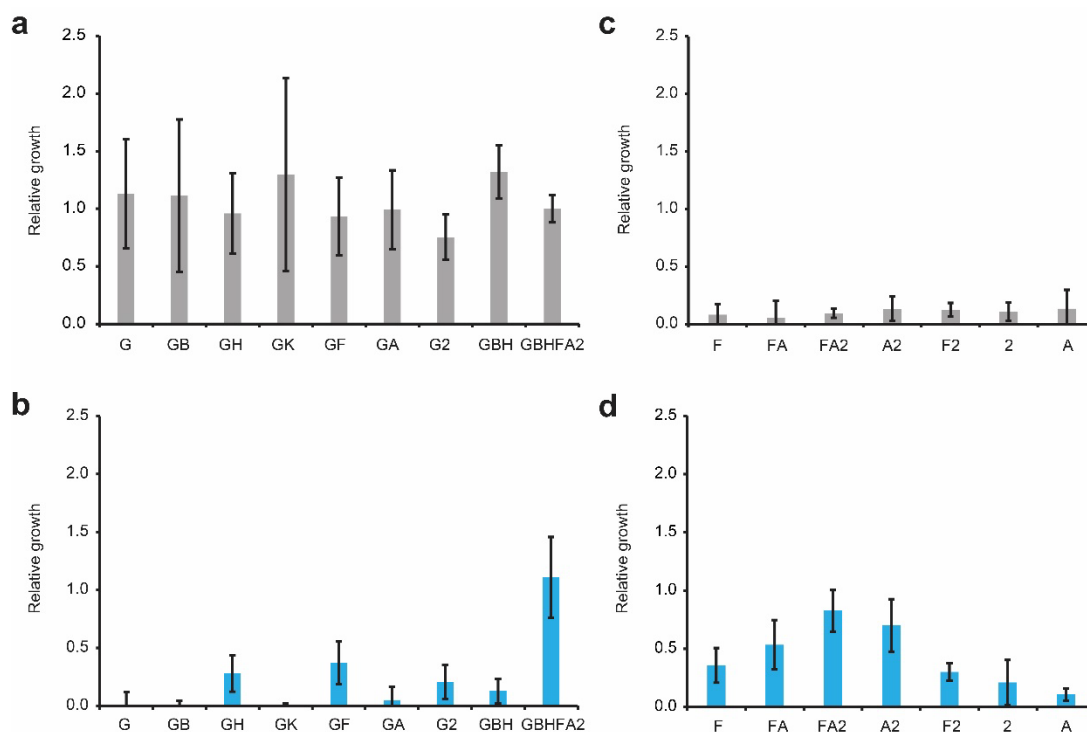
Figure 7. Identification of defined medium that supports independent growth.
Panels a and c, Growth of *B. theta* in dropout medium. **Panels b and d,** Growth of *M. smithii* in dropout medium. Data for each panel was obtained from triplicate biological and 8 technical replicates (n=24). Error bars represent standard deviation. G, 0.5% glucose; B, vitamin B_{12}; H, hematin; K, vitamin K_3; F, 10mM formate; A, 10mM acetate; 2, 5% H_2 atmosphere.
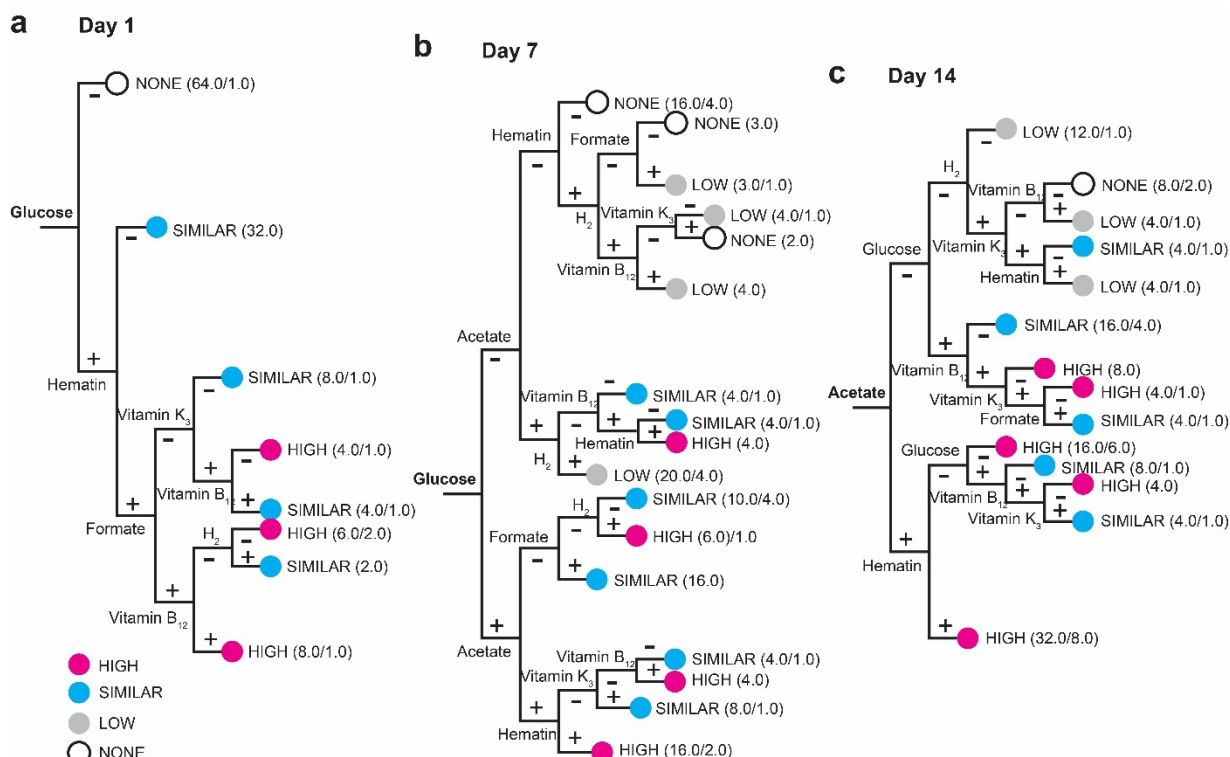
Figure 8. Decision Trees of co-culture growth results. Triplicate *B. theta + M. smithii* cocultures were grown in replicates of 8 on glucose defined medium supplemented with 64 different combinations of vitamin B_{12}, hematin, vitamin K_3, acetate, formate, and a 5% H_2 atmosphere. **Panel a,** Co-cultures after 1 day of growth **Panel b,** Co-cultures after 7 days of growth. **Panel c**, Cocultures after 14 days of growth. Data were obtained from triplicate biological and eight technical replicates (n=24). Growth relative to the positive control is indicated as follows; open circles: no growth (NONE < 0.25), gray circles: low growth (LOW ≥ 0.25, < 0.75); blue circles: similar growth (SIMILAR ≥ 0.75, < 1.25); and pink circles: high growth (HIGH ≥ 1.25).
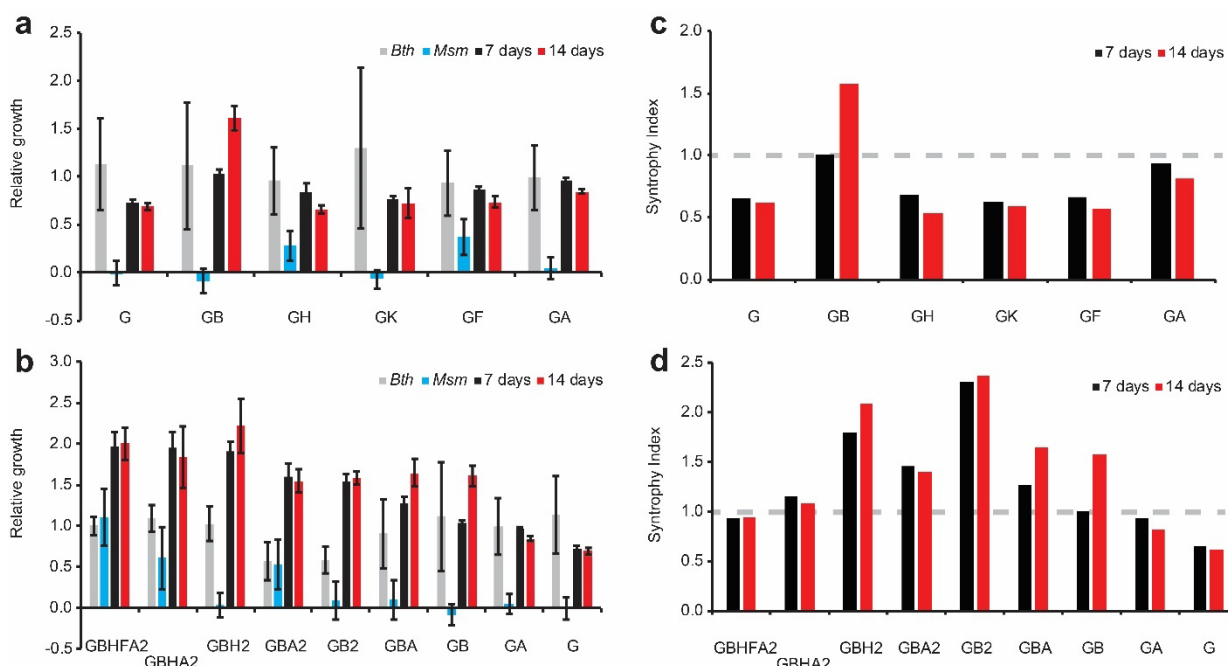
Figure 9. Metabolic Synergistic Interaction Index (SI). Panel a, Effect of nutrient supplementation on growth. **Panel b**, Effect of nutrient combinations of on growth. **Panels c and d**, SI of conditions shown in panels a and b, respectively. An index of 1 (dotted gray line) indicates the null hypothesis where organisms grow independently in co-culture. An index greater than 1 indicates the relative growth of the co-culture is greater than the sum of the monocultures, suggesting a syntrophic relationship. An index of less than one indicates a competitive or inhibitory effect. Error bars represent standard deviation from triplicate biological and eight technical replicates (n=24). G, 0.5% glucose; B, vitamin B_{12}; H, heme; K, vitamin K_3; F, 10mM formate; A, 10mM acetate; 2, 5% H_2 atmosphere.

Table 2. Synergistic Interaction Index Statistics		
Index range ($I_i =$)	**Number of treatments**	
	Day 7	**Day 14**
>1.5	2	7
>1.25	8	11
$0.75 \geq x \geq 1.25$	9	5
< 0.75	24	29
< 0.5	2	1
Extrema	**Index Value ($I_i =$)**	
	Day 7	**Day 14**

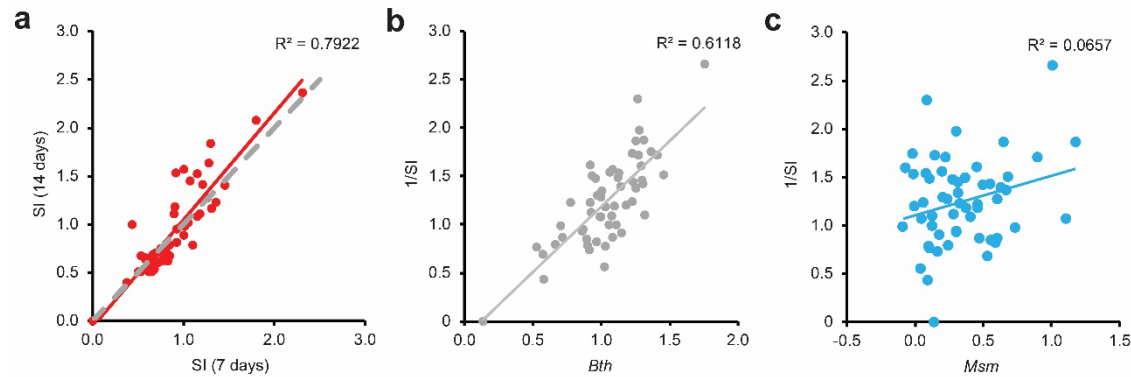| Maximum	2.307	2.366
Minimum	0.376	0.397
Positive Control[a]	0.928	0.950
a: Defined medium supplemented with glucose, histidine and hematin, vitamin B_{12}, formate, acetate, and H_2. In this treatment *B. theta* and *M. smithii* are provided nutrients for both to grow independently.		

Figure 10. Synergistic coculture growth is inversely related to *B. theta* growth. Panel a, Metabolic relationships are established and stable between 7 and 14 days in culture. **Panel b**, *B. theta* monoculture relative growth is inversely correlated to the 7-day Synergistic Interaction index (SI). **Panel c**, *M. smithii* monoculture relative growth is not correlated with the 7-day SI.
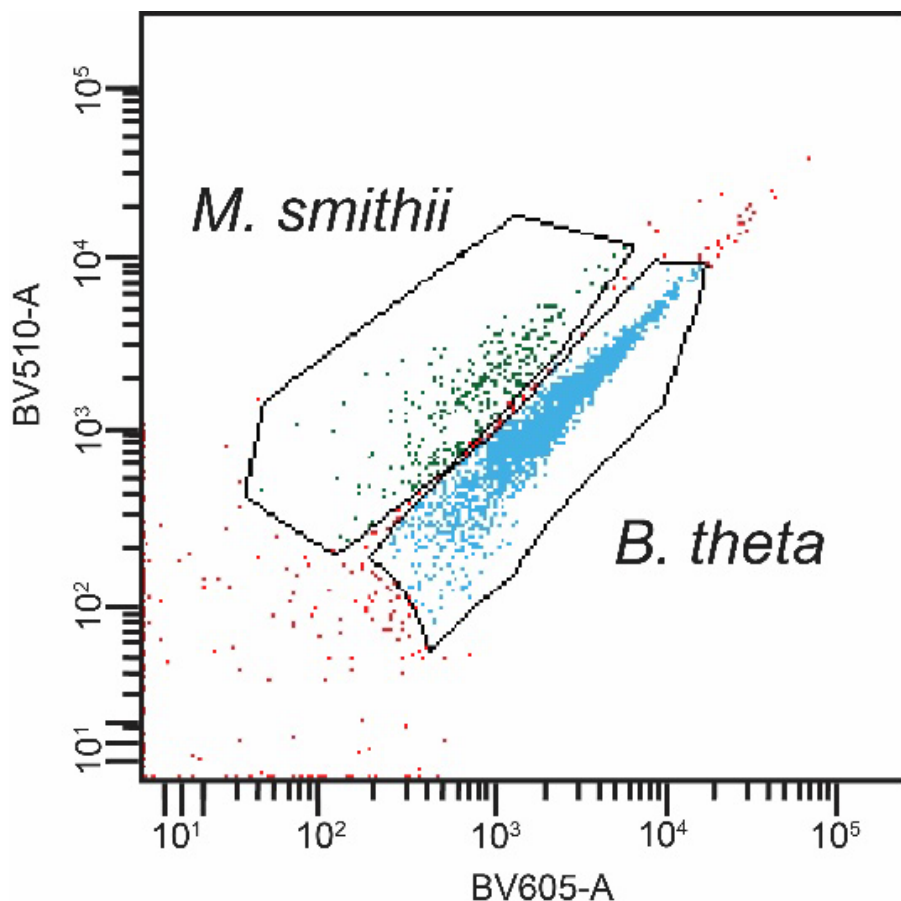
Figure S1. Flow cytometry gating. Cells were harvested, washed in phosphate buffer, and stained as described in the Materials and Methods. B. theta and M. smithii cells were cultured anaerobically in rich medium until stationary phase (4 days for *B. theta* and 9 days for *M. smithii)* as determined by measuring optical density (OD) at 600nm. Cells were mixed with an OD ratio of 10:1 *B. theta*:*M. smithii* and concentrated anaerobically via centrifugation at a 500 x *g* for 10 minutes in a ThermoScientific Sorvall Legend centrifuge fitted with a Micro21 rotor (ThermoFisher Scientific, Waltham, MA), washed with phosphate-buffered saline (PBS; 137mM NaCl, 2.7mM KCl, 10mM Na_2HPO_4, 1.8mM KH_2PO_4) and resuspended to a concentration of approximately 1.0×10^6 cells per mL. Cells were dyed using LIVE/DEAD^{TM} Fixable Yellow Dead Cell Stain Kit (Invitrogen, Waltham, MA) according to the manufacturer instructions. Flow cytometry was performed by exciting with a 405nm laser and 10,000 events were recorded. The axes display the level of fluorescence detected at 510nm and 605nm. Blue dots indicate *B. theta* cells. Green dots indicate *M. smithii* cells which fluoresce more strongly at 510nm due to the presence of cofactor F420 and due to staining with amine-reactive dye, as *M. smithii* has a proteinaceous S-layer instead of a cell wall and has no outer membrane. Red dots indicate signals which do not cluster strongly with either signal.